I=2 S-wave Pion Scattering Phase Shift with Two Flavor Dynamical Quark Effect

Takeshi YAMAZAKI

A dissertation submitted to the Doctoral Program
in Physics, the University of Tsukuba
in partial fulfillment of the requirements
for the degree of Doctor of Philosophy in Science

January 2004

Abstract

We present the isospin $I = 2$ S-wave pion scattering phase shift with two-flavor dynamical quark effect obtained from lattice QCD. The calculation uses two-flavor full QCD configurations previously generated with a renormalization group improved gauge action and clover quark action with a tadpole improved clover coefficient at three different bare couplings, corresponding to $a \approx 0.22, 0.16$ and 0.11 fm, for the continuum extrapolation. This is the first calculation for the scattering phase including the two flavor dynamical quark effect and taken to the continuum limit. The scattering phase is obtained through the finite volume method in the center of mass system, and its extension to the non-rest system. While the inclusion of the non-rest system requires little extra computational cost, the use of the system allows significantly more dense sampling of the scattering phase. We observe a reasonable fit with the results obtained from the calculations in the different systems. We also find that the pion mass and the lattice spacing dependences for the scattering phase are large. These dependences cause large systematic errors at the physical pion mass and in the continuum limit. The result for the scattering phase in the continuum limit agrees with the experimental result. Furthermore as an extension of this work we calculate the two-pion wave function. The wave function contains various information of the scattering. From the wave function we obtain the effective potential, its interaction range and the scattering length.

Contents

1 Introduction

The strong interaction is described by Quantum chromodynamics (QCD) in the Standard Model. It is formulated in terms of quarks and gluons which are the basic degrees of freedom that make up hadronic matter. It has been very successful in predicting phenomena involving large momentum transfer. In this region the strong coupling constant becomes small due to asymptotic freedom, which is a property of QCD, so that perturbative calculation is a reliable tool. However, at the scale of the hadronic world the coupling constant is order of unity and perturbative methods fail. In this domain lattice QCD is a powerful tool of non-perturbative calculations. From first principles lattice QCD can be used to address issues like hadronic spectrum, matrix elements of any operator within these hadronic states, the mechanism of confinement and chiral symmetry breaking, the role of topology, and the equilibrium properties of QCD at finite temperature or density.

Lattice QCD is QCD formulated on a discrete Euclidean space time grid with a finite lattice spacing a. QCD is reconstructed in the limit of the continuum, $a \to 0$, and the infinite volume. Since a finite lattice spacing corresponds to an ultraviolet energy cut-off at $O(1/a)$, no new parameters or field variable are introduced in this discretization. Lattice QCD retains the fundamental character of QCD, and there are no infinities at finite a. Furthermore renormalized physical quantities have a finite limit in the continuum limit. Since lattice QCD is formulated on discrete space-time, it is possible to simulate on the computer using methods analogous to those used for statistical mechanics systems. These simulations allow us to calculate correlation functions of hadronic operators and matrix elements of any operator between hadronic states in terms of the fundamental quark and gluon degrees of freedom.

So far most of lattice QCD calculations have focused on 'static' physical quantities, e.g., hadronic spectrum, and succeeded in this region. CP-PACS Collaboration studied the light hadronic spectrum with quenched approximation [1] of ignoring the dynamical effects of sea quarks, and with two-flavor full QCD [2] which contains the dynamical effects of u, d quarks. They obtained results consistent with experiment within 10% order for quenched QCD. Recently a more realistic calculation with three flavor full QCD has been pursued by HPQCD/UKQCD/MILC/Fermilab [3] and CP-PACS/JLQCD [4] Collaborations. On the other hand, for 'dynamical' physical quantities, such as scattering amplitudes and decay widths, there have been few studies. Calculation of the scattering phase shift is a challenging study beyond the static physical quantities to understand hadronic dynamics based on (lattice) QCD.

However, calculation of the phase shift poses several problems from the technical point of view. One of them is that Euclidean hadron correlation functions calculated by Monte Carlo evaluation methods of lattice QCD are generally only indirectly connected to real time scattering amplitudes. An elegant solution to this problem is the finite volume method, proposed by Lüscher [5, 6], relating the phase shifts to the energy of two hadron states on a finite volume lattice with periodic boundary condition. Another problem is the extraction of the energy of the two-hadron state. Since a two-hadron correlation function behaves as a sum of exponentials due to the presence of a number of states having the same quantum numbers, it is non-trivial to extract the two-hadron energy eigenvalue of the excited states. To solve this problem Lüscher and Wolff [7] proposed a diagonalization method, which have succeeded in many works with effective theory [7, 8, 9].

Historically the first attempt toward a lattice calculation of hadron scattering length,

which is defined as the threshold value of the scattering phase shift, was made by Guagnelli, Marinari and Parisi [10] for $\pi\pi$ and π-N scattering cases. They found a finite volume shift of the energy of two-hadron states and examined the volume dependence. However, they did not calculate full diagrams, and thus the results cannot compared with the physical scattering lengths. Gupta, Kilcup, Patel and Sharpe [11, 12] developed an analysis of the physical $\pi\pi$ scattering length for the isospin $I = 2$ channel. Kuramashi *et al.* [13] studied the scattering lengths in various channels, $\pi\pi$ in $I = 0, 2$, π-N in $I = 1/2, 3/2$, K-N and $\overline{K}$-N in $I = 0, 1$, and baryon scattering N-N. JLQCD Collaboration [14] and Liu, Zhang, Chen and Ma [15] obtained the $I = 2$ $\pi\pi$ scattering length in the continuum limit within the quenched approximation. Recently Meng, Miao, Du and Liu [16] reported K-N scattering length in the $I = 0$ channel, and BGR Collaboration [17] studied the $I = 2$ $\pi\pi$ scattering length in the small pion mass region. These works employed the quenched approximation.

Due to the difficulty of extraction of two-hadron energy for momentum excited states, calculation of the scattering phase shift is more difficult than that of the scattering length. So far only pioneering works in $I = 2$ $\pi\pi$ scattering system have been reported. The isospin $I = 2$ $\pi\pi$ scattering is the simplest hadronic scattering, because in the low energy region $E < 4m_\pi$ physical states with the quantum number $I = 2$ are only $\pi\pi$ state. Fiebig *et al.* [18] used an effective potential calculated from lattice simulation to estimate the phase shift. Since their calculation did not take into account the multi-exponential behavior of the pion four-point function, the result has a strange behavior. CP-PACS Collaboration [19] attempted a direct calculation for the phase shift employing the finite volume method [5, 6]. They observed a 30% smaller result in magnitude than the experiment. Very recently Kim [20] have explored a calculation through the finite volume method with anti-periodic boundary conditions. This boundary conditions allow an easier extraction of the two-pion energy with momentum.

All the previous works for the phase shift have employed quenched approximation, and did not take the continuum limit. Bernard and Golterman [21], and Colangelo and Pallante [22] claimed that the quenched approximation causes divergence of the scattering length in the chiral limit where the pion mass vanishes. In the phase shift, the same problem also occurs. Furthermore the approximation violates unitarity. Unitarity is expected to become more important in the calculation of scatterings and decays than in that of the hadron mass spectrum. For these reasons calculations without the quenched approximation are required to evaluate realistic physical phase shifts.

In this work we aim to obtain a realistic scattering phase shift for the $I = 2$ $\pi\pi$ scattering system. To do this, we calculate the scattering phase on the gauge configurations with dynamical u, d quarks effect, at three different lattice spacings for the continuum extrapolation. We use the configurations previously generated for study of light hadron spectroscopy [2]. Since the result can get rid of the uncertainties of unitary violation and effects of finite lattice spacing, it is expected to be a more realistic phase shift than those of the previous works. In this calculation we attempt to apply the finite volume method not only in the center of mass system [5, 6], where the total momentum of two pions is zero, but also in non-rest system, where the total momentum is non-zero. The method in the non-rest system was proposed by Rummukainen and Gottlieb [8]. The inclusion of the non-rest system adds little extra computational cost, and yet the use of the system allows a significantly more dense sampling of the energy states. The method in the non-rest system has been employed only in effective theory [8]. The result in this work is the first not only with two-flavor full QCD in the continuum limit, but also employing the non-rest system method in QCD. We

compare our result in the continuum limit with the experimental results [23, 24] and the prediction extracted in the framework of chiral perturbation theory [25], an effective theory of Goldstone bosons.

In the finite volume method it is an important assumption that the interaction range of scattering is contained in the finite volume considered. Check this assumption, a simple method is to examine the volume dependence of the phase shift, but the examination demands calculations with changing volume. In stead we explore a direct observation of the interaction range from the two-pion wave function calculated on lattice. A similar study of the wave function have been carried out previously by Balog *et al.* [26] for the two-dimensional XY model, but the calculation in the four-dimensional lattice QCD has not been carried out. From the wave function we extract the interaction range and the scattering length.

The understanding of hadronic dynamics is also important for evaluations of hadronic effect included in the cross section observed experimentally. Since the effect cannot be estimated by perturbation theory, the lattice calculation is a powerful tool. For example, the CP violation parameter $\varepsilon^{'}/\varepsilon$ and the $\Delta I = 1/2$ selection rule of $K \to \pi\pi$ decay are famous open problems. There are a number of difficulties in the calculation, which are summarized in Ref. [27]. Main difficulties are the following two points: (i)extraction of the on-shell amplitude at $m_K^2 = 4(m_\pi^2 + p^2)$ with $p \neq 0$, (ii)the relation between the amplitude calculated on a finite volume lattice and that in the infinite volume. Lellouch and Lüscher [28] proposed a solution of the second difficulty. The solution, however, assumed that the first difficulty have been solved. The first difficulty has not solved. Some strategies [29] have been suggested to avoid the difficulty, and its applications [30] have been reported. However, even the recent works have not obtained results consistent with the experiment. The first difficulty is related to the final state interaction, i.e., the $\pi\pi$ scattering. Thus the study of the $\pi\pi$ scattering is a first step toward the calculation of $K \to \pi\pi$ decay [31].

This article is organized as follows. In Sec. 2 we review the results obtained from theoretical and experimental sides. On the theoretical side we focus on the results of chiral perturbation theory. The formulation of lattice QCD is described in Sec. 3. In Sec. 4, the previous studies for the $\pi\pi$ scattering calculated from lattice QCD are summarized. In Sec. 5 we explain the two finite volume methods in the center of mass system proposed by Lüscher, and in general systems proposed by Rummukainen and Gottlieb, which are methods to extract the scattering phase shift from the two-pion energy calculated on lattice. To employ the finite volume method, we need to extract the two-pion energy from the pion four-point function. The extraction method is discussed in Sec. 6. Then we show our work in Sec 7–9. In Sec. 7 the detailed calculation method to obtain the scattering phase shift, and the simulation parameters are given. The results for the scattering length and phase shift at each lattice spacings and in the continuum limit are presented in Sec. 8. We present the pioneering work of the two-pion wave function in Sec. 9. In Sec. 10 we summarize this work, and we list future problems related to this thesis in Sec. 11.

2 $\pi\pi$ scattering

In this section we first present the theoretical results predicted by chiral perturbation theory (ChPT), which is an effective theory of Goldstone bosons. Later we show the experimental results with several approaches.

2.1 Theoretical results

The study of $\pi\pi$ scattering is a classical subject in the field of strong interactions. The properties of the pions are intimately related to an approximate chiral symmetry of QCD. In the chiral limit, where m_u and m_d vanish, this symmetry becomes exact, the Lagrangian being invariant under the group $\mathrm{SU(2)_R}\times\mathrm{SU(2)_L}$ of chiral rotations. The symmetry is spontaneously broken to the isospin subgroup $\mathrm{SU(2)_V}$. The pions represent the corresponding Goldstone bosons.

The properties of the Goldstone bosons are strongly constrained by chiral symmetry. In the chiral limit, the scattering amplitude vanishes when the momenta of the pions tend to zero. To first order in the symmetry breaking, the S-wave scattering lengths are proportional to the square of the pion mass:

$$a_0^0 m_\pi = \frac{7m_\pi^2}{32\pi F^2}, \quad a_0^2 m_\pi = -\frac{m_\pi^2}{16\pi F^2}, \tag{1}$$

where a_l^I stands for the scattering length in the isospin I channel with angular momentum l, and F is the pion decay constant in the chiral limit. The two low energy theorems eq.(1) are valid only at leading order in a series expansion in powers of the quark masses. The next-to-leading order corrections were calculated in [32], and even the next-to-next-to-leading order corrections are also known [33].

2.1.1 Scattering amplitude

We consider elastic $\pi\pi$ scattering in the framework of QCD and restrict our analysis to the isospin symmetry limit, where the masses of the up and down quarks are taken equal and the electro magnetic interaction is ignored. The pion is denoted as the isovector particle π^a for $a = 1, 2, 3$. In this case, the scattering process is described by a single Lorentz invariant amplitude $A(s,t,u)$,

$$\begin{aligned}&\langle \pi^d(p_4)\pi^c(p_3)\ \mathrm{out}|\pi^a(p_1)\pi^b(p_2)\ \mathrm{in}\rangle \\ &= \delta_{fi} + (2\pi)^4 i\delta^4(P_f - P_i)\{\delta^{ab}\delta^{cd}A(s,t,u) + \delta^{ac}\delta^{bd}A(t,u,s) + \delta^{ad}\delta^{bc}A(u,s,t)\}.\end{aligned} \tag{2}$$

The amplitude depends only on the Mandelstam variables s, t, u,

$$s = (p_1+p_2)^2, t = (p_3-p_1)^2, u = (p_4-p_1)^2, \tag{3}$$

which are constrained by $s + t + u = 4m_\pi^2$. Moreover, crossing symmetry implies the interchange symmetry of the second and third arguments,

$$A(s,t,u) = A(s,u,t). \tag{4}$$

The pion can be described by the $I_z = \pm 1, 0$ components as

$$\pi^\pm = \mp\frac{1}{\sqrt{2}}(\pi^1 \pm i\pi^2), \quad \pi^0 = \pi^3. \tag{5}$$

In the isospin basis, the two-pion is classified into the $I = 0, 1$ and 2 state as

$$\begin{aligned} I=0: \quad \frac{1}{\sqrt{3}}(\pi^+\pi^- + \pi^-\pi^+ - \pi^0\pi^0) &= -\frac{1}{\sqrt{3}}\sum_{a=1}^{3}\pi^a\pi^a, \\ I=1: \quad \pi^+\pi^0 - \pi^0\pi^+ &= -\frac{1}{2}(\pi^1\pi^0 - \pi^0\pi^1 + i(\pi^2\pi^0 - \pi^0\pi^2)), \\ I=2: \quad \pi^+\pi^+ &= \frac{1}{2}(\pi^1\pi^1 + i(\pi^1\pi^2 + \pi^2\pi^1) - \pi^2\pi^2). \end{aligned} \tag{6}$$

Substituting eq.(6) to eq.(2), one obtains the s-channel isospin I components of the amplitude T^I,

$$T^0(s,t) = 3A(s,t,u) + A(t,u,s) + A(u,s,t), \tag{7}$$
$$T^1(s,t) = A(t,u,s) - A(u,s,t), \tag{8}$$
$$T^2(s,t) = A(t,u,s) + A(u,s,t). \tag{9}$$

The partial wave decomposition reads

$$\begin{aligned} T^I(s,t) &= 32\pi\sum_l (2l+1)P_l(\cos\theta)\; t_l^I(s), \\ t_l^I(s) &= \frac{1}{2i\sigma(s)}\{e^{2i\delta_l^I(s)} - 1\}, \\ \sigma(s) &= \sqrt{1 - \frac{4m_\pi^2}{s}}, \end{aligned} \tag{10}$$

where $P_l(\cos\theta)$ is the Legendre function and $\cos\theta$ is given by the Mandelstam variables,

$$\cos\theta = 1 + \frac{2t}{s - 4m_\pi^2}, \tag{11}$$

and the real parameter $\delta_l^I(s)$ is the scattering phase shift with $s = 4(m_\pi^2 + p^2)$. The threshold parameters are given by the coefficients of the expansion

$$\mathrm{Re}\, t_l^I(p) = \left(\frac{p}{m_\pi}\right)^{2l}\left\{a_l^I m_\pi + b_l^I\left(\frac{p}{m_\pi}\right)^2 + \cdots\right\}. \tag{12}$$

Using the definition of $t_l^I(s)$ eq.(12), we find that the amplitude $T^I(s,t)$ is normalized by the S-wave scattering length a_0^I,

$$T^0(4m_\pi^2, 0) = 32\pi a_0^0 m_\pi, \quad T^1(4m_\pi^2, 0) = 0, \quad T^2(4m_\pi^2, 0) = 32\pi a_0^2 m_\pi. \tag{13}$$

2.1.2 A simple parametrization of scattering phase shift

In the elastic scattering region the partial wave amplitudes are written by eq.(10) with the phase shift for isospin I with angular momentum l. Schenk [34] proposed a simple parametrization of the phase shifts using the following properties of the amplitudes:

(i) The threshold behavior of the scattering amplitude T^I is described by eqs.(10) and (12).

(ii) The phase shifts δ_0^0 and δ_1^1 pass through 90^o at some measured values m_σ and m_ρ

$$\delta_0^0(\sqrt{s} = m_\sigma) = \delta_1^1(\sqrt{s} = m_\rho) = 90^o. \tag{14}$$

(iii) The quantity

$$\sqrt{\frac{s}{s-4m_\pi^2}}\frac{m_\pi^2}{p^2}\left(\frac{s-m_\rho^2}{4m_\pi^2-m_\rho^2}\right)\tan\delta_1^1(s) \tag{15}$$

is very smooth below $\sqrt{s} \approx 1$ GeV. In this region $\tan\delta_1^1(s)$ can be described by a simple Breit-Wigner form

$$\tan\delta_1^1(s) = \frac{m_\rho\Gamma_\rho}{m_\rho^2 - s}, \tag{16}$$

where Γ_ρ is the decay width of the rho meson.

A simple parametrization, respecting all three conditions, is given by

$$\tan\delta_l^I(s) = \sqrt{\frac{s}{s-4m_\pi^2}}\left(\frac{p}{m_\pi}\right)^{2l}\left(a_l^I m_\pi + \overline{b}_l^I\left(\frac{p}{m_\pi}\right)^2 + \cdots\right)\left(\frac{4m_\pi^2 - s_l^I}{s - s_l^I}\right), \tag{17}$$

where the threshold expansion is reproduced with

$$\overline{b}_l^I = b_l^I - a_l^I m_\pi \frac{4m_\pi^2}{s_l^I - 4m_\pi^2} + (a_l^I m_\pi)^3\delta_{l0}. \tag{18}$$

2.1.3 Chiral perturbation theory

In order to obtain the scattering amplitude T^I in eq.(10), most studies employ chiral perturbation theory (ChPT). We show the framework of ChPT in this section.

If the quark masses are set equal to zero, the QCD Lagrangian

$$L_{QCD} = -\frac{1}{4}F_{\mu\nu}F^{\mu\nu} + \overline{q}i\not{D}q, \quad q = (\overbrace{u, d, s, \cdots}^{N_f}) \tag{19}$$

is symmetric under the chiral group $\mathrm{SU}(N_f)\times\mathrm{SU}(N_f)$. One assumes that the ground state of the theory spontaneously breaks this symmetry down to $\mathrm{SU}(N_f)$. The hidden symmetry then manifests itself in the occurrence of $N_f^2 - 1$ pseudoscalar Goldstone bosons; in the $N_f = 2$ case $\pi^\pm$ and π^0 appear.

In reality, the QCD Lagrangian contains a quark mass term which breaks the symmetry. The vector and axial currents are not exactly conserved,

$$\partial_\mu(\overline{u}\gamma^\mu d) = i(m_u - m_d)\overline{u}d, \tag{20}$$

$$\partial_\mu(\overline{u}\gamma^\mu\gamma_5 d) = i(m_u + m_d)\overline{u}\gamma_5 d. \tag{21}$$

Since the masses of u and d quarks, however, are tiny, the divergence of the currents approximately vanishes. Deviations from chiral symmetry may be studied by treating the quark mass

$$\hat{m} = (m_u + m_d)/2, \tag{22}$$

in the Lagrangian as a perturbation.

Let us consider effective theory containing only the Goldstone modes in the isospin symmetry limit. Our basic assumption is the pattern of spontaneous symmetry breaking,

$$\mathrm{SU}(2) \times \mathrm{SU}(2) \to \mathrm{SU}(2)_V. \tag{23}$$

We denote by ϕ^a $(a = 1, 2, 3)$ the coordinates describing the Goldstone fields in the broken symmetry $\mathrm{SU}(2)\times\mathrm{SU}(2)/\mathrm{SU}(2)_V$. We choose the two-by-two unitary matrix

$$U(\phi) = \exp\left(i\sqrt{2}\Phi/F\right), \tag{24}$$

where F is the pion decay constant in the chiral limit, and Φ gives a convenient parameterization of the Goldstone fields

$$\Phi = \frac{\tau^a}{\sqrt{2}}\phi^a = \begin{pmatrix} \pi^0/\sqrt{2} & \pi^+ \\ \pi^- & -\pi^0/\sqrt{2} \end{pmatrix}. \tag{25}$$

The $U(\phi)$ linearly transforms under the chiral symmetry $(\overline{g}_L, \overline{g}_R) \equiv \mathrm{SU}(2)_L\times\mathrm{SU}(2)_R$ as

$$U(\phi) \to \overline{g}_R U(\phi) \overline{g}_L^\dagger, \tag{26}$$

but the transformation of the Goldstone fields is highly non-linear.

Since the low energy effective Lagrangian can be organized in terms of $U(\phi)$ and increasing powers of momentum, the Lagrangian contains an even number of derivatives due to parity conservation;

$$\mathcal{L}_{\mathrm{eff}}(U) = \sum_n \mathcal{L}_{2n}. \tag{27}$$

At lowest order, the Lagrangian is given in term of,

$$\mathcal{L}_2 = \frac{F^2}{4}\mathrm{Tr}\left[\partial_\mu U^\dagger \partial^\mu U\right]. \tag{28}$$

Let us consider an extended effective Lagrangian including the mass term, which explicitly breaks chiral symmetry. To do this, we extend the QCD Lagrangian to

$$\mathcal{L}_{\mathrm{QCD}} + \overline{q}\gamma^\mu(v_\mu + a_\mu\gamma_5)q - \overline{q}(s - i\gamma_5 p)q, \tag{29}$$

where the external fields $v_\mu(x), a_\mu(x), s(x)$ and $p(x)$ are Hermitian flavor two-by-two matrices. The $s(x)$ at the leading order is related to the mass matrix M as

$$s = M = \hat{m} \cdot \mathbf{1}. \tag{30}$$

The Lagrangian eq.(29) is invariant under the following local transformations $(g_L, g_R) \equiv \mathrm{SU}(2)_L\times\mathrm{SU}(2)_R$,

$$\begin{array}{lll} q_L \to g_L q_L, & q_R \to g_R q_R, \\ r_\mu \equiv v_\mu + a_\mu & \to & g_R r_\mu g_R^\dagger + i g_R \partial_\mu g_R^\dagger, \\ l_\mu \equiv v_\mu - a_\mu & \to & g_L l_\mu g_L^\dagger + i g_L \partial_\mu g_L^\dagger, \\ s - ip & \to & g_R(s - ip) g_L^\dagger. \end{array} \tag{31}$$

We use this symmetry to build a generalized effective Lagrangian with these external fields. Due to the local symmetry, only v_μ and a_μ appear in the covariant derivatives,

$$D_\mu U = \partial_\mu U - i r_\mu U + i U l_\mu, \quad D_\mu U^\dagger = \partial_\mu U^\dagger - i r_\mu U^\dagger + i l_\mu U^\dagger. \tag{32}$$

At the lowest order, the generalized effective Lagrangian is given by

$$\mathcal{L}_2 = \frac{F^2}{4}\mathrm{Tr}\Big[D_\mu U^\dagger D^\mu U + U^\dagger\chi + \chi^\dagger U\Big], \tag{33}$$

where

$$\chi = 2B(s - ip). \tag{34}$$

The parameter B is related to the quark condensate as

$$B = -\langle 0|\overline{q}q|0\rangle/F^2. \tag{35}$$

We can extract the pseudoscalar mass term from the χ term in eq.(33) by taking the external fields as $s = M$ eq.(30) and $p = 0$, and expanding in Φ,

$$\begin{aligned}\frac{F^2}{4}2B\mathrm{Tr}\Big[M(U^\dagger + U)\Big] &= -B\hat{m}\mathrm{Tr}\Big[\Phi^2\Big] + O(\Phi^4/F^2) &(36)\\ &= -\frac{1}{2}2B\hat{m}(\pi^+\pi^- + \pi^-\pi^+ + \pi^0\pi^0) + O(\Phi^4/F^2), &(37)\end{aligned}$$

where we drop constant terms. So we obtain the relation between the physical pion mass and the quark mass at lowest order,

$$m^2_{\pi^\pm,0} = 2B\hat{m}. \tag{38}$$

This relation means m_π^2 is treated as the same order as the quark mass. The expansion of the quark mass is not rather than the one of m_π^2. The momentum expansion of the effective Lagrangian eq.(27) is also carried out by taking into account the order of the momentum $p^2 \sim m_\pi^2$.

The scattering amplitude for the isospin $I = 0, 2$ at the lowest order can be calculated from $\mathcal{L}_2$ as,

$$\begin{aligned}t_0^0(s) &= \frac{2s - m_\pi^2}{32\pi F^2},\\ t_0^2(s) &= -\frac{s - 2m_\pi^2}{32\pi F^2}.\end{aligned} \tag{39}$$

In the limit $s \to 4m_\pi^2$ and $t = u \to 0$, we find the scattering lengths of the lowest order eq.(1).

The effective Lagrangian of order p^4 was given by Gasser and Leutwyler [32],

$$\begin{aligned}\mathcal{L}_4 &= l_1\left(\mathrm{Tr}\Big[D^\mu U^\dagger D_\mu U\Big]\right)^2 + l_2\mathrm{Tr}\Big[D^\mu U^\dagger D^\nu U\Big]\,\mathrm{Tr}\Big[D_\mu U^\dagger D_\nu U\Big]\\ &\quad + l_3\left(\mathrm{Tr}\Big[\chi^\dagger U + \chi U^\dagger\Big]\right)^2 + l_4\mathrm{Tr}\Big[D^\mu\chi^\dagger D_\mu U + D^\mu\chi D_\mu U^\dagger\Big] + \cdots,\end{aligned} \tag{40}$$

which is the part of $\mathcal{L}_4$ related to the scattering amplitude eq.(10). The low energy constants l_i are divergent and renormalized with the divergences generated by one loop graphs from $\mathcal{L}_2$. The renormalized constants l_i^r logarithmically depend on the renormalization scale μ [32],

$$l_i^r = \frac{\gamma_i}{32\pi^2}\left(\bar{l}_i + \ln\frac{m_\pi^2}{\mu^2}\right);\ \gamma_1 = \frac{1}{3},\ \gamma_2 = \frac{2}{3},\ \gamma_3 = -\frac{1}{2},\ \gamma_4 = 2. \tag{41}$$

Here $\overline{l}_i$ is scale independent constants. At this order the pion mass and pion decay constant in terms of F and m^2, which is the pion mass at the lowest order, are given by

$$m_\pi^2 = m^2\left\{1 - \frac{m^2}{32\pi^2F^2}\overline{l}_3 + O(m^4)\right\}, \tag{42}$$

$$f_\pi = F\left\{1 + \frac{m^2}{16\pi^2F^2}\overline{l}_4 + O(m^4)\right\}. \tag{43}$$

The complete effective Lagrangian $\mathcal{L}_6$ of order p^6 is not yet available. The list of necessary counter terms has been published [35], but their divergence structure is under investigation.

2.1.4 Amplitude at two loop order

The scattering amplitude at two loop order was calculated by Bijnens *et al.* [33]. The momentum expansion of the amplitude amounts to a Taylor series in

$$\xi = \left(\frac{m_\pi}{4\pi f_\pi}\right)^2. \tag{44}$$

The following amplitude at two-loop order was obtained

$$\begin{aligned} A(s,t,u) = \quad & \xi[-(4\pi)^2 + (4\pi)^2\overline{s}] \\ & +\xi^2[b_1 + b_2\overline{s} + b_3\overline{s}^2 + b_4(\overline{t}-\overline{u})^2] \\ & +\xi^2[F^{(1)}(\overline{s}) + G^{(1)}(\overline{s},\overline{t}) + G^{(1)}(\overline{s},\overline{u})] \\ & +\xi^3[b_5\overline{s}^3 + b_6\overline{s}(\overline{t}-\overline{u})^2] \\ & +\xi^3[F^{(2)}(\overline{s}) + G^{(2)}(\overline{s},\overline{t}) + G^{(2)}(\overline{s},\overline{u})] \\ & +O(\xi^4), \end{aligned} \tag{45}$$

where the coefficients b_i for $i = 1, \cdots, 6$ include the renormalized couplings l_i^r for $i = 1, \cdots, 4$ and r_i^r for $i = 1, \cdots, 6$ from $\mathcal{L}_4$ and $\mathcal{L}_6$, respectively. The coefficients and the functions $G^{(1)}, G^{(2)}, F^{(1)}$ and $F^{(2)}$ are given in appendix A. Here $\overline{s}, \overline{t}, \overline{u}$ are the Mandelstam variables normalized by the physical pion mass squared m_π^2,

$$\overline{s} = \frac{s}{m_\pi^2}, \quad \overline{t} = \frac{t}{m_\pi^2}, \quad \overline{u} = \frac{u}{m_\pi^2}. \tag{46}$$

From the expression for the scattering amplitude in eq.(45), it is straightforward to evaluate the scattering length a_0^I. Using the parameter ξ and the coefficients b_i, one finds

$$a_0^0 m_\pi = \frac{7m_\pi^2}{32\pi f_\pi^2}\left\{1 + \frac{\xi}{7}\left[49 + 5b_1 + 12b_2 + 48b_3 + 32b_4\right]\right. \tag{47}$$

$$\left. +\xi^2\left[\frac{7045}{63} - \frac{215\pi^2}{126} + 10b_1 + 24b_2 + 96b_3 + 64b_4 + \frac{192}{7}b_5\right]\right\}, \tag{48}$$

$$a_0^2 m_\pi = -\frac{m_\pi^2}{16\pi f_\pi^2}\left\{1 - \xi\left[2 + b_1 + 16b_4\right] + \xi^2\left[\frac{262}{9} - \frac{22\pi^2}{9} + 4b_1 + 64b_4\right]\right\}. \tag{49}$$

In order to obtain the values of the scattering lengths, Bijnens *et al.* [33] used l_i^r estimated from the scale independent couplings $\overline{l}_i$. The $\overline{l}_i$ was evaluated by the experimental inputs as

$$\begin{array}{lcll} \overline{l}_1 & = & -1.7 \pm 1.0 & K_{e4} \text{ decay and } \pi\pi \text{ scattering [36]} \\ \overline{l}_2 & = & 6.1 \pm 0.5 & K_{e4} \text{ decay and } \pi\pi \text{ scattering [36]} \\ \overline{l}_3 & = & 2.9 \pm 2.4 & u, d, s \text{ SU(3) symmetry breaking [32]} \\ \overline{l}_4 & = & 4.3 \pm 0.9 & \text{pion scalar radius } \langle r^2\rangle_s \text{ [32]}, \end{array} \tag{50}$$

The scalar radius related to $\bar{l}_4$ shows up in the scalar form factor

$$\langle\pi(p')|m_u\overline{u}u + m_d\overline{d}d|\pi(p)\rangle = \sigma_\pi\left(1 + \frac{1}{6}\langle r^2\rangle_s q^2 + O(q^4)\right),\ q = p - p', \tag{51}$$

where σ_π is the pion σ-term related to a derivative of m_π^2 with respect to quark mass $\hat{m} = (m_u + m_d)/2$, $\sigma_\pi = \hat{m}\cdot\partial m_\pi^2/\partial\hat{m}$. The effective coupling $\bar{l}_4$ is strongly constrained, because $\bar{l}_4$ is almost determined by only $\langle r^2\rangle_s$ at one loop order [32],

$$\langle r^2\rangle_s = \frac{3}{8\pi^2 f_\pi^2}\left(\bar{l}_4 - \frac{13}{12}\right) + O(\xi^2). \tag{52}$$

The low energy constants l_i were evaluated at $\mu = 1$ GeV from these values.

The couplings r_i^r were estimated by Bijnens *et al.* [33] from the vector meson resonance, the scalar meson resonance and the K meson and the eta meson contributions. They obtained the following numerical estimates,

$$\begin{aligned} r_1^r &= -0.6\cdot 10^{-4} \\ r_2^r &= \ \ 1.3\cdot 10^{-4} \\ r_3^r &= -1.7\cdot 10^{-4} \\ r_4^r &= -1.0\cdot 10^{-4} \\ r_5^r &= \ \ 1.1\cdot 10^{-4} \\ r_6^r &= \ \ 0.3\cdot 10^{-4}. \end{aligned} \tag{53}$$

They ignored the scale dependence of these couplings.

Using the center values for these couplings the scattering lengths were obtained at two-loop order [33] as

$$a_0^0 m_\pi = 0.217 \tag{54}$$

$$a_0^2 m_\pi = -0.0417. \tag{55}$$

They also obtained the scattering phase shifts. In Fig. 1 the results for the scattering phase difference $\delta_0^0 - \delta_0^1$ and the $I = 2$ scattering phase δ_0^2 are presented. In the figure the result with the parameters eq.(50) is denoted as set I, and the one with $\bar{l}_1 = -1.5$ and $\bar{l}_2 = 4.5$ ($\bar{l}_3$,$\bar{l}_4$ unchanged) is denoted as set II.

2.1.5 Result with phenomenological representation

Colangelo *et al.* [25] utilized the scattering amplitude at the two-loop order of ChPT, which is different from eq.(49) in the two loop part, and the phenomenological representation based on the Roy equation [37]. The phenomenological representation is obtained from the available experimental information.

The two loop representation of the scattering amplitude is denoted with the chiral expansion of the partial waves by

$$t_l^I(s) = t_l^I(s)_2 + t_l^I(s)_4 + t_l^I(s)_6 + O(p^8), \tag{56}$$

where $t_l^I(s)_n$ is obtained from the effective Lagrangian $\mathcal{L}_n$. For $I = 0, 2$ at the leading order S-wave amplitudes $t_0^I(s)$ are presented above eq.(39). Since inelastic reactions start to contribute only at $O(p^8)$, the optical theorem reads,

$$\mathrm{Im}t_l^I(s) = \sigma(s)|t_l^I(s)|^2 + O(p^8), \quad \sigma(s) = \sqrt{1 - \frac{4m_\pi^2}{s}}. \tag{57}$$

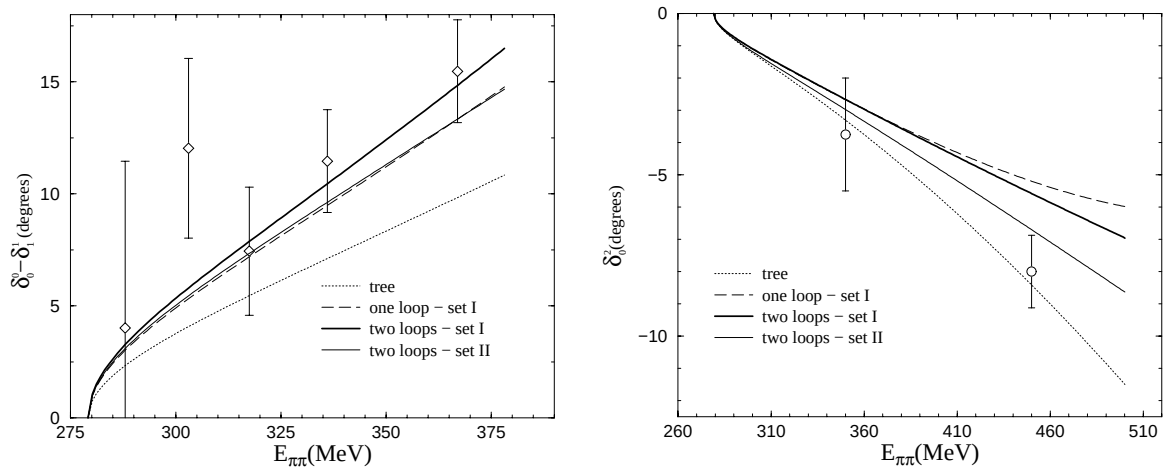

Figure 1: Scattering phase shifts [33] at lowest, one-loop and two-loop order in ChPT. The data points are from Ref. [41]. The set I uses $\bar{l}_1 = -1.7, \bar{l}_2 = 6.1, \bar{l}_3 = 2.9$ and $\bar{l}_4 = 4.3$, while the set II uses $\bar{l}_1 = -1.5, \bar{l}_2 = 4.5$ and $\bar{l}_3, \bar{l}_4$ unchanged.

This unitarity condition leads the following relation between the two loop imaginary amplitude and the real part of the lowest and one loop amplitude as,

$$\mathrm{Im}t_l^I(s) = \sigma(s) t_l^I(s)_2 \left(t_l^I(s)_2 + 2\mathrm{Re}t_l^I(s)_4 \right) + O(p^8). \tag{58}$$

From the discussion the scattering amplitude is given by three functions, $U^I(s)$ for $I = 0, 1, 2$, describing the unitary correction [25],

$$\begin{aligned} A(s,t,u) &= C(s,t,u) + 32\pi \left(\frac{1}{3} U^0(s) + \frac{3}{2}(s-u) U^1(s) + \frac{3}{2}(s-t) U^1(u) \right. \\ &\left. + \frac{1}{2} U^2(t) + \frac{1}{2} U^2(u) - \frac{1}{3} U^2(s) \right) + O(p^8). \end{aligned} \tag{59}$$

The first term is a crossing symmetric polynomial

$$C(s,t,u) = c_1 + s c_2 + s^2 c_3 + (t-u)^2 c_4 + s^3 c_5 + s(t-u)^2 c_6, \tag{60}$$

where the parameters c_i are constructed by the effective couplings l_i and r_i which appear in $\mathcal{L}_4$ and $\mathcal{L}_6$, respectively. The c_i are given in appendix B.1. The functions $U^0(s), U^1(s)$ and $U^2(s)$ are written by dispersion integrals in the form,

$$U^0(s) = \frac{s^4}{\pi} \int_{4m_\pi^2}^{\infty} ds' \frac{\sigma(s') t_0^0(s')_2 \left(t_0^0(s')_2 + 2\mathrm{Re}t_0^0(s')_4 \right)}{s'^4 (s' - s)}, \tag{61}$$

$$U^1(s) = \frac{s^3}{\pi} \int_{4m_\pi^2}^{\infty} ds' \frac{\sigma(s') t_1^1(s')_2 \left(t_1^1(s')_2 + 2\mathrm{Re}t_1^1(s')_4 \right)}{s'^3 (s' - 4m_\pi^2)(s' - s)}, \tag{62}$$

$$U^2(s) = \frac{s^4}{\pi} \int_{4m_\pi^2}^{\infty} ds' \frac{\sigma(s') t_0^2(s')_2 \left(t_0^2(s')_2 + 2\mathrm{Re}t_0^2(s')_4 \right)}{s'^4 (s' - s)}. \tag{63}$$

While the phenomenological representation [25] was obtained in the same manner, the representation includes only two uncertainties, a_0^0 and a_0^2, and other quantities are described

by the experimental information. The phenomenological amplitude takes the form,

$$\begin{aligned} A(s,t,u) &= 16\pi a_0^2 + \frac{4\pi}{3m_\pi^2}(2a_0^0 - 5a_0^2) + \overline{P}(s,t,u) \\ &\quad +32\pi\left(\frac{1}{3}W^0(s) + \frac{3}{2}(s-u)W^1(s) + \frac{3}{2}(s-t)W^1(u)\right. \\ &\quad \left. +\frac{1}{2}W^2(t) + \frac{1}{2}W^2(u) - \frac{1}{3}W^2(s)\right) + O(p^8), \end{aligned} \tag{64}$$

where the three functions are given by

$$W^0(s) = \frac{s^4}{\pi}\int_{4m_\pi^2}^{\infty} ds^{'} \frac{\mathrm{Im}t_0^0(s^{'})}{s^{'4}\,(s^{'}-s)}, \tag{65}$$

$$W^1(s) = \frac{s^3}{\pi}\int_{4m_\pi^2}^{\infty} ds^{'} \frac{\mathrm{Im}t_1^1(s^{'})}{s^{'3}\,(s^{'}-4m_\pi^2)\,(s^{'}-s)}, \tag{66}$$

$$W^2(s) = \frac{s^4}{\pi}\int_{4m_\pi^2}^{\infty} ds^{'} \frac{\mathrm{Im}t_0^2(s^{'})}{s^{'4}\,(s^{'}-s)}. \tag{67}$$

The crossing symmetry polynomial $\overline{P}(s,t,u)$ is defined by

$$\overline{P}(s,t,u) = \overline{p}_1 + s\overline{p}_2 + s^2\overline{p}_3 + (t-u)^2\overline{p}_4 + s^3\overline{p}_5 + s(t-u)^2\overline{p}_6. \tag{68}$$

These parameters $\overline{p}_i$ can be explained by the integrations of the imaginary part of the partial wave [25], and presented in appendix B.2.

The chiral and phenomenological representations have the same structure. The polynomial $C(s,t,u)$ and the functions $U^I(s)$ in the chiral representation, however, involve uncertainties at higher loop order. This implies that the difference from these representations starts showing up at three loop $O(p^8)$. We show the differences of the functions $U^I(s)$ and $W^I(s)$ as,

$$W^0(s) = U^0(s) + O(p^8), \tag{69}$$

$$W^1(s) = U^1(s) + O(p^6), \tag{70}$$

$$W^2(s) = U^2(s) + O(p^8). \tag{71}$$

The two polynomials $C(s,t,u)$ and $\overline{P}(s,t,u)$ also agree up to $O(p^8)$,

$$C(s,t,u) = 16\pi^2 a_0^2 m_\pi + \frac{4}{3m_\pi}(2a_0^0 - 5a_0^2)s + \overline{P}(s,t,u) + O(p^8). \tag{72}$$

This leads the relation of the coefficients c_i and $\overline{p}_i$,

$$\begin{array}{ll} c_1 = 16\pi^2 a_0^2 + \overline{p}_1 + O(p^8), & c_2 = \dfrac{4}{3m_\pi^2}(2a_0^0 - 5a_0^2) + \overline{p}_2 + O(p^6), \\ c_3 = \overline{p}_3 + O(p^4), & c_4 = \overline{p}_4 + O(p^4), \\ c_5 = \overline{p}_5 + O(p^2), & c_6 = \overline{p}_6 + O(p^2). \end{array} \tag{73}$$

The coefficients c_i in the chiral representation are written by the effective couplings of ChPT, while the $\overline{p}_i$ are experimentally determined but the scattering lengths a_0^0, a_0^2 are unknown constants. From the above relations eq.(73) we can determine the scattering lengths

in terms of the coefficients c_i. In order to determine the scattering lengths, Colangelo *et al.* [25] defined the quantities

$$C_1 \equiv f_\pi^2 \left(c_2 + 4m_\pi^2(c_3 - c_4)\right), \quad C_2 \equiv \frac{f_\pi^2}{m_\pi^2}\left(-c_1 + 4m_\pi^4(c_3 - c_4)\right). \tag{74}$$

These combinations include only two effective couplings $\bar{l}_3, \bar{l}_4$ up to the one loop order [25],

$$C_1 = 1 + \xi\left(2\bar{l}_4 - \frac{887}{420}\right) + O(\xi^2), \quad C_2 = 1 + \xi\left(\frac{\bar{l}_3}{2} + 2\bar{l}_4 - \frac{18}{7}\right) + O(\xi^2), \tag{75}$$

where $\xi = (m_\pi/4\pi f_\pi)^2$. Substituting c_i in eq.(73) into C_1 and C_2, one finds the relation for the scattering lengths,

$$a_0^0 m_\pi = \frac{7m_\pi^2}{32\pi f_\pi^2}C_0 - \left(\frac{5}{32\pi}\overline{p}_1 + \frac{3m_\pi^2}{8\pi}\overline{p}_2 + \frac{3m_\pi^4}{4}(\overline{p}_3 - \overline{p}_4)\right) + O(\xi^2), \tag{76}$$

$$a_0^2 m_\pi = -\frac{m_\pi^2}{16\pi f_\pi^2}C_2 - \left(\frac{1}{16\pi}\overline{p}_1 - \frac{m_\pi^4}{4}(\overline{p}_3 - \overline{p}_4)\right) + O(\xi^2), \tag{77}$$

where C_0 is given by the following combination,

$$C_0 = \frac{1}{7}(12C_1 - 5C_2). \tag{78}$$

It is noted that the relation for the scattering lengths are different from the expression of ChPT at two loop eq.(49), because this form includes the phenomenological coefficients $\overline{p}_i$.

The four variables $a_0^0, a_0^2, \bar{l}_1$ and $\bar{l}_2$ can be determined through the coefficients $\overline{p}_1, \cdots, \overline{p}_4$, when $\bar{l}_3, \bar{l}_4$ and the coupling constants $r_1, \cdots, r_4$ from $\mathcal{L}_6$ are treated as known. Colangelo *et al.* [25] obtained the following results for the scattering lengths,

$$a_0^0 m_\pi = 0.220 \pm 0.05 \tag{79}$$

$$a_0^2 m_\pi = -0.0444 \pm 0.0010. \tag{80}$$

While $\bar{l}_4$ is strongly constrained by the experimental data of the scalar radius eq.(51), $\bar{l}_3$ is not strongly constrained as shown eq.(50). Hence both scattering lengths are approximately controlled by $\bar{l}_3$. This causes the correlation between the scattering lengths. From the correlation a_0^2 can be determined as a function of a_0^0 [25],

$$a_0^2 m_\pi = -0.0444 \pm 0.0008 + 0.236\Delta_0 - 0.61\Delta_0^2 - 9.9\Delta_0^3, \tag{81}$$

where $\Delta_0 = a_0^0 m_\pi - 0.22$.

The scattering phase shifts for $I = 0, 1$ and 2 were also obtained from the framework of the two representations. The results are displayed in Fig. 2. In the figures the central curves are described by the simple parametrization of the phase shift eq.(17) given by,

$$\tan\delta_l^I = \sqrt{1 - \frac{4m_\pi^2}{s}}\frac{p^{2l}}{m_\pi^{2l}}\left\{A_l^I + B_l^I\frac{p^2}{m_\pi^2} + C_l^I\frac{p^4}{m_\pi^4} + D_l^I\frac{p^6}{m_\pi^6}\right\}\left(\frac{4m_\pi^2 - s_l^I}{s - s_l^I}\right), \tag{82}$$

where $s = 4(m_\pi^2 + p^2)$. The values of the coefficients are tabulated in following,

$$\begin{array}{lll} A_0^0 = 0.220, & A_1^1 = 0.379 \cdot 10^{-1}, & A_0^2 = -0.444 \cdot 10^{-1}, \\ B_0^0 = 0.268, & B_1^1 = 0.140 \cdot 10^{-4}, & B_0^2 = -0.857 \cdot 10^{-1}, \\ C_0^0 = -0.139 \cdot 10^{-1}, & C_1^1 = -0.673 \cdot 10^{-4}, & C_0^2 = -0.221 \cdot 10^{-2}, \\ D_0^0 = -0.139 \cdot 10^{-2}, & D_1^1 = 0.163 \cdot 10^{-7}, & D_0^2 = -0.129 \cdot 10^{-3}. \end{array} \tag{83}$$

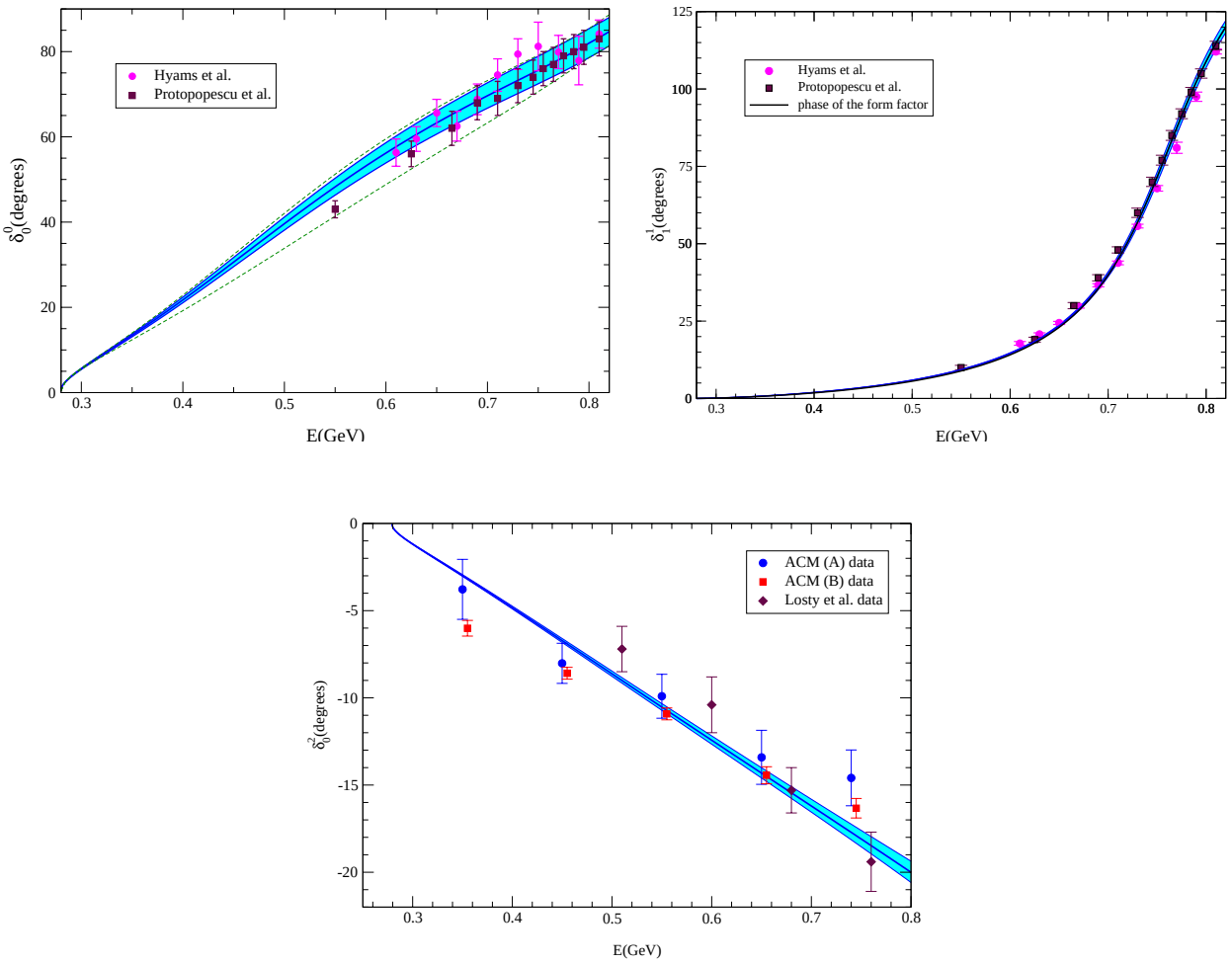

Figure 2: Scattering phase shift in $I = 0, 1, 2$ channels obtained from analysis with chiral and phenomenological representations [25]. Solid lines are center value, and shaded regions correspond to uncertainties. In the δ_0^0 figure dotted lines indicate region allowed if constrains imposed by chiral symmetry are ignored [40].

The constants A_0^0 and A_0^2 show the scattering lengths $a_l^I m_\pi$ for each isospin. The parameters s_l^I specify the value of s where δ_l^I passes through $90°$, and are given by,

$$s_0^0 = 36.77 m_\pi^2, \quad s_1^1 = 30.72 m_\pi^2, \quad s_0^2 = -21.62 m_\pi^2. \tag{84}$$

The corresponding energies for $I = 0, 1$ are 846 MeV and 774 MeV, respectively. In the $I = 2$ channel there are no such resonance particles, so that an exotic negative s_0^2 is applied. These results are compared with the experimental data, which are given by Hyams *et al.* [38], Protopopescu *et al.* [39], Hoogland *et al.*(ACM) [23] and Losty *et al.* [24].

In our analysis these results for the scattering length a_0^2 and the scattering phase shift δ_0^2 are referred for comparing with our results. In the following we call them the predictions of ChPT.

2.2 Experimental results

For the determination of the scattering lengths, because of the experimental intractability of a direct determination of the $\pi\pi$ scattering lengths through measurements of $\pi\pi$ scattering, indirect techniques have been utilized. The reactions that have been most extensively investigated include the K_{e4} K meson decays ($K^+ \to \pi^+\pi^- e^+\nu_e$) which are sensitive to the isospin $I = 0$ with angular momentum $l = 0$ scattering length a_0^0, and pion-induced pion production reactions such as ($\pi p \to \pi\pi n$) which are sensitive to both the $I = 0, 2$ scattering lengths a_0^0 and a_0^2. An interesting experiment have begun, which is based on the fact that $\pi^+\pi^-$ atoms decay into a pair of neutral pions, through the strong transition $\pi^+\pi^- \to \pi^0\pi^0$. The experiment is sensitive to the difference $a_0^0 - a_0^2$.

We list the properties and the recent results for each experiment in the following.

2.2.1 K_{e4} decay

Among the long list of possible charged K meson decay the rare K_{e4} decay $K^\pm \to \pi^+\pi^- e^\pm \nu_e(\overline{\nu}_e)$ has received particular attention because it could provide important information on the structure of the weak hadronic currents and also on $\pi\pi$ scattering at low energies. What made this four-body semileptonic decay attractive despite its low branching ratio, which is of order 10^{-5}, is that the two pions are the only hadrons in the final states. Thus experimental studies of the K_{e4} decay are seen as the cleanest method to determine a_0^0. The phase shift difference $\delta_0^0 - \delta_1^1$ could be extracted from the experiments. The experiments of the K meson decay have been carried out assuming that the $\Delta I = 1/2$ rule suppresses the $I = 2$ and $l = 0$ partial wave.

The Geneva-Saclay Collaboration [41] gathered about 30,000 events, and provided its final results in 1977. The results are the often quoted values $a_0^0 m_\pi = 0.26(5)$ and $a_0^2 m_\pi = -0.028(12)$ [42, 43].

Recently a new measurement has been published by the E865 Collaboration [44] at Brookhaven who collected 400,000 K_{e4} events, and the statistics improved by more than a factor of 10. From the analysis [45] the scattering lengths are reported with a smaller uncertainty

$$a_0^0 m_\pi = 0.216 \pm 0.013 \pm 0.004 \pm 0.002, \tag{85}$$

$$a_0^2 m_\pi = -0.0454 \pm 0.0031 \pm 0.0010 \pm 0.0008, \tag{86}$$

where the first, second and third errors correspond to statistical, systematic and theoretical errors, respectively. The $a_0^2 m_\pi$ is determined by the correlation between a_0^2 and a_0^0 eq.(81) [25].

Similar experiments are proposed by the NA48 Collaboration at CERN[46] and the KLOE Collaboration at DAΦNE[47].

2.2.2 $(\pi, 2\pi)$ reaction

The $A\pi \to A'2\pi$ reactions are sensitive to $\pi\pi$ scattering because one pion exchange is dominant mechanism, although additional sizable backgrounds from other processes also contribute. There is least one other hadron present in the final state. However, the experiment is sensitive to both the $I = 0, 2$ S-wave scattering lengths a_0^0 and a_0^2. The $\pi^- p \to \pi^-\pi^+ n$ reaction involves both the $I = 0, 2$ $\pi\pi$ interaction amplitudes, while the $\pi^+ p \to \pi^+\pi^+ n$ reaction involves only $I = 2$.

In 1974, Aachen-Cern-Munich Collaboration [23] reported an experiment on the $\pi^+ p \to \pi^+\pi^+ n$ reaction and Losty *et al.* [24] on the $\pi^- p \to \Delta^{++}\pi^-\pi^-$ reaction. Both collaborations

focused on the $I = 2$ channel. In 1978, Kravtsov *et al.* [48] obtained information on the $\pi^+ p \to \pi^+\pi^+ n$ reaction from measurements of the charge symmetric reaction extracted from the more complex $\pi^- d \to \pi^-\pi^- pp$ reaction. In 1989, Sevior *et al.* [49] determined the energy dependence of the total cross section for $\pi^+ p \to \pi^+\pi^+ n$ reaction in the threshold region. They provided better data for evaluating the $I = 2$ scattering length,

$$a_0^2 m_\pi = -0.040 \pm 0.001 \pm 0.003. \tag{87}$$

At the same time the OMICRON Collaboration [50] reported the result that is in disagreement with the results of Kravtsov *et al.* and Sevior *et al.* near the threshold.

Recently the experiment on $\pi^- p \to \pi^-\pi^+ n$ and $\pi^+ p \to \pi^+\pi^+ n$ reactions were reported by Lange *et al.* [51]. They obtained the $I = 0, 2$ scattering length,

$$a_0^0 m_\pi = 0.23 \pm 0.08, \tag{88}$$

$$a_0^2 m_\pi = -0.031 \pm 0.008. \tag{89}$$

The CHAOS Collaboration [52] proposed a similar experiment on the $\pi^+ A \to \pi^+\pi^\pm A'$ reactions for several nuclei.

2.2.3 Lifetime of $\pi^+\pi^-$ atom

An experiment is under way by the DIRAC Collaboration [53] at CERN, which is based on the fact that $\pi^+\pi^-$ atoms decay into a pair of neutral pions, through the strong transition $\pi^+\pi^- \to \pi^0\pi^0$. Since the momentum transfer nearly vanishes, only the scattering lengths are relevant. The ground state lifetime τ is related to the $I = 0, 2$ S-wave scattering length difference [54]

$$\frac{1}{\tau} = \frac{2}{9}\alpha^3 \sqrt{m_\pi^2 - m_{\pi^0}^2 - \alpha^2 m_\pi^2/4}\,|a_0^0 - a_0^2|^2 (1 + \delta), \tag{90}$$

where α is the fine structure constant, m_π the mass of the charged pion, m_{π^0} the mass of neutral pion and δ the next-to-leading order correction ($\delta = 0.058$). The DIRAC Collaboration reported recently a preliminary result,

$$\tau = (3.1^{+0.9}_{-0.7} \pm 1.0) \times 10^{-15} s, \tag{91}$$

where the first and second error correspond to the statistical and a rough estimated systematic errors, respectively.

3 Lattice QCD

In this section we describe formulations of lattice QCD. We also introduce improvements of action which are employed in this work.

3.1 Standard action

3.1.1 Gauge action

On the lattice the gauge action is constructed by the link variable $U_{x,\mu} \equiv e^{iagA_\mu(x)}$ where a is the lattice spacing, g is the bare coupling and $A_\mu(x)$ is the gauge field. The simplest gauge invariant quantity constructed by the links is 1×1 Wilson loop "plaquette",

$$P_{\mu\nu}(x) = \mathrm{Tr}[U_{x,\mu}U_{x+\hat{\mu},\nu}U^\dagger_{x+\hat{\nu},\mu}U^\dagger_{x,\nu}]. \tag{92}$$

Here $\hat{\mu}$ denotes a unit vector in μ-direction. Using the plaquette the standard action S_g is given by

$$S_g = \beta \sum_{x,\mu>\nu} \left(1 - \frac{1}{3}\mathrm{Re}\left[P_{\mu\nu}(x)\right]\right). \tag{93}$$

Since in the continuum limit $a \to 0$, the S_g should reconstruct the continuum gauge action in Euclidean space-time,

$$S_g \overset{a\to 0}{\to} \frac{1}{4}\int d^4x F_{\mu\nu,c}F_{\mu\nu,c} + O(a^2), \quad F_{\mu\nu,c} = \partial_\mu A_\nu - \partial_\nu A_\mu + ig[A_\mu, A_\nu]. \tag{94}$$

The coefficient β in eq.(93) is determined by the normalization in the continuum limit as $\beta = 6/g^2$.

3.1.2 Quark action

In the free case the quark action is constructed in terms of the quark field ψ_x as,

$$S_q^{\mathrm{naive}} = \sum_{x,y} \overline{\psi}_x D^{\mathrm{naive}}_{x,y}\psi_y, \tag{95}$$

where

$$D^{\mathrm{naive}}_{x,y} = \frac{1}{2a}\sum_\mu \gamma_\mu \left[\delta_{x+\hat{\mu},y} - \delta_{x,y+\hat{\mu}}\right] + m\delta_{x,y}. \tag{96}$$

This action is called the naive quark action. In the continuum limit S_q^{naive} reconstructs the continuum quark action in Euclidean space-time,

$$S_q^{\mathrm{naive}} \overset{a\to 0}{\to} \int d^4x \overline{\psi}(x)\left(\partial_\mu\gamma_\mu + m\right)\psi(x) + O(a^2). \tag{97}$$

However, the action produces a physical pole and unphysical fifteen poles in the free quark propagator. This is the well-known doubling problem.

To avoid the problem Wilson [55] proposed to add a Laplacean term, which is called the Wilson term, as,

$$S_q^W = S_q^{\mathrm{naive}} - a\frac{r}{2}\overline{\psi}_x \Box_{x,y}\psi_y, \tag{98}$$

where r is the Wilson coefficient usually chosen as $r = 1$, and the Laplacean $\Box_{x,y}$ is given by

$$\Box_{x,y} = \sum_{\mu} \frac{1}{a^2} \left(\delta_{x+\hat{\mu},y} + \delta_{x,y+\hat{\mu}} - 2\delta_{x,y} \right). \tag{99}$$

This term breaks chiral symmetry even when $m = 0$ at a finite lattice spacing. However, the unphysical poles decouple from the physical one, since their masses diverge in the continuum limit. This action is called Wilson quark action. In actual calculations the quark field is rescaled by

$$\psi \to \sqrt{2\kappa} a^{-3/2} \psi \quad \text{where} \quad \kappa = \frac{1}{2ma + 8} \text{ with } r = 1, \tag{100}$$

for simplicity.

Gauge symmetry requires that the quark bilinear fields $\overline{\psi}_x \psi_{x+\hat{\mu}}$ should be connect by the link variable as

$$\overline{\psi}_x \psi_{x+\hat{\mu}} \to \overline{\psi}_x U_{x,\mu} \psi_{x+\hat{\mu}}. \tag{101}$$

Considering the connection and the normalization eq.(100), Wilson action with interaction is written by

$$\begin{aligned} S_q^W &= \sum_{x,y} \overline{\psi}_x D^W_{x,y} \psi_y, \\ D^W_{x,y} &= \delta_{x,y} - \kappa \sum_{\mu} \left\{ (1-\gamma_\mu) U_{\mu,x} \delta_{x+\hat{\mu},y} + (1+\gamma_\mu) U^\dagger_{x,\mu} \delta_{x,y+\hat{\mu}}) \right\}. \end{aligned} \tag{102}$$

Here κ is called hopping parameter. The quark mass is then defined by

$$ma = \frac{1}{2} \left(\frac{1}{\kappa} - \frac{1}{\kappa_c} \right), \tag{103}$$

where $\kappa_c = 1/8 + O(g^2)$. The Wilson action deviates from the continuum action by $O(a)$ due to the Wilson term.

3.2 Continuum limit

Lattice QCD allows construction of the continuum theory of QCD in the continuum limit. In order to compare a physical quantity calculated in lattice QCD with the experimental value, we need the continuum extrapolation. The extrapolation requires calculations at several different lattice spacings. The lattice spacing a is a function of the bare coupling g^2. From the renormalization group argument, the relation between a and g^2 is given by

$$a\Lambda_{\rm L} = (\beta_0 g^2)^{-\beta_1/2\beta_0^2} e^{-1/2\beta_0 g^2}, \quad g^2 \to 0. \tag{104}$$

Here $\Lambda_{\rm L}$ is a scale and β_i for $i = 0, 1$ are defined by

$$\beta_0 = \frac{1}{(4\pi^2)} \left(11 - \frac{2}{3} N_f \right), \quad \beta_1 = \frac{1}{(4\pi)^4} \left(102 - \frac{38}{3} N_f \right), \tag{105}$$

where N_f is the number of quark flavor. Therefore the continuum limit $a \to 0$ is understood as $g^2 \to 0$ or $\beta \to \infty$.

3.3 Improvement

In order to extract physical quantities near the continuum limit from calculations carried out at coarse lattice spacings, some improvement methods of the action have been proposed. Since the lattice action reproduces the continuum action in the continuum limit, one can add higher order terms of the lattice spacing to the standard lattice actions eqs.(93) and (102), to reduce effects of a finite lattice spacing. In this section we present the improvement methods employed in this work.

3.3.1 Renormalization group improvement

In principle we can add infinite terms with dimensional couplings to the lattice action, since such actions reproduce the same continuum physics as the standard action eq.(93). From the renormalization group argument, there is the renormalized trajectory (RT) in infinite dimensional coupling parameter space. The actions on the RT, which are called perfect action, give the same physics at the continuum limit. If an infinite number of coupling parameters are admitted, a perfect action is achieved. But such the action is not acceptable for numerical calculations. It is necessary to truncate the action to a small numbers of couplings.

Iwasaki [56] applied the block spin renormalization group analysis in perturbation theory to survey the parameter space, and proposed a renormalization group gauge improved action which adds only one term to the standard action eq.(93). This improved action is written in terms of the parts of the 1×1 and 1×2 Wilson loops $W_{\mu\nu}^{1\times 1}$ and $W_{\mu\nu}^{1\times 2}$,

$$S_g^{\mathrm{RG}} = \frac{\beta}{6}\left(c_0 \sum_{x,\mu<\nu} W_{\mu\nu}^{1\times 1}(x) + c_1 \sum_{x,\mu,\nu} W_{\mu\nu}^{1\times 2}(x) \right). \tag{106}$$

The coefficient $c_1 = -0.331$ is fixed by the block spin renormalization group analysis, and $c_0 = 1 - 8c_1 = 3.648$ by the normalization condition in the continuum limit.

3.3.2 Clover action

The Wilson action deviates from the continuum quark action by $O(a)$ due to the Wilson term in eq.(98). Sheikholeslami and Wohlert [57] proposed an improved quark action, which is called SW/clover quark action, to reduce $O(a)$ errors for on-shell quantities without spoiling Wilson's resolution of doublers. The clover quark action is constructed by the quark bilinear fields which are invariant under gauge, discrete rotations, parity and charge conjugation transformations. The explicit form of the action is written by the Wilson quark action and the clover term with a coefficient c_{SW} as,

$$S_q^{\mathrm{SW}} \;=\; S_q^W - c_{\mathrm{SW}}\kappa \sum_{x,\mu<\nu} \overline{\psi}_x \sigma_{\mu\nu} F_{\mu\nu} \psi_x, \tag{107}$$

where κ is the hopping parameter and $F_{\mu\nu}$ is the standard lattice discretization of the field strength. At tree level Sheikholeslami and Wohlert [57] derived $c_{\mathrm{SW}} = 1$. Tuning the clover coefficient c_{SW} appropriately, one can reduce the discretization error for the on-shell quantities.

3.3.3 Tadpole improvement

The expansion of the link variable is given by

$$U_{x,\mu} = e^{iagA_\mu(x)} = 1 + iagA_\mu(x) - \frac{a^2g^2}{2}A_\mu^2(x) + \cdots. \tag{108}$$

The first two terms contribute to the continuum action, but other higher terms are lattice artifacts. On a finite lattice spacing, the third term in eq.(108) gives rise to the tadpole diagram. Since the diagram generates ultraviolet divergence $O(1/a^2)$ that is canceled out by the coefficient factor a^2, the contribution is suppressed by powers of only g^2. This causes a poor match between short distance quantities and their perturbative estimates, and large coefficients in the perturbative lattice expansions.

To avoid the difficulties, Lepage and Mackenzie [58] proposed tadpole improvement, which replaces the link variable by its mean value u_0 and fluctuation $\tilde{U}$,

$$U_{x,\mu} \to u_0 \tilde{U}_{x,\mu}. \tag{109}$$

The u_0 is almost dominated by the tadpole contribution. This rescaling of all links by $u_0 < 1$ keeps the theory gauge invariant. Under this rescaling the bare coupling in the standard gauge action eq.(93) is replaced by

$$\beta \to \tilde{\beta} \equiv \beta u_0^4, \quad \text{or} \quad g^2 \to \tilde{g}^2 \equiv g^2/u_0^4, \tag{110}$$

to keep the original form of the action. For the clover action eq.(107) the rescaling keeping the action of the same form corresponds to

$$\kappa \to \tilde{\kappa} \equiv \kappa u_0, \quad c_{\rm SW} \to \tilde{c}_{\rm SW} \equiv c_{\rm SW} u_0^3. \tag{111}$$

At tree level the tadpole improved clover coefficient gives

$$\tilde{c}_{\rm SW} = 1 \quad \text{corresponding to} \quad c_{\rm SW} = 1/u_0^3. \tag{112}$$

This choice of $c_{\rm SW}$ is called tadpole (a mean field) improved choice.

There are two choices of the tadpole factor u_0. The first is that the fourth root of the plaquette value $P^{1/4}$, and the second is that the expectation value of the link in Landau gauge. In this work we employ the first choice.

4 Previous results for $\pi\pi$ scattering

In this section we review the results of the previous lattice calculations for the S-wave $\pi\pi$ scattering. We describe several results of the scattering length for the isospin $I = 0, 2$ channels. We then present the two pioneering results for the $I = 2$ $\pi\pi$ scattering phase shift, one used the effective potential [18], and the other calculated directly [19] through the finite volume method proposed by Lüscher [5, 6]. All previous works employed quenched approximation.

4.1 Scattering length

Kuramashi *et al.* [12] calculated the scattering length in $I = 0, 2$ channels. Since the $I = 0$ scattering length is much more difficult due to the presence of box and disconnected contributions, there have been no other calculations of the $I = 0$ channel so far. The calculation was carried out using the standard gauge action. For quark action they used the Kogut-Susskind quark action, which has U(1) axial symmetry, and Wilson quark action described in Sec. 3.1.2. As shown in Fig. 3 they compared the dimensionless ratio $32\pi(f_\pi^{lat})^2/m_\pi \cdot a_0^I$ for $I = 0, 2$, where f_π^{lat} is measured for each pion mass on the lattice, with the prediction of current algebra eq.(1),

$$\frac{32\pi f_\pi^2}{m_\pi} a_0^0 = 7, \quad \frac{32\pi f_\pi^2}{m_\pi} a_0^2 = -2, \tag{113}$$

where a_l^I is the scattering length for isospin I with angular momentum l, and $f_\pi = 93$ MeV. In the figure the $I = 2$ results of Refs. [11, 12] with Wilson and Kogut-Susskind quark actions are also plotted. They observed an agreement of lattice results with current algebra predictions up to quite heavy quark masses ($m_\pi/m_\rho \approx 0.7$–0.8) for both $I = 0$ and 2 channels.

The most recent calculation was carried out by BGR Collaboration [17]. They explored the calculation of $I = 2$ scattering length in small pion mass region, $m_\pi/m_\rho \approx 0.35$ and $m_\pi \approx 0.3$ GeV, with fixed point gauge action [59] and chirality improved quark action [60]. The calculation was carried out on three physical volumes, $L \approx 1.2, 1.8$ and 2.4 fm. Cutoff effects were studied in smaller volumes with several lattice spacings. Their results are compared with the results of other groups and the prediction for the mass dependence of the quenched ChPT, as shown in Fig. 4. It was pointed out by Barnard and Golterman [21], and by Colangelo and Pallante [22], that the scattering length a_0/m_π in quenched theory diverges as δ^2/m_π^2 in the chiral limit. From the figure BGR Collaboration concluded that the effect of the δ^2/m_π^2 term is still not entirely visible at the pion mass region they examined.

JLQCD Collaboration [14] and Liu *et al.* [15] obtained the $I = 2$ scattering length in the continuum limit. JLQCD Collaboration employed the standard gauge action and Wilson quark action at $\beta = 5.9, 6.1$ and 6.3, corresponding to the lattice spacings $a \approx 0.10, 0.07$ and 0.06 fm. Since the relation of the energy shift and the pion four-point function is not simple due to effects from intermediate off-shell two-pion states [11] and quenching effects [21], they used several analyses to extract the energy shift which is related to the scattering length through the finite volume formula [5, 6]. The continuum extrapolations for the two results are shown in Fig. 5. The figure shows that the difference of the results vanishes in the continuum limit.

Liu *et al.* [15] calculated with a tadpole improved gauge and clover quark actions on

coarse anisotropic lattice. The spatial lattice spacing is roughly between 0.18 and 0.39 fm where the physical size of the lattice range from 0.7 to 3.2 fm. They extrapolated the dimensionless combination $a_0 m_\rho^2/m_\pi$ to the physical pion mass and the infinite volume. It was argued in Refs [11, 13, 21] that in a quenched calculation the form of the finite volume formula is invalidated. Therefore they carried out two infinite volume extrapolations calling them scheme I (extrapolating according to $1/L^3$) and scheme II (extrapolating according to $1/L^2$), respectively. The continuum extrapolations of these results are also shown in Fig. 5. The results for both schemes are consistent in the continuum limit.

We summarize the result of the $I = 2$ scattering length in the continuum limit as follows. JLQCD Collaboration obtained the results as,

$$a_0 m_\pi = \begin{cases} -0.0409(68)\ (\mathbf{Exp}) \\ -0.0405(47)\ (\mathbf{Lin}) \end{cases} , \tag{114}$$

where (**Exp**) and (**Lin**) corresponds to those in Fig. 5, and Liu *et al.* obtained,

$$a_0 m_\pi = \begin{cases} -0.0342(75)\ (\text{scheme I}) \\ -0.0459(91)\ (\text{schem II}) \end{cases} . \tag{115}$$

All results are consistent with the prediction of ChPT [25],

$$a_0 m_\pi = -0.0444(10). \tag{116}$$

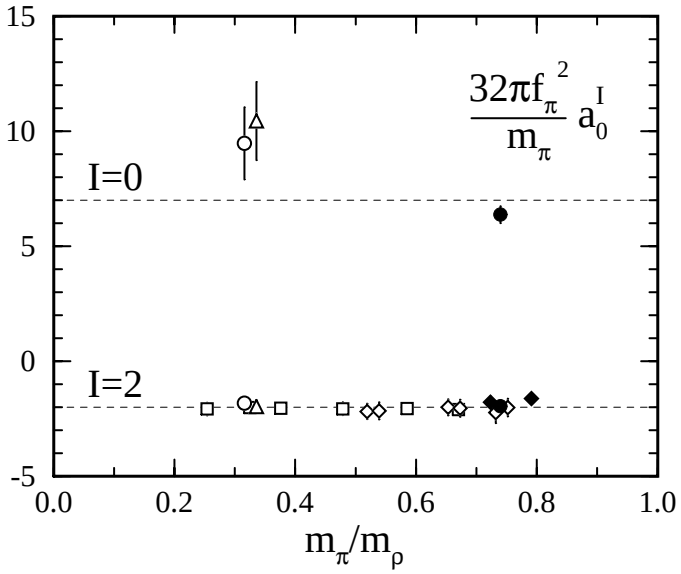

Figure 3: $I = 0$ and 2 S-wave $\pi\pi$ scattering lengths a_0^I from Ref. [13]. Closed and open symbols denote Wilson and Kogut-Susskind results. Triangles are the results with Coulomb gauge fixing. Squares and diamonds for $I = 2$ are the results from Refs. [11, 12]. Dotted lines indicated predictions of current algebra eq.(113).

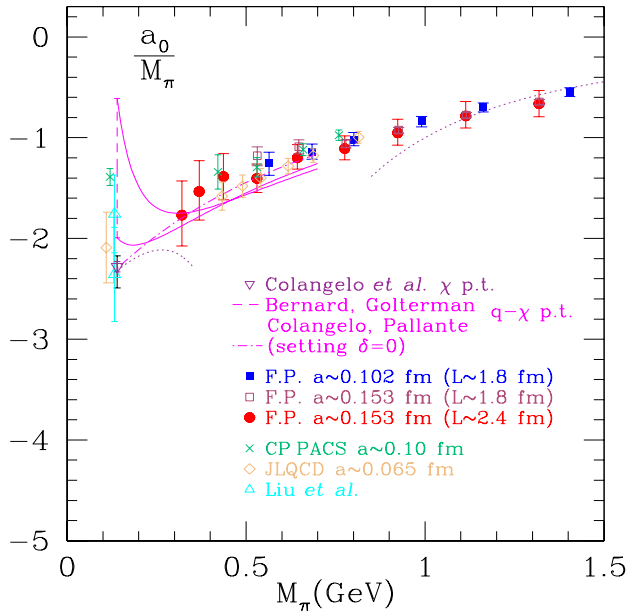

Figure 4: Results of the isospin $I = 2$ scattering length a_0/m_π GeV^{-2} for BGR Collaboration [17] and other groups. The down triangle is the prediction of ChPT [25]. The spread in the quenched ChPT calculation [21, 22] corresponds to the range $0.10 < \delta < 0.20$. The cross, diamond and up triangle symbols denote the results of CP-PACS [19], JLQCD Collaborations [14] and Liu *et al.* [15].

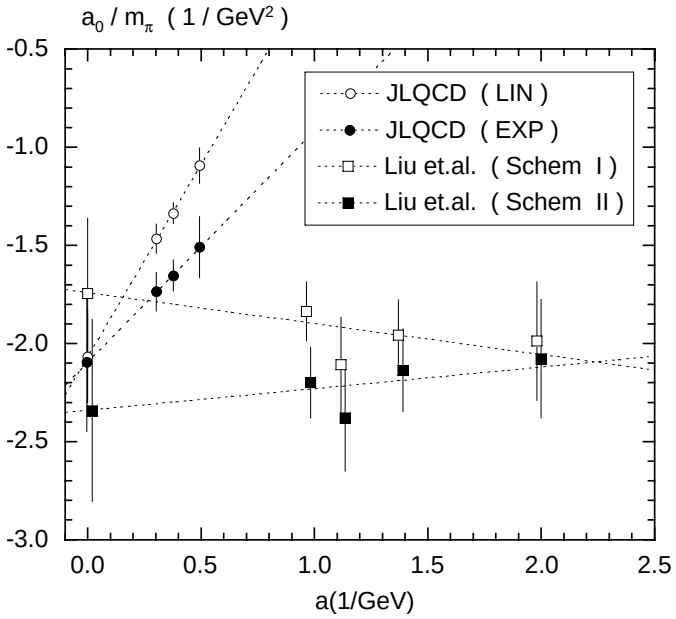

Figure 5: Continuum extrapolation for the isospin $I = 2$ scattering length a_0/m_π GeV^{-2} obtained by JLQCD Collaboration [14] and Liu *et al.* [15]. Data denoted by JLQCD (LIN) and JLQCD (EXP) were extracted by different analyses. Difference of Scheme I and II is also analysis method.

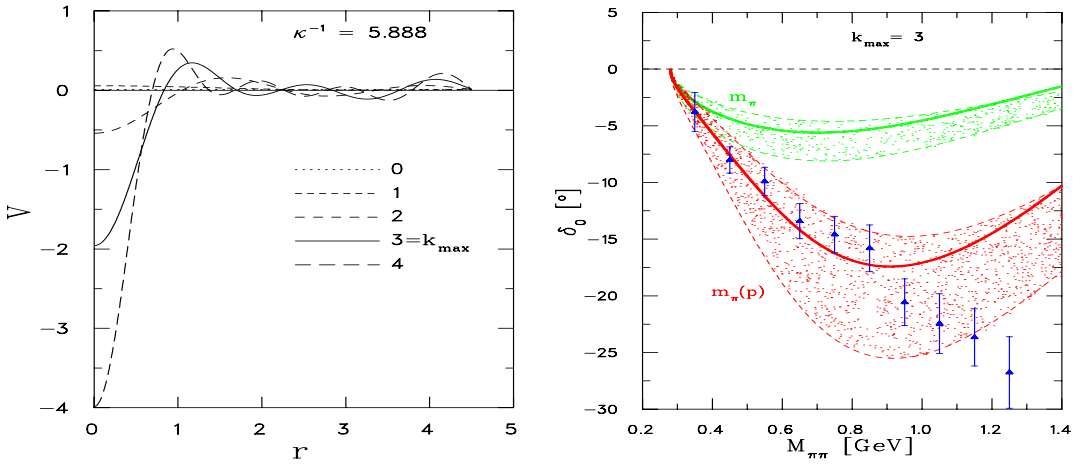

Figure 6: Effective potential (left figure) of the isospin $I = 2$ $\pi\pi$ scattering, and phase shift (right figure) evaluated by the potential [18]. The k_{max} denotes energy state cut-off. In order to estimate error of non-relativistic potential, they compared phase shifts estimated with m_π and $m_\pi(p) = \sqrt{m_\pi^2 + p^2}$. Triangle symbols in right figure are experiment [23].

4.2 Scattering phase shift

Fiebig *et al.* [18] and CP-PACS Collaboration [19] carried out a pioneering study for the $I = 2$ $\pi\pi$ scattering phase shift. Fiebig *et al.* used effective potential for $\pi\pi$ scattering, and CP-PACS Collaboration employed finite volume method in the center of mass system which is described in Sec. 5.1.

4.2.1 Effective potential

Fiebig *et al.* [18] estimated the phase shift through the effective potential of $\pi\pi$ scattering obtained from the pion four-point function. The simulation was carried out with a tree level $O(a)$ tadpole improved action in quenched approximation. The lattice size $L^3 \times T$ employed was $9^3 \times 13$, and the lattice spacing was about 0.4 fm.

An example of the obtained effective potential is shown in Fig. 6. The $k_{\max}$ in the figure is the cut-off of the energy state. The short distance region $r < 1$ for $k_{\max} \geq 2$ is an attractive potential. Since the experiment shows that the $I = 2$ $\pi\pi$ scattering is repulsive, this is a strange result. A possible reason of the behavior is that they employed a naive single exponential fit for the extraction of the two-pion energy even for higher states. They evaluated the potential from Fourier transformation of two-pion energy. As mentioned in Sec. 1 there is a difficulty to extract the two-pion energy for higher states, so that one needs some method, such as the diagonalization method described in Sec. 6.1, to solve the difficulty. Their results for $k_{\max} \geq 2$ may include such a higher state effect.

They estimated the scattering phase shift from the effective potential. The result obtained with $k_{\max} = 3$ is shown in Fig. 6. The upper solid curve is evaluated with the physical reduced mass of $m_\pi/2$. In order to estimate the magnitude of the error due to the non-relativistic potential scattering theory they used the relativistic dispersion relation $m_\pi(p) = \sqrt{m_\pi^2 + p^2}$. This result is also plotted in the figure. The results were compared with the experimental result [23]. As well as the effective potential, the phase shift in the high energy region (small distance region) has a strange behavior.

4.2.2 Finite volume method

CP-PACS Collaboration [19] carried out a direct calculation for the phase shift at one lattice spacing ($\beta = 5.90$), and three physical volumes of about 2.4, 3.2 and 4.8 fm. The collaboration used the standard gauge and Wilson quark actions. They employed the diagonalization method [7] to extract the energy shift for the momentum excited states, and the finite volume method in the center of mass system [5, 6] to obtain the scattering phase shift from the energy shift. These finite volume and diagonalization methods are described in Sec. 5.1 and Sec. 6.1, respectively. This is the first study to apply the finite volume method to lattice QCD.

The result for the phase shift $\delta(p)$ at the physical pion mass $m_\pi = 0.14$ GeV is shown in Fig. 7. In the figure the experimental data [23, 24] and the curve [25] parametrized by experimental input are also presented. The values of the phase shift at several momenta are tabulated in Table I.

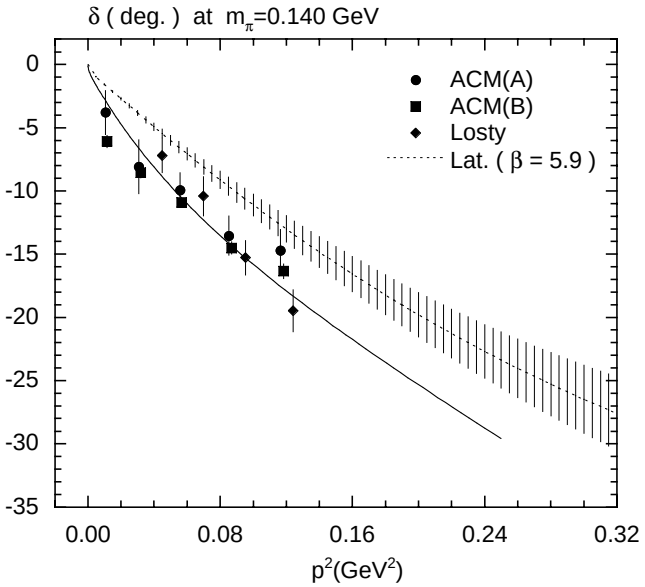

Figure 7: Scattering phase shift in the isospin $I = 2$ system obtained by CP-PACS Collaboration [19]. The symbols, ACM(A) and ACM(B) [23] and Losty [24], are experimental data. The solid curve [25] is parametrized by the experimental inputs.

p^2 [GeV^2]	$\sqrt{s}$ [GeV]	$\delta(p)$ [deg.]
0.02	0.40	-2.71(12)
0.07	0.60	-8.09(59)
0.14	0.80	-14.8(12)
0.23	1.00	-22.0(20)
0.34	1.20	-28.6(31)

Table I: Result for the isospin $I = 2$ $\pi\pi$ scattering phase shift [19] at the physical pion mass $m_\pi = 0.14$ GeV.

5 Finite volume method

We describe here the finite volume method proposed by Lüscher [5, 6] in the center of mass system, and its extension proposed by Rummukainen and Gottlieb [8] in general systems, where the total momentum of two particles is not constrained. The method relates the scattering phase shift in the infinite volume to the two-particle energy on a finite volume with periodic boundary condition. Lüscher derived the method in the center of mass system by the framework of all orders perturbation theory, and the two-particle wave function. Rummukainen and Gottlieb extended the discussion of the wave function to general systems. We explain both methods from the discussion of the wave function. Here we focus only on a scattering of two spinless bosons, such as pions.

5.1 Center of mass system

At first Lüscher derived the finite volume formula in quantum mechanics, and later he discussed the extension of quantum field theory. We describe here the derivation only in quantum mechanics, and a brief discussion of the extension.

5.1.1 Wave function in a box

We now consider that two particles are enclosed in a box of size L^3 with the periodic boundary conditions, and the total momentum of two particles is zero. The states are described by wave function $\psi(\mathbf{r})$ satisfying

$$\psi(\mathbf{r} + \mathbf{n}L) = \psi(\mathbf{r}) \quad \text{for all } \mathbf{n} \in Z^3. \tag{117}$$

Here $\mathbf{r}$ is the relative coordinate of two particles. The symmetry of the two spinless bosons constrains the wave function as $\psi(\mathbf{r}) = \psi(-\mathbf{r})$. The Hamiltonian operator, defined by

$$H = -\frac{1}{2\mu}\nabla^2 + V_{\text{p.b.}}(r), \quad V_{\text{p.b.}}(r) = \sum_{\mathbf{n}\in Z^3} V(|\mathbf{r} + \mathbf{n}L|), \tag{118}$$

takes into account interactions "around the world" and thus respects the periodicity of the wave functions. Here $r = |\mathbf{r}|$ and $\mu = m/2$ is the reduced mass of the system. The potential $V(r)$ is assumed to be effective in a finite range R,

$$V(r) = 0 \quad \text{for} \quad r > R, \tag{119}$$

where $L/2 > R$.

Suppose now that $\psi(\mathbf{r})$ is such an eigenfunction with energy $E = \overline{p}^2/2\mu$,

$$H\psi(\mathbf{r}) = E\psi(\mathbf{r}). \tag{120}$$

The two-particle energy on the finite volume is shifted by $O(1/L^3)$ [5] due to the potential $V(r)$. This means that the momentum is also shifted by $O(1/L^3)$ from $p^2 = (2\pi/L)^2 \cdot n$ where n is an integer. In follows we denote the shifted momentum as $\overline{p}$. In the exterior region $|\mathbf{r} + \mathbf{n}L| > R$ for all $\mathbf{n} \in Z^3$, it is obvious that $\psi(\mathbf{r})$ is a periodic solution of the Helmholtz equation

$$(\nabla^2 + \overline{p}^2)\psi(\mathbf{r}) = 0. \tag{121}$$

It is possible to expand $\psi(\mathbf{r})$ by the spherical harmonics

$$\psi(\mathbf{r}) = \sum_{l=0}^{\infty} \sum_{m=-l}^{l} Y_{lm}(\theta, \phi)\psi_{lm}(r), \tag{122}$$

where $\mathbf{r} = r(\sin\theta\cos\phi, \sin\theta\sin\phi, \cos\theta)$. The expansion is rapidly convergent. Furthermore the spherical components $\psi_{lm}(r)$ are regular solutions of the radial Schrödinger equation

$$\left(\frac{\mathrm{d}^2}{\mathrm{d}r^2} + \frac{2}{r}\frac{\mathrm{d}}{\mathrm{d}r} - \frac{l(l+2)}{r^2} + \overline{p}^2 - 2\mu V_{\mathrm{p.b.}}(r)\right)\psi_{lm}(r) = 0. \tag{123}$$

Since there is only one such solution for fixed $\overline{p}$ and l, $\psi_{lm}(r)$ is a linear combination of the spherical Bessel function $j_l(\overline{p}r)$ and Noeman function $n_l(\overline{p}r)$[1]

$$\psi_{lm}(r) = b_{lm}(\alpha_l(\overline{p})j_l(\overline{p}r) + \beta_l(\overline{p})n_l(\overline{p}r)) \tag{124}$$

for some constants b_{lm} and all $R < r < L/2$. In the limit $\overline{p}r \to 0$ these functions have the asymptotic behaviors as

$$j_l(\overline{p}r) \;\to\; \frac{1}{(2l+1)!!}(\overline{p}r)^l \tag{125}$$

$$n_l(\overline{p}r) \;\to\; (2l-1)!!(\overline{p}r)^{-l-1}. \tag{126}$$

For real $\overline{p} > 0$ and angular momentum l, the associated scattering phase shift $\delta_l(\overline{p})$ is given by

$$\tan\delta_l(\overline{p}) = \frac{\beta_l(\overline{p})}{\alpha_l(\overline{p})}. \tag{127}$$

We introduce an angular momentum cut-off Λ on the interaction. This is a reason that in the actual calculation we cannot consider scattering phase shifts for all angular momenta. A modified Hamiltonian is defined by

$$H_\Lambda = -\frac{1}{2\mu}\nabla^2 + Q_\Lambda V_{\mathrm{p.b.}}(r), \tag{128}$$

where

$$Q_\Lambda\psi(\mathbf{r}) = \sum_{l=0}^{\Lambda} \sum_{m=-l}^{l} Y_{lm}(\theta, \phi)\psi_{lm}(r) \tag{129}$$

denotes the projector on the space of wave functions with angular momenta $l \leq \Lambda$. For all $l \leq \Lambda$, the scattering phases of the modified system are equal to those of the original system, while for all $l > \Lambda$ the scattering phases are equal to zero.

5.1.2 Definition

We consider that a function $\psi(\mathbf{r})$ is called a singular periodic solution of the Helmholtz equation if it has the following properties.

(i)The $\psi(\mathbf{r})$ is a smooth function defined for all $\mathbf{r} \neq 0 \pmod{L}$, and satisfies the Helmholtz equation eq.(121) for some value of $\overline{p}$.

[1]All conventions regarding Legendre polynomials, spherical harmonics and spherical Bessel and Noeman functions are as in Ref. [6]. Another convention of $\psi_{lm}(r)$ is $\psi_{lm}(r) \propto \alpha_l(\overline{p})j_l(\overline{p}r) - \beta_l(\overline{p})n_l(\overline{p}r)$ with $n_0(\overline{p}r) \propto -\cos(\overline{p}r)$.

(ii)The $\psi(\mathbf{r})$ is periodic with period L, in other words it satisfies eq.(117).
(iii)Near the origin, $\psi(\mathbf{r})$ is bounded by a power of $1/r$. That is

$$\sup_{0<r<L/2} |r^{\Lambda+1}\psi(\mathbf{r})| < \infty \tag{130}$$

for some integer Λ.

For values of $\overline{p}$ in the set

$$\overline{p} = \pm\frac{2\pi}{L}|\mathbf{n}| \quad \text{for some } \mathbf{n} \in Z^3, \tag{131}$$

the Helmholtz equation has periodic plane wave solutions, and these tend to complicate the situation. In these cases a different treatment is needed. We do not describe the treatment, while it is discussed in Ref. [6].

From eq.(126) and the condition (iii), We can show that $\psi(\mathbf{r})$ is written by

$$\psi(\mathbf{r}) = \sum_{l=0}^{\Lambda}\sum_{m=-l}^{l} c_{lm}Y_{lm}(\theta,\phi)\overline{p}^{l+1}n_l(\overline{p}r) + \hat{\psi}(\mathbf{r}), \tag{132}$$

where the remainder $\hat{\psi}(\mathbf{r})$ is a smooth solution of the Helmholtz equation in an open neighborhood of the origin $r = 0$.

5.1.3 General solution

Lüscher found that a solution of the Helmholtz equation on the finite periodic box L^3 is given by the Green function

$$G(\mathbf{r};\overline{p}^2) = L^{-3}\sum_{\mathbf{k}} \frac{e^{i\mathbf{k}\cdot\mathbf{r}}}{\mathbf{k}^2 - \overline{p}^2}, \tag{133}$$

where the summation is carried out in $\mathbf{k} = (2\pi/L)\cdot\mathbf{n}$ for some $\mathbf{n} \in Z^3$. The Green function is obviously periodic, and it has the property

$$(\nabla^2 + \overline{p}^2)G(\mathbf{r};\overline{p}^2) = -\sum_{\mathbf{n}\in Z^3}\delta(\mathbf{r}+\mathbf{n}L). \tag{134}$$

To determine the singularity of $G(\mathbf{r};\overline{p}^2)$ at the origin explicitly, first note that

$$(\nabla^2 + \overline{p}^2)n_0(\overline{p}r) = -\frac{4\pi}{\overline{p}}\delta(\mathbf{r}). \tag{135}$$

Using eq.(134) the Green function is written by

$$G(\mathbf{r};\overline{p}^2) = \frac{\overline{p}}{4\pi}n_0(\overline{p}r) + \text{regular part of a function.} \tag{136}$$

Further singular solutions can be generated from the Green function by differentiating with respect to $\mathbf{r}$. This can be achieved by introducing the harmonic polynomials

$$\mathcal{Y}_{lm}(\mathbf{r}) = r^l Y_{lm}(\theta,\phi) \tag{137}$$

and defining

$$G_{lm}(\mathbf{r};\overline{p}^2) = \mathcal{Y}_{lm}(\nabla)G(\mathbf{r};\overline{p}^2). \tag{138}$$

It is trivial that these functions are singular periodic solutions of the Helmholtz equation of degree l.

We determine their singularities precisely. The crucial identity is

$$\mathcal{Y}_{lm}(\nabla)n_0(\overline{p}r) = (-\overline{p})^l Y_{lm}(\theta,\phi)n_l(\overline{p}r), \tag{139}$$

which is described in appendix B of Ref. [6]. From eq.(136) we find that the singular part can be expressed by the spherical Noeman function $n_l(\overline{p}r)$. The regular part is written by a summation of the spherical Bessel function $j_l(\overline{p}r)$, because $j_l(\overline{p}r)$ is regular at the origin. We then conclude that

$$G_{lm}(\mathbf{r};\overline{p}^2) = \frac{(-1)^l}{4\pi}\overline{p}^{l+1}\left\{ Y_{lm}(\theta,\phi)n_l(\overline{p}r) + \sum_{l'=0}^{\infty}\sum_{m'=-l'}^{l'} \mathcal{M}_{lm,l'm'}Y_{l'm'}(\theta,\phi)j_{l'}(\overline{p}r)\right\}. \tag{140}$$

We need the explicit expression of the matrix $\mathcal{M}_{lm,l'm'}$ to obtain the scattering phase. To this end it is useful to start with the simplest case,

$$G(\mathbf{r};\overline{p}^2) = \frac{\overline{p}}{4\pi}n_0(\overline{p}r) + \sum_{l=0}^{\infty}\sum_{m=-l}^{l} g_{lm}Y_{lm}(\theta,\phi)j_l(\overline{p}r). \tag{141}$$

The simple relation between the coefficients g_{lm} and the spherical zeta function $Z_{lm}(s;\overline{n})$, which is discussed in appendix D of Ref. [6], is given by

$$g_{lm} = \frac{i^l}{\pi L\overline{n}^{l/2}}Z_{lm}(1;\overline{n}), \tag{142}$$

where

$$Z_{lm}(s;\overline{n}) = \sum_{\mathbf{n}\in Z^3}\mathcal{Y}_{lm}(\mathbf{n})(\mathbf{n}^2-\overline{n})^{-s}, \tag{143}$$

and $\overline{p}^2 = (L/2\pi)^2\cdot\overline{n}$. The calculation method of $Z_{lm}(1;\overline{n})$ at $l=0$ is explained in appendix C.1.

To obtain the expansion in the spherical harmonics of $G_{lm}(\mathbf{r};\overline{p}^2)$, we apply differential operator $\mathcal{Y}_{lm}(\nabla)$ to the series eq.(141). The action of this operator on the singular term is given by eq.(139). The corresponding identity for the regular terms reads

$$\mathcal{Y}_{lm}(\nabla)Y_{js}(\theta,\phi)j_j(\overline{p}r) = \frac{\overline{p}^l}{\sqrt{4\pi}}\sum_{l'=|j-l|}^{j+l}\sum_{m'=-l'}^{l'} C_{lm,js,l'm'}Y_{l'm'}(\theta,\phi)j_{l'}(\overline{p}r), \tag{144}$$

where the tensor $C_{lm,js,l'm'}$ is related to the Wigner $3j$-symbols through

$$\begin{aligned} C_{lm,js,l'm'} &= (-1)^{m'}i^{l-j+l'}\sqrt{(2l+1)(2j+1)(2l'+1)} \\ &\quad\times\begin{pmatrix} l & j & l' \\ 0 & 0 & 0\end{pmatrix}\begin{pmatrix} l & j & l' \\ m & s & m'\end{pmatrix}. \end{aligned} \tag{145}$$

The Wigner $3j$-symbols are related to the Clebsch-Gordan coefficients $\langle lm,js|l'\ -m'\rangle$ as

$$\begin{pmatrix} l & j & l' \\ m & s & m'\end{pmatrix} = (-1)^{l-j-m'}(2l'+1)^{-1/2}\langle lm,js|l'\ -m'\rangle. \tag{146}$$

The proof of these formulae is given in appendix B of Ref. [6]. We collect all contributions and obtain the final result

$$\mathcal{M}_{lm,l'm'} = \frac{(-1)^l}{\pi^{3/2}} \sum_{j=|l-l'|}^{l+l'} \sum_{s=-j}^{j} \frac{i^j}{\overline{n}^{(j+1)/2}} Z_{js}(1;\overline{n}) C_{lm,js,l'm'}. \tag{147}$$

5.1.4 Matching of wave function and Green function

The expansion of the energy eigenfunction $\psi(\mathbf{r})$ with degree Λ is written by

$$\psi(\mathbf{r}) = \sum_{l=0}^{\infty} \sum_{m=-l}^{l} Y_{lm}(\theta,\phi) b_{lm} \alpha_l(\overline{p}) j_j(\overline{p}r) + \sum_{l=0}^{\Lambda} \sum_{m=-l}^{l} Y_{lm}(\theta,\phi) b_{lm} \beta_l(\overline{p}) n_j(\overline{p}r). \tag{148}$$

On the other hand, $\psi(\mathbf{r})$ is expanded by the spherical component of the Green function $G_{lm}(\mathbf{r};\overline{p}^2)$ given by eq.(140) as

$$\psi(\mathbf{r}) = \sum_{l=0}^{\Lambda} \sum_{m=-l}^{l} v_{lm} G_{lm}(\mathbf{r};\overline{p}^2) \tag{149}$$

with arbitrary coefficient v_{lm}. Using the explicit expression of $G_{lm}(\mathbf{r};\overline{p}^2)$ given in eq.(140), we obtain the following equations

$$b_{lm}\alpha_l(\overline{p}) = \sum_{l'=0}^{\Lambda} \sum_{m'=-l'}^{l'} v_{l'm'} \frac{(-1)^{l'}}{4\pi} \overline{p}^{l'+1} \mathcal{M}_{l'm',lm} \tag{150}$$

$$b_{lm}\beta_l(\overline{p}) = v_{lm} \frac{(-1)^l}{4\pi} \overline{p}^l, \tag{151}$$

where we use the identity $\mathcal{M}_{lm,l'm'} = \mathcal{M}_{l'm',lm}$. The second equation can be used to eliminate v_{lm}. After that one is left with a homogeneous linear system for the coefficients b_{lm}. Since the number of equations is equal to the number of unknowns, a non-zero solution exists if and only if the associated determinant vanishes. This will happen for a discrete set of values of $\overline{p}$, corresponding to the eigenvalues of H_Λ.

Let $\mathcal{H}_\Lambda$ be the space of complex vectors v with components v_{lm}. The matrix $\mathcal{M}_{lm,l'm'}$ can be regarded as a linear operator M in $\mathcal{H}_\Lambda$. Two further operators A and B may be defined through

$$[Av]_{lm} = \alpha_l(\overline{p}) v_{lm}, \quad [Bv]_{lm} = \beta_l(\overline{p}) v_{lm}, \tag{152}$$

and from these one obtains the matrix

$$e^{2i\delta} = (A + iB)/(A - iB). \tag{153}$$

The condition for the existence of a non-zero solution of the linear equations eqs.(150) and (151) can now be written in the closed form

$$\det[A - BM] = 0. \tag{154}$$

The determinant $\det[(A-iB)(M-i)]$ is well defined and non-zero, because M is hermitian and because the eigenvalues of $A-iB$ do not vanish. It is clear then that eq.(154) may be divided by the factor without affecting the set of solutions,

$$\begin{aligned} -i2\det[A-BM] &= \det[(A+iB)(M-i)-(A-iB)(M+i)] && (155)\\ &= \det[(A-iB)(M-i)]\det[e^{2i\delta}-U], && (156)\end{aligned}$$

where $U=(M+i)/(M-i)$. We thus show that eq.(154) is equivalent to

$$\det[e^{2i\delta}-U]=0. \tag{157}$$

5.1.5 Finite volume formula in A_1^+ representation

In follows we focus on states in A_1^+ representation. The states correspond to S-wave states in the continuum, ignoring effects from states with angular momentum $l \geq 4$. For $\Lambda < 4$ eq.(157) reduces to

$$e^{2i\delta_0} = \frac{\mathcal{M}_{00,00}+i}{\mathcal{M}_{00,00}-i}, \tag{158}$$

where

$$\mathcal{M}_{00,00} = \frac{1}{\pi^{3/2}} Z_{00}(1;\overline{n}), \tag{159}$$

which is obtained from eq.(147). This formula is rewritten by

$$\tan\delta_0(\overline{p}) = \frac{\pi^{3/2}\sqrt{\overline{n}}}{Z_{00}(1;\overline{n})}, \tag{160}$$

which is the finite volume formula for S-wave $l=0$ in the center of mass system.

5.1.6 Large-L expansion

The previous works for the S-wave scattering lengths [10, 11, 12, 13, 14, 15, 17] and scattering phase shift [19] employed the expansion of eq.(160) by a power series of $1/L$. We show the expansion in this section.

In general the solutions of eq.(160) satisfy

$$\overline{n} \overset{L\to\infty}{=} n + O(1/L), \quad \text{or} \quad \overline{p}^2 \overset{L\to\infty}{=} \left(\frac{2\pi}{L}\right)^2 n + O(1/L^3), \tag{161}$$

where n is some integer. We expand the zeta function $Z_{00}(1;\overline{n})$ in eq.(160) around $\overline{n}=n$. To expand the zeta function, we define the subtracted zeta function through

$$Z_{00}^{sub}(s;\overline{n}) = \lim_{\overline{n}\to n}\left\{\sqrt{4\pi}Z_{00}(s;\overline{n}) - \nu_n(n-\overline{n})^{-s}\right\}, \tag{162}$$

where $\nu_n \equiv \sum_{\mathbf{n}'}\delta_{n,\mathbf{n}'^2}$. Using this function, the zeta function is denoted as

$$\sqrt{4\pi}Z_{00}(1;\overline{n}) = \frac{\nu_n}{n-\overline{n}} + Z_{00}^{sub}(1;\overline{n}). \tag{163}$$

Since $Z_{00}^{sub}(1;\overline{n})$ is not singular at $\overline{n}=n$, we can expand it as,

$$Z_{00}^{sub}(1;\overline{n}) = \sum_{l=0}^{\infty}(\overline{n}-n)^l Z_{00}^{sub}(l+1;n). \tag{164}$$

Now it is obvious from eq.(160) that

$$n - \overline{n} = t\left(\nu_n + (n-\overline{n})Z_{00}^{sub}(1;n) - (n-\overline{n})^2 Z_{00}^{sub}(2;n) + \cdots\right), \tag{165}$$

where the expansion parameter t occurring here is defined by

$$t = \left\{\frac{\tan\delta_0(\overline{p})}{\pi L\overline{p}}\right\}_{\overline{p}^2=(2\pi/L)^2 n}. \tag{166}$$

In order to solve the equation by a recursive procedure we obtain the final expression

$$\overline{n} = n - \nu_n t\left\{1 + tZ_{00}^{sub}(1;n) + t^2\left[Z_{00}^{sub}(1;n)^2 - \nu_n Z_{00}^{sub}(2;n)\right]\right\} + O(1/L^4). \tag{167}$$

In particular the equation in the $n = 0$ case was used in many works for the scattering length. In this case the expansion parameter is given by $t = a_0/\pi L$, where a_0 is the scattering length, and eq.(167) becomes the relation of a_0 and the momentum $\overline{p}^2 = (2\pi/L)^2 \cdot \overline{n}$,

$$\frac{\overline{p}^2}{m} = -\frac{4\pi a_0}{mL^3}\left(1 + c_1\frac{a_0}{L} + c_2\frac{a_0^2}{L^2}\right) + O(1/L^6), \tag{168}$$

where $c_1 = Z_{00}^{sub}(1;0)/\pi$ and $c_2 = (Z_{00}^{sub}(1;0)^2 - Z_{00}^{sub}(2;0))/\pi^2$. The values of the coefficients c_1 and c_2 are known such that $c_1 = -2.837297$ and $c_2 = 6.375183$ [5]. In the actual calculation the left hand side is approximated by the energy shift $\Delta\overline{E} = \overline{E} - 2m \approx \overline{p}^2/m$, where $\overline{E}$ is the two-particle energy in the interacting case, given by $\overline{E}^2 = 4(m^2 + \overline{p}^2)$.

5.1.7 Relativistic case

We note here the extension of eq.(160) toward quantum field theory briefly. In quantum field theory Lüscher derived the relation between the momentum in a finite volume and the scattering amplitude in the framework of the Feynman diagram expansion [5]. The crucial observation is that the effective Schrödinger equation can be derived, which reads

$$-\frac{1}{2\mu}\nabla^2\psi(\mathbf{r}) + \frac{1}{2}\int d^3r' U_E(\mathbf{r},\mathbf{r}')\psi(\mathbf{r}) = E\psi(\mathbf{r}), \tag{169}$$

where the parameter $E = \overline{p}^2/2\mu$ is related to the true energy $\overline{E}$ of the system through

$$\overline{E} = 2\sqrt{m^2 + \overline{p}^2}. \tag{170}$$

The effective potential $U_E(\mathbf{r},\mathbf{r}')$ is the Fourier transformation of the modified Bethe-Salpeter (or two-particle irreducible) kernel $\hat{U}_E(\mathbf{k},\mathbf{k}')$ introduced in Ref. [5]. It depends on E and is a smooth function of the coordinates $\mathbf{r}$ and $\mathbf{r}'$, decaying exponentially in all directions. When the potential is rotationally invariant, one can pass to the radial effective Schrödinger equation. The corresponding regular solution behaves exactly same as in quantum mechanics, except that the large r form eq.(124) only holds up to exponentially small correction, because the potential does not strictly vanish for r greater than some radius R.

If we assume that the potential vanishes, in the framework of the relativistic quantum mechanics the derivation of the Helmholtz equation eq.(121) in the center of mass system is not so difficult from the Klein-Gordon equation. This is described in Ref. [8] and also in Sec. 5.2.1.

5.2 General system

We consider general systems where two particles have any total momentum. We first derive the Helmholtz equation from the Klein-Gordon equation in the center of mass system. We then describe solutions of the Helmholtz equation and the finite volume formulae in the general systems. We shall call the system with non-zero total momentum as the laboratory system.

5.2.1 Lorentz transformation of wave function

Let us consider a two-particle wave function in the infinite volume. The state of the system is described by the scalar wave function $\Psi(r_1, r_2)$, where $r_i = (r_i^0, \mathbf{r}_i)$ are the four-dimensional Minkowski space-time coordinates of the i-th particle. The wave function transforms in the Lorentz transformations as

$$\Psi(r_1, r_2) = \Psi(r_1^{'}, r_2^{'}) = \Psi(\Lambda r_1, \Lambda r_2), \tag{171}$$

where $r_\mu^{'} = \Lambda_\mu{}^\nu r_\nu$ denotes the Lorentz transformation of the four-vector r. It is convenient to consider only the case $r_1^0 = r_2^0$.

Let us first consider the free case. In this case the wave function satisfies the Klein-Gordon equations,

$$(\hat{p}_{i\mu}\hat{p}_i^\mu - m^2)\Psi(r_1, r_2) = 0, \quad i = 1, 2, \tag{172}$$

where $\hat{p}_{i\mu} = -i\partial/\partial r_i^\mu$. The above equations can be transformed with the change of variables

$$X = (r_1 + r_2)/2, \quad r = r_1 - r_2, \tag{173}$$

into the form

$$[4(\hat{p}_\mu\hat{p}^\mu - m^2) + \hat{P}_\mu\hat{P}^\mu]\Psi(X, r) = 0, \tag{174}$$

$$\hat{p}_\mu\hat{P}^\mu\Psi(X, r) = 0, \tag{175}$$

where $\hat{p} = (\hat{p}_1 - \hat{p}_2)/2$, and $\hat{P} = \hat{p}_1 + \hat{p}_2$ is the total four-momentum operator.

In the absent of external potentials, the total momentum is conserved even when the two-particle interaction is turned on, so that we can write the wave function as an eigenfunction of the total momentum P,

$$\Psi(X, r) = e^{-iP_\mu X^\mu}\psi(r). \tag{176}$$

In the center of mass system the total momentum vanishes $\mathbf{P} = 0$. We shall focus only on the positive energy solution $P_0 = E$. From eq.(175) it follows that

$$\hat{p}_0\psi(r) = 0, \tag{177}$$

so that the wave function depends only on the time variable $X^0 = t$ and the relative separation of the two particles $\mathbf{r} = \mathbf{r}_1 - \mathbf{r}_2$:

$$\Psi_{\rm CM}(t, \mathbf{r}) = e^{-iEt}\psi_{\rm CM}(\mathbf{r}). \tag{178}$$

From eqs.(174) and (178) we note that the wave function in the center of mass system satisfies the Helmholtz equation

$$(\nabla_{\mathbf{r}}^2 + p^2)\psi_{\rm CM}(\mathbf{r}) = 0, \tag{179}$$

where $p^2 = E^2/4 - m^2$. Therefore we can derived the Helmholtz equation from the relativistic formulation.

Let us now consider the situation in the laboratory system where $\mathbf{P} \neq 0$. The transformation from the laboratory system to the center of mass system can be written as $r^\mu = \Lambda^\mu_\nu r^\nu_L$, where r is any four-vector and a quantity with $(_L)$ refers to the laboratory system. The transformation is written by

$$r^0 = \gamma(r^0_L + \mathbf{v}\cdot\mathbf{r}_L), \tag{180}$$
$$\mathbf{r} = \vec{\gamma}(\mathbf{r}_L + \mathbf{v}r^0_L), \tag{181}$$

where $\mathbf{v} = \mathbf{P}/E_L$ is the center of mass three-velocity in the laboratory system with $P^0_L = E_L$, and $\gamma = 1/\sqrt{1-\mathbf{v}^2}$ is the Lorentz boost factor. Here $\vec{\gamma}\mathbf{r} = \gamma\mathbf{r}_{||} + \mathbf{r}_\perp$ where $\mathbf{r}_{||}$ and $\mathbf{r}_\perp$ are components of $\mathbf{r}$ parallel and perpendicular to the velocity $\mathbf{v}$: $\mathbf{r}_{||} = (\mathbf{r}\cdot\mathbf{v})\mathbf{v}/\mathbf{v}^2$ and $\mathbf{r}_\perp = \mathbf{r} - \mathbf{r}_{||}$. Using the transformation eq.(171), the identity $P_{\mu L}X^\mu_L = P_\mu X^\mu$ and eq.(176), the laboratory system wave function can be written as $\Psi_{\rm L}(X_L, r_L) = e^{-iP_{\mu L}X^\mu_L}\psi_{\rm L}(r_L)$, where

$$\psi_{\rm L}(r^0_L, \mathbf{r}_L) = \psi_{\rm CM}(\gamma(r^0_L + \mathbf{v}\cdot\mathbf{r}_L), \vec{\gamma}(\mathbf{r}_L + \mathbf{v}r^0_L)). \tag{182}$$

In the center of mass system the wave function has the complicated coordinates. However, we are interested in the case where both of the particles have equal time coordinate, i.e. $r^0_L = 0$. (More specifically, on the lattice all two-particle operators act on single spacelike hyperplane.) Since from eq.(177) we know the wave function in the center of mass system is independent of r^0, the relation in eq.(182) becomes simple

$$\psi_{\rm L}(0, \mathbf{r}_L) = \psi_{\rm CM}(\vec{\gamma}\mathbf{r}_L). \tag{183}$$

In the laboratory system the relation is transformed as

$$\Psi_{\rm L}(0, \mathbf{r}_L, t_L, \mathbf{X}_L) = e^{-iE_L t_L + i\mathbf{P}\cdot\mathbf{X}_L}\psi_{\rm L}(0, \mathbf{r}_L) = e^{-iEt}\psi_{\rm CM}(\vec{\gamma}\mathbf{r}_L). \tag{184}$$

The total energies in the two systems are related by $E^2_L = E^2 + \mathbf{P}^2$.

5.2.2 boundary condition of wave function

Let us now consider the laboratory system in a box of size L^3 with periodic boundary conditions. Since in this discussion the time is not important, we take the time direction of the box is infinite.

The wave function $\Psi_{\rm L}$ in the laboratory systems is periodic with respect to the position of either of the particles

$$\Psi_{\rm L}(\mathbf{r}_1, \mathbf{r}_2) = \Psi_{\rm L}(\mathbf{r}_1 + \mathbf{n}L, \mathbf{r}_2 + \mathbf{m}L) \quad \text{for all } \mathbf{n}, \mathbf{m} \in Z^3. \tag{185}$$

From the boundary condition and the form of the wave function given by eq.(184) we yield the result

$$\psi_{\rm L}(\mathbf{r}_L) = (-1)^{\mathbf{d}\cdot\mathbf{n}}\psi_{\rm L}(\mathbf{r}_L + \mathbf{n}L), \tag{186}$$

where $\mathbf{d} = \mathbf{P}L/2\pi$ and $\mathbf{d}, \mathbf{n} \in Z^3$. The periodicity of the wave function depends on the direction and the value of $\mathbf{d}$.

We can use eq.(183) to obtain the corresponding periodicity rule for the center of mass wave function. For fixed vector $\mathbf{d}$,

$$\psi_{\rm CM}(\mathbf{r}) = (-1)^{\mathbf{d}\cdot\mathbf{n}}\psi_{\rm CM}(\mathbf{r} + \vec{\gamma}\mathbf{n}L) \quad \text{for all } \mathbf{n} \in Z^3. \tag{187}$$

The energy E_L and the box size L determine the boost factor $\vec{\gamma} = \mathbf{d}/\sqrt{(LE_L/2\pi)^2 - \mathbf{d}^2}$. We shall call the functions obeying the rule eq.(187) **d**-periodic functions. The eq.(187) has an simple interpretation: the center of mass system sees the laboratory system torus expanded by the boost factor γ to the direction of the total momentum, while the length scales to the perpendicular directions are preserved.

5.2.3 Scattering interaction

In the center of mass system, the interaction has the same period as the wave function but without the antiperiodicity

$$V_{\rm p.b.}(|\mathbf{r}|) = \sum_{\mathbf{n}\in Z^3} V(|\mathbf{r} + \vec{\gamma}\mathbf{n}L|). \tag{188}$$

We assume that a potential $V(|\mathbf{r}|)$ has a finite range

$$V(|\mathbf{r}|) = 0 \quad \text{for all } |\mathbf{r} + \vec{\gamma}\mathbf{n}L| > R. \tag{189}$$

We consider that the potential is expanded by γ in the laboratory system, but if R exists in center of mass system, there is the zero potential region in also the laboratory system. Then the Klein-Gordon equations (172) hold when $|\mathbf{r}| > R$, and in this region $\psi_{\rm CM}(\mathbf{r})$ satisfies the Helmholtz equation eq.(179).

5.2.4 Singular d-periodic solutions

Our task is now to obtain solutions of the Helmholtz equation with **d**-periodic boundary condition in the center of mass system, when the interaction turns on. The strategy is same as in Sec. 5.1.3 – 5.1.4, expanding general solutions of the Helmholtz equation in terms of the spherical harmonics and the Bessel and Noeman functions in the region $R < |\mathbf{r}| < L/2$, and extracting the relation between the scattering phase shift and the expansion coefficients.

In the following we shall call a function $\psi(\mathbf{r})$ in the center of mass system a singular **d**-periodic solution of the Helmholtz equation, when it satisfies the following conditions.

(i)The $\psi(\mathbf{r})$ is a smooth function defined for all $\mathbf{r} \neq 0 \pmod{\vec{\gamma}\mathbf{n}L}$, $\mathbf{n} \in Z^3$), and it satisfies the Helmholtz equation eq.(179)

$$(\nabla^2 + \overline{p}^2)\psi(\mathbf{r}) = 0, \tag{190}$$

for some value of $\overline{p} > 0$. Here $\overline{p}$ is the center of mass momentum given by

$$\overline{p}^2 = \overline{E}^2/4 - m_\pi^2, \quad \text{where} \quad \overline{E}^2 = \overline{E}_L^2 - \mathbf{P}^2. \tag{191}$$

We denote quantities in the interacting case with the overline.

(ii)The $\psi(\mathbf{r})$ obeys the **d**-periodicity rule

$$\psi(\mathbf{r}) = (-1)^{\mathbf{d}\cdot\mathbf{n}}\psi(\mathbf{r} + \vec{\gamma}\mathbf{n}L) \quad \text{for all } \mathbf{n} \in Z^3. \tag{192}$$

(iii)We also require that the function is bounded by a power of $1/|\mathbf{r}|$ near the origin

$$\lim_{\mathbf{r}\to 0} |\mathbf{r}^{\Lambda+1}\psi(\mathbf{r})| < \infty, \tag{193}$$

for some positive integer Λ which called the degree of $\psi(\mathbf{r})$.

In this discussion we also assume that the value of $\overline{p}$ is not singular,

$$\overline{p} \neq \sqrt{\overline{n}}\frac{2\pi}{L}|\vec{\gamma}^{-1}(\mathbf{n}+\mathbf{d}/2)| \quad \text{for all } \mathbf{n} \in Z^3, \quad \overline{n} = \left(\frac{L\overline{p}}{2\pi}\right)^2. \tag{194}$$

We can define the Green function

$$G^{\mathbf{d}}(\mathbf{r};\overline{p}^2) = \gamma^{-1}L^{-3}\sum_{k\in\Gamma_{\mathbf{d}}}\frac{e^{i\mathbf{k}\cdot\mathbf{r}}}{\mathbf{k}^2-\overline{p}^2}, \tag{195}$$

where the sum is over the momentum lattice

$$\Gamma_{\mathbf{d}} = \left\{\mathbf{k} = \frac{2\pi}{L}\vec{\gamma}^{-1}(\mathbf{n}+\mathbf{d}/2) \quad \text{for all } \mathbf{n} \in Z^3\right\}. \tag{196}$$

We can show that the Green function satisfies the **d**-periodicity rule using

$$\mathbf{k}\cdot(\mathbf{r}+\vec{\gamma}\mathbf{m}L) = \mathbf{k}\cdot\mathbf{r} + \pi\mathbf{d}\cdot\mathbf{m} + 2\pi\mathbf{n}\cdot\mathbf{m} \quad \text{for all } \mathbf{n},\mathbf{m} \in Z^3. \tag{197}$$

The **d**-periodicity arises from the second term in the right hand side. The Green function also satisfies the equation

$$(\nabla^2+\overline{p}^2)G^{\mathbf{d}}(\mathbf{r};\overline{p}^2) = -\sum_{\mathbf{n}\in Z^3}(-1)^{\mathbf{d}\cdot\mathbf{n}}\delta(\mathbf{r}+\vec{\gamma}\mathbf{n}L). \tag{198}$$

Thus, the Green function $G^{\mathbf{d}}(\mathbf{r};\overline{p}^2)$ is an example of singular **d**-periodic solutions of the Helmholtz equation. Further solutions can be obtained by differentiating $G^{\mathbf{d}}(\mathbf{r};\overline{p}^2)$ with respect to $\mathbf{r}$ as well as eq.(138),

$$G^{\mathbf{d}}_{lm}(\mathbf{r};\overline{p}^2) = \mathcal{Y}_{lm}(\nabla)G^{\mathbf{d}}(\mathbf{r};\overline{p}^2), \tag{199}$$

where $\mathcal{Y}_{lm}(\mathbf{r})$ is defined by eq.(137). Since $\mathcal{Y}_{lm}(\nabla)$ commutes with ∇^2, the functions $G^{\mathbf{d}}_{lm}(\mathbf{r};\overline{p}^2)$ are also singular **d**-periodic solutions of the Helmholtz equation. As well as in Sec. 5.1.4 the singular **d**-periodic solution of degree Λ is given by a linear combination of the functions $G^{\mathbf{d}}_{lm}(\mathbf{r};\overline{p}^2)$ with $l \leq \Lambda$,

$$\psi_\Lambda(\mathbf{r}) = \sum_{l=0}^{\Lambda}\sum_{m=-l}^{l} v_{lm}G^{\mathbf{d}}_{lm}(\mathbf{r};\overline{p}^2). \tag{200}$$

The expansion of $G^{\mathbf{d}}_{lm}(\mathbf{r};\overline{p}^2)$ by the spherical Bessel and Noeman functions is straightforward with the same way in Sec. 5.1.3, and we obtain the form by changing $G_{lm}(\mathbf{r};\overline{p}^2) \to G^{\mathbf{d}}_{lm}(\mathbf{r};\overline{p}^2)$ and $\mathcal{M}_{lm,l'm'} \to \mathcal{M}^{\mathbf{d}}_{lm,l'm'}$ in eq.(140). We need the explicit form of the matrix $\mathcal{M}^{\mathbf{d}}_{lm,l'm'}$ to obtain the final formula. The form is given by

$$\mathcal{M}^{\mathbf{d}}_{lm,l'm'} = \gamma^{-1}\frac{(-1)^l}{\pi^{3/2}}\sum_{j=|l-l'|}^{l+l'}\sum_{s=-j}^{j}\frac{i^j}{\overline{n}^{(j+1)/2}}Z^{\mathbf{d}}_{js}(1;\overline{n})C_{lm,js,l'm'}, \tag{201}$$

where the tensor $C_{lm,js,l'm'}$ is given by eq.(145). Here the generalized spherical zeta function $Z^{\mathbf{d}}_{js}(1;\overline{n})$ is defined by

$$Z^{\mathbf{d}}_{lm}(s;\overline{n}) = \sum_{\mathbf{r}\in\mathbf{P}_{\mathbf{d}}}\mathcal{Y}_{lm}(\mathbf{r})(\mathbf{r}^2-\overline{n})^{-s}, \tag{202}$$

where $\overline{n} = (L\overline{p}/2\pi)^2$ and the summation is over the set

$$\mathbf{P_d} = \left\{ \mathbf{r} = \vec{\gamma}^{-1}(\mathbf{n} + \mathbf{d}/2) \quad \text{for all } \mathbf{n} \in Z^3 \right\}. \tag{203}$$

We show the calculation of the zeta function $Z^{\mathbf{d}}_{lm}(s; \overline{n})$ in the $l = 0$ case in appendix C.1.

5.2.5 Generalized finite volume formula in $\mathbf{A}_1^+$ representation

As well as in Sec. 5.1.5 we restrict ourselves to the state in A_1^+ representation. For angular momentum cut-off $\Lambda = 0$ we can obtain the simple finite volume formula

$$\tan\delta_0(\overline{p}) = \frac{1}{\mathcal{M}^{\mathbf{d}}_{00,00}} = \frac{\gamma\pi^{3/2}\sqrt{\overline{n}}}{Z^{\mathbf{d}}_{00}(1;\overline{n})}, \quad \overline{n} = \left(\frac{L\overline{p}}{2\pi}\right)^2. \tag{204}$$

Substituting $|\mathbf{d}| = 0$ and $\gamma = 1$, eq.(204) is transformed to the relation in the center of mass system eq.(160). For other value of Λ the formula becomes a complicated form depending on the direction $\mathbf{d}$. In $|\mathbf{d}| = 1, 2$ systems the same form is obtained in the case of $\Lambda \leq 1$ [8].

6 Extraction of two-particle energy

In this section we introduce extraction methods of two-particle energies on lattice. In Sec. 5 we show that the scattering phase shift in the infinite volume can be evaluated from two-particle energy on a finite box. However, there is a problem to calculate such energies from a two-particle four-point function. We first explain the problem considering in a simple model, and later describe a method to solve it, which was proposed by Lüscher and Wolff [7]. This method succeeded in many works with effective theory [7, 8, 9]. After that we present another method with the maximum entropy method [61], and its application to $O(4)$ ϕ^4 theory [62].

In this section the discussion is only in the center of mass system, although the extension to general systems is straightforward.

6.1 Diagonalization method

6.1.1 Simple model and definition

Let us consider for simplicity a lattice theory of a single scalar field $\phi(x)$, such as the ϕ^4-theory in two-dimension (t, x). Suppose $\phi \to -\phi$ is an unbroken symmetry of the system and that the particle spectrum consists of a single massive particle, which has odd parity under this symmetry, in other words the particle is spinless. The two-particle states live in the sector with even parity, zero total momentum and energies $0 < \overline{E} < 4m$, where $\overline{E}$ is the two-particle energy with the interaction.

We define the two-particle operator

$$\Omega_n(t) = \sum_{x,y} e^{ip(x-y)} \phi(x,t)\phi(y,t) \tag{205}$$

where $p = (2\pi/L) \cdot n$ and n is an integer. We now construct four-point function by the operator as

$$G_{nm}(t) = \langle 0|\Omega_n^*(t)\Omega_m(0)|0\rangle - \langle 0|\Omega_n^*(t)|0\rangle\langle 0|\Omega_m(0)|0\rangle. \tag{206}$$

The general form of the spectral decomposition of $G_{nm}(t)$ is, for $t \geq 0$,

$$G_{nm}(t) = \sum_{\alpha=0}^{\infty} V_{n\alpha}^T V_{\alpha m} e^{-\overline{E}_\alpha t}, \quad V_{\alpha m} = \langle \overline{\Omega}_\alpha | \Omega_m(0)|0\rangle, \tag{207}$$

where $|\overline{\Omega}_\alpha\rangle$ is the interacting two-particle state with the energy $\overline{E}_\alpha > 0$. We note that n, m label the operator and α label the two-particle state. The label is ordered by the two-particle levels. We assume for simplicity that $\overline{E}_0 < \overline{E}_1 < \cdots < \overline{E}_A < 4m$ and $\overline{E}_\alpha \geq 4m$ for $\alpha > A$.

6.1.2 Difficulty of two-particle state on lattice

The traditional analysis method to extract the energy is a single exponential fit of the correlation function with assuming the asymptotic behavior for large time. Since the only ground state contribution in $G_{nm}(t)$ remains in the large time region, $G_{nm}(t)$ behaves in this region as

$$G_{nm}(t) \to V_{n0}^T V_{0m} e^{-\overline{E}_0 t}, \quad t \to \infty, \tag{208}$$

for any n, m. The extraction of the contribution for the ground state $\alpha = 0$ is easy. However, we cannot obtain other state contributions by the single exponential analysis. This is the

serious problem to calculate the scattering phase shift, because we need the two-particle energy for also $\alpha \neq 0$ states to evaluate the phase shift through the finite volume method as shown in Sec. 5.

This is related to a problem of calculation of the weak matrix element for the K meson non-leptonic decay $K \to \pi\pi$. The problem is so called Maiani-Testa problem [27]. In the calculation we need the amplitude

$$\langle K|H_W|\overline{\Omega}_\alpha\rangle \quad \text{at } m_K = \overline{E}_\alpha = 2\sqrt{m_\pi^2 + \overline{p}_\alpha^2}, \tag{209}$$

where $\overline{p}_\alpha \neq 0$. Here H_W is an effective weak interaction operator. From above argument we cannot the on-shell amplitude by the single exponential analysis. So far to avoid the problem various methods were proposed [29].

6.1.3 Diagonalization method

Since in the actual numerical simulation we cannot calculate all components of $G_{nm}(t)$, we introduce a cut-off N for the operator number, and for the state.

The matrix $V_{\alpha n}$ is assumed to be linearly independent because we assume the two-particle energy is not degenerate. The linear independence of the two-particle operator is guaranteed when we choose $0 \leq n < L/2$.

The eigenvalues $\lambda_\alpha(t)$ of $G(t)$ are ordered such that $\lambda_0 \geq \lambda_1 \geq \cdots \geq \lambda_A$. Lüscher and Wolff discussed in Ref.[7] that $\lambda_\alpha(t)$ for all $\alpha = 0, \cdots, A$ are given by

$$\lambda_\alpha(t) = c_\alpha e^{-\overline{E}_\alpha t}\left[1 + O(e^{-\Delta\overline{E}_\alpha t})\right], \quad t \gg 1, \tag{210}$$

where $c_\alpha > 0$ and $\Delta\overline{E}_\alpha = \min_{\alpha\neq\beta}|\overline{E}_\alpha - \overline{E}_\beta|$. In principle it is possible to extract the eigenvalues by the diagonalization of the matrix $G(t)$ at large time region, but $G(t)$ cannot usually be determined very accurately at this region. Hence it may not be possible to guarantee that the error term in eq.(210) is negligible.

Let us now consider the generalized eigenvalue problem

$$G(t)w = \lambda(t, t_0)G(t_0)w, \tag{211}$$

where t_0 is fixed and may be chosen as small. This problem is well posed if $G(t_0)$ is non-singular. This is guaranteed in the case, because the two-particle operator $\Omega_n(t)$, $n = 0, \cdots, N$, are linearly independent. Thus, there are N independent solutions to eq.(211), and the corresponding eigenvalues $\lambda_\alpha(t, t_0)$, $\alpha = 0, \cdots, A$, are different from that in eq.(210). More precisely we can expect that the coefficients are given by $c_\alpha \approx e^{\overline{E}_\alpha t_0}$ and that the sub-leading coefficients in eq.(210) are suppressed, so that the leading term in eq.(210) dominates at moderately large values of t.

To see this, by appropriate selection of the state $|\overline{\Omega}_\alpha\rangle$ with $\alpha = 0, \cdots, N$, the truncated four-point function matrix

$$G^0_{nm}(t) = \sum_{\alpha=0}^{N} V^T_{\alpha n} V_{\alpha m} e^{-\overline{E}_\alpha t} \tag{212}$$

can be expected to approximate $G(t)$ rather well. It is not difficult to show that the spectrum of the eigenvalues $\lambda^0_\alpha(t, t_0)$ of the associated modified eigenvalue problem is exactly given by

$$\lambda^0_\alpha(t, t_0) = e^{-\overline{E}_\alpha(t-t_0)} \quad \text{for all } \alpha = 1, \cdots, N. \tag{213}$$

The proof is given by rewriting eq.(211) in the truncated case as

$$Vw = \Delta(t)^{-1}\lambda^0(t,t_0)\Delta(t_0)Vw, \tag{214}$$

where we use $G^0(t) = V^T\Delta(t)V$ and $\Delta_\alpha(t) = e^{-\overline{E}_\alpha t}$. Thus, we obtain $\lambda^0_\alpha(t,t_0) = \Delta(t)\Delta(t_0)^{-1}$. Now we consider full $G(t)$. At least the larger eigenvalues ($\alpha = 0, \cdots, N$ states) should not be strongly affected by the lower eigenvalues ($\alpha > N$ states), and the larger ones are approximately equal to $\lambda^0_\alpha(t,t_0)$.

Finally we can extract the eigenvalues of $G(t)$ to solve the eigenvalue problem

$$M(t,t_0)w' = \lambda(t,t_0)w' \tag{215}$$

where $M(t,t_0) = G^{-1/2}(t_0)G(t)G^{-1/2}(t_0)$ and $w' = G^{1/2}(t_0)w$ with the eigenvector w in eq.(211). The two-particle energies are possible to be obtained from $\lambda_\alpha(t,t_0)$ by a single exponential fit.

6.1.4 Extraction of spectral amplitude

It is useful for calculating physical quantities, e.g., $K \to \pi\pi$ weak matrix element, to determine the spectral amplitude $V_{\alpha n}$. It is obtained from the equation

$$V = \Delta^{-1/2}(t_0)w'^T G^{1/2}(t_0). \tag{216}$$

We show the derivation of the equation briefly in the following.

The eigenvalue problem eq.(215) is rewritten by

$$X^T(t_0)\Delta(t)X(t_0) = \Delta(t), \tag{217}$$

where $X(t_0) = VG^{-1/2}(t_0)w'\Delta^{1/2}(t_0)$. When we assume that the two-particle is not degenerate, the following condition is derived as

$$X(t_0) = \mathbf{1}. \tag{218}$$

Thus we can obtain the equation eq.(216).

6.2 Maximum entropy method

In this section we show a method to extract two-particle energy using the maximum entropy method [61] (MEM). The MEM can decompose states contributing to a correlation function through the spectral function. This method has been applied to lattice QCD to obtain the excited state mass [63], to study the properties of the spectral function in a finite temperature [64], and to investigate the theta term [65]. Applications of the MEM to an unstable particle system have been carried out by Allton *et al.* [66] in the three-dimensional four-fermion model, and by us [62] in the four-dimension $O(4)$ ϕ^4 theory. We focus on the later work here.

6.2.1 Spectral function

The spectral function is defined through a correlation function as

$$G(t) = \langle 0|O^\dagger(t)O(0)|0\rangle = \int d\omega f(\omega)e^{-\omega t}, \tag{219}$$

where O is an operator, such as Ω_n in eq.(206), and $f(\omega)$ is the spectral function. In a finite volume the energy states are discretized, so that the spectral function is written by

$$f(\omega) = \sum_{\alpha=0}^{\infty} C_\alpha \delta(\omega - \overline{E}_\alpha), \quad C_\alpha = |\langle \overline{O}_\alpha | O(0) | 0 \rangle|^2, \tag{220}$$

where $|\overline{O}_\alpha\rangle$ is a state has same quantum numbers with operator O, and $\overline{E}_\alpha$ is its energy. In the case $O = \Omega_n$ the coefficient $C_\alpha = |V_{\alpha n}|^2$. From $f(\omega)$ we can extract the energy for each state.

Furthermore if the system includes $\sigma \to \pi\pi$ decay, in other words the σ particle has the same quantum number with the $\pi\pi$ state, $f(\omega)$ includes the contribution from the σ state, such as C_σ.

If one could reconstruct $f(\omega)$ directly from $G(t)$ using data at all t, information of various states would be extracted from one correlation function. Since the number of data for $G(t)$ with a discrete set of time t is much smaller than the number of degree of freedom necessary for the reconstruction of $f(\omega)$ in general, however, the standard χ^2 fit is ill-posed for this problem. In condensed matter physics, the reconstruction of the spectral function in quantum Monte Carlo simulations has been attempted with the MEM[61]. The MEM can numerically reconstruct the most probable spectral function, using the Bayes's theorem in probability theory, without any strong constraints on its form.

6.2.2 Results of decomposition

We show here the result of an exploring study for the MEM [62] in the four-dimensional $O(4)$ ϕ^4 theory, which contains the pion and the σ particle. For $m_\sigma > 2m_\pi$, the σ particle is unstable and can decay to the $I = 0$ $\pi\pi$ state. We decomposed the σ and $\pi\pi$ states with the zero momentum contributed to the pion four-point function, such as G_{00} in eq.(206), and σ correlation function. Numerical simulations were carried out for several spatial lattice sizes in the range $10^3 - 28^3$ to investigate the volume dependence of the spectral functions and the energies.

The results of the spectral functions are shown in Fig. 8. We denote the spectral functions extracted from the σ correlation function and the pion four-point function as $f_\sigma(\omega)$ and $f_{\pi\pi}(\omega)$, respectively. The sharp peaks are observed in both the spectral functions, which can be identified as the $\pi\pi$ state at the first peak and the σ state at the second peak. The decrease of the peak height for the $\pi\pi$ state in $f_\sigma(\omega)$ and for the σ state in $f_{\pi\pi}(\omega)$ agrees with the perturbation theory [62].

The σ mass m_σ and the $\pi\pi$ state energy $E_{\pi\pi}$ were obtained from the peak positions of the spectral functions. The results are shown in Figs. 9 by circles. These energies were also obtained by the diagonalization method for the comparisons. The results are plotted by cross symbols in Fig. 9. These are consistent with those with the MEM, while the statistical error with the diagonalization method is much smaller.

It is an advantage of MEM that only the single particle correlation function of the unstable particle is needed to analyze both the particle itself and the multi-particle decaying states. Furthermore it works even when the dominant states in the correlation functions are not known, but the diagonalization does not work in such case.

The isospin $I = 2$ S-wave $\pi\pi$ scattering system includes only two-pion states, however. Since we know all states contributed to the pion four-point functions, in this thesis we employ the diagonalization method.

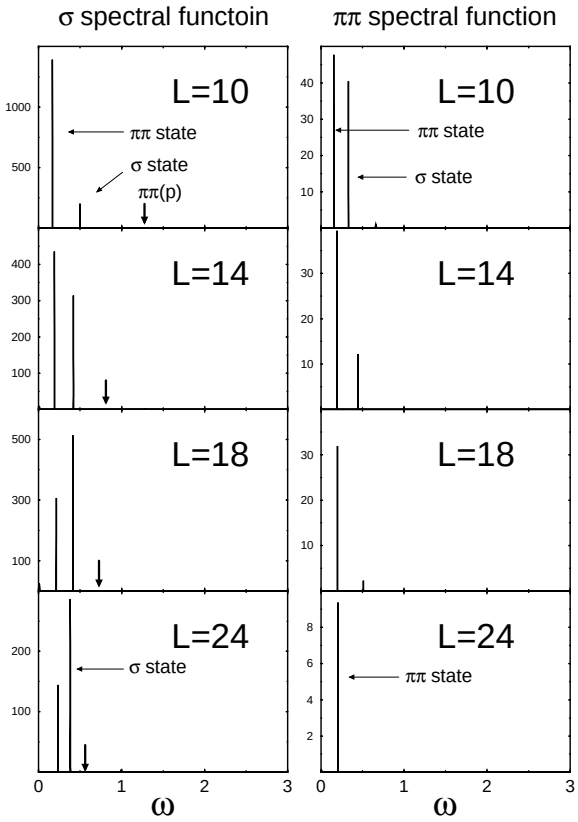

Figure 8: Spectral functions reconstructed from the σ (left line) and $\pi\pi$ (right line) correlation functions in $O(4)$ ϕ^4 theory [62]. First and second peaks correspond to $\pi\pi$ and σ states, respectively.

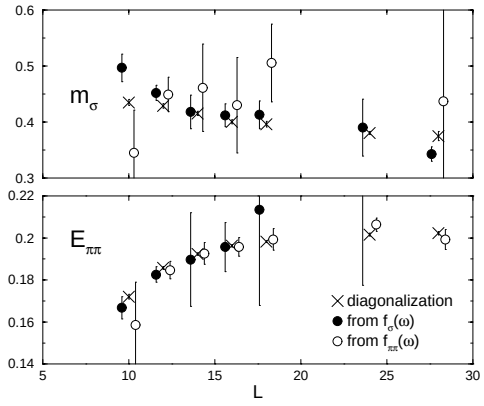

Figure 9: Energies for σ (top figure) and $\pi\pi$ (bottom figure) states with MEM and diagonalization in $O(4)$ ϕ^4 theory [62]. Closed and open circles are the results obtained from σ and $\pi\pi$ correlation functions, respectively. Cross symbols denote result with diagonalization method.

7 Calculation method

Following sections are based on our original works. In this section and next section we describe the calculation of the isospin $I = 2$ S-wave $\pi\pi$ scattering phase shift, which is the main work in this thesis. We first explain the outline of the actual analysis with the finite volume methods, described in Sec. 5, and fix the notations. We then briefly describe the calculation of the pion four-point functions, and the extraction of the two-pion energy eigenvalues by the diagonalization method, discussed in Sec. 6.1. Finally the parameters for the configuration [2] and for the calculation of the pion four-point function are given.

7.1 Finite volume method

We employ the finite volume method, described in Sec. 5, proposed by Lüscher [5, 6] in the center of mass system, and proposed by Rummukainen and Gottlieb [8] in the system with the non-zero total momentum to evaluate the scattering phase shift. We explain the methods used in the actual analysis here.

7.1.1 Center of mass system

In the center of mass system the energy eigenvalue of two-pion on a finite periodic box L^3 without the two-pion interaction is given by,

$$E_n = 2\sqrt{m_\pi^2 + \mathbf{p}_n^2}, \quad \mathbf{p}_n^2 = (2\pi/L)^2 n, \quad n \in Z. \tag{221}$$

In the interacting case the energy eigenvalue of the n-th state is given by,

$$\overline{E}_n = 2\sqrt{m_\pi^2 + \overline{p}_n^2}, \quad \overline{p}_n^2 = (2\pi/L)^2 \overline{n}, \quad \overline{n} \notin Z. \tag{222}$$

Since the interaction shifts the two-pion energy on L^3, $\overline{n}$ is not an integer. The momentum $\overline{p}_n$ satisfies the relation eq.(160),

$$\tan\delta(\overline{p}_n) = \frac{\pi^{3/2}\sqrt{\overline{n}}}{Z_{00}(1;\overline{n})}, \tag{223}$$

where $\delta(\overline{p}_n)$ is the phase shift in the infinite volume and $Z_{00}(1;\overline{n})$ is the spherical zeta function [5, 6] defined by

$$Z_{00}(s;\overline{n}) = \frac{1}{\sqrt{4\pi}} \sum_{\mathbf{n}\in Z^3} (\mathbf{n}^2 - \overline{n})^{-s}. \tag{224}$$

The calculation method of $Z_{00}(s;\overline{n})$ is explained in appendix C.1.

7.1.2 Laboratory system

Here let us consider a two-pion system in a periodic box L^3, where two pions have momenta $\mathbf{p}_1$ and $\mathbf{p}_2$ with the non-zero total momentum $\mathbf{P} = \mathbf{p}_1 + \mathbf{p}_2 \neq 0$. We shall call the system as the laboratory system in following.

In the laboratory system the energy eigenvalue for the n-th energy state E_n without the interaction is given by

$$E_{n,L} = \sqrt{m_\pi^2 + \mathbf{p}_{1,n}^2} + \sqrt{m_\pi^2 + \mathbf{p}_{2,n}^2}, \tag{225}$$

where $\mathbf{p}_{i,n}$ is the i-th pion momentum of the n-th energy state. These momenta take discrete values due to a finite volume with the periodic boundary condition. The two-pion interaction shifts $E_{n,L}$ to $\overline{E}_{n,L}$ also in this system, where $\overline{E}_{n,L}$ is the interacting two-pion energy in the laboratory system. The quantity in the laboratory system can be transformed to the one in the center of mass system by the Lorentz transformation, for example,

$$\overline{E}_n = \gamma^{-1}\overline{E}_{n,L}, \tag{226}$$

where $\overline{E}_n$ is the center of mass two-pion energy and the Lorentz boost factor γ is given by $\gamma = \overline{E}_{n,L}/\sqrt{\overline{E}^2_{n,L} - \mathbf{P}^2}$. It is noted that the total momentum $\mathbf{P}$ is conserved even when the interaction exists. The center of mass momentum $\overline{p}_n$ is determined from $\overline{E}_n$ as

$$\overline{p}_n^2 = \overline{E}_n^2/4 - m_\pi^2 = (2\pi/L)^2\overline{n}, \quad \overline{n} \notin Z. \tag{227}$$

The momentum $\overline{p}_n$ is related to the phase shift in the infinite volume through the relation eq.(204),

$$\tan\delta(\overline{p}_n) = \frac{\gamma\pi^{3/2}\sqrt{\overline{n}}}{Z^{\mathbf{d}}_{00}(1;\overline{n})}, \tag{228}$$

where the spherical zeta function $Z^{\mathbf{d}}_{00}(1;\overline{n})$ [8] in the system with $\mathbf{d} = (L/2\pi)\mathbf{P}$ is given by

$$Z^{\mathbf{d}}_{00}(s;\overline{n}) = \frac{1}{\sqrt{4\pi}}\sum_{\mathbf{r}\in P_d}(\mathbf{r}^2 - \overline{n})^{-s}, \tag{229}$$

with $P_d = \{\mathbf{r} = \vec{\gamma}^{-1}(\mathbf{n} + \mathbf{d}/2), \mathbf{n} \in Z^3\}$. Here $\vec{\gamma}^{-1}\mathbf{n} = \gamma^{-1}\mathbf{n}_{||} + \mathbf{n}_\perp$ where $\mathbf{n}_{||}$ and $\mathbf{n}_\perp$ are components of $\mathbf{n}$ parallel and perpendicular to the direction $\mathbf{d}$: $\mathbf{n}_{||} = (\mathbf{n}\cdot\mathbf{d})\mathbf{d}/\mathbf{d}^2$ and $\mathbf{n}_\perp = \mathbf{n} - \mathbf{n}_{||}$. The calculation of $Z^{\mathbf{d}}_{00}(s;\overline{n})$ is also given in appendix C.1. Therefore the phase shift is extracted by the two-pion energy eigenvalue calculated from lattice simulation in both the center of mass and laboratory systems.

7.2 Extraction of two-pion energy eigenvalue

We describe here the actual calculations for the pion four-point function matrix and the diagonalization method which is discussed in Sec. 6.

In this work we consider $\pi^+\pi^+$ scattering, which is one of the $I = 2$ scattering. The π^+ operator is defined by

$$\pi(\mathbf{x},t) = -\overline{d}(\mathbf{x},t)\gamma_5 u(\mathbf{x},t), \tag{230}$$

and the pion operator with the momentum $\mathbf{p}$ is given by

$$\pi(\mathbf{p},t) = \sum_{\mathbf{x}}\pi(\mathbf{x},t)e^{i\mathbf{p}\cdot\mathbf{x}}. \tag{231}$$

To extract the two-pion energy eigenvalues we construct the pion four-point function matrix in each system with $\mathbf{P}$

$$G^{(N_R)}_{nm}(t) = \langle 0|\Omega_n(t)\Omega^{(N_R)}_m(t_S)|0\rangle, \tag{232}$$

where t_S is the source point. We omit labels of the systems, such as $\mathbf{P}$. The $\Omega_n(t)$ is a two-pion operator at time t, which is coupled to the n-th energy eigenstate, and is given by,

$$\Omega_n(t) = \frac{1}{N_n}\sum_{\mathbf{p}_1,\mathbf{p}_2}\pi(\mathbf{p}_1,t)\pi(\mathbf{p}_2,t)\,\delta\Big(E^{\mathbf{P}}_n - \sqrt{m_\pi^2+\mathbf{p}_1^2} - \sqrt{m_\pi^2+\mathbf{p}_2^2}\Big)\delta\Big(\mathbf{P} - \mathbf{p}_1 - \mathbf{p}_2\Big), \tag{233}$$

where $\mathbf{p}_1, \mathbf{p}_2$ are the lattice momenta. Here the number N_n is the degeneracy of the n-th energy as,

$$N_n = \sum_{\mathbf{p}_1,\mathbf{p}_2} \delta\Big(E_n^{\mathbf{P}} - \sqrt{m_\pi^2 + \mathbf{p}_1^2} - \sqrt{m_\pi^2 + \mathbf{p}_2^2}\Big)\delta\Big(\mathbf{P} - \mathbf{p}_1 - \mathbf{p}_2\Big). \tag{234}$$

The only states with the same total momentum $\mathbf{P}$ are coupled to the operator $\Omega_n(t)$ which belongs to the system with $\mathbf{P}$. This is the reason that we do not write a label for the system explicitly in $G_{nm}(t)$ and $\Omega_n(t)$. In all systems the operator numbers increase with the energy levels.

In Table II we compile the degeneracy N_n for three systems as, the center of mass system and two laboratory systems with the total momentum as $|(L/2\pi)\mathbf{P}| = |\mathbf{d}| = 1$ and 2, so that we denote them as CM, L1 and L2 systems, respectively. For concreteness, we choose the direction of the non-zero total momentum in the L1 and L2 systems as $\mathbf{d} = (1,0,0)$ and $(1,1,0)$. To calculate the n-th two-pion energy $E_n^{\mathbf{P}}$ in eqs.(233) and (234), we use a typical momentum set $\mathbf{p}_{1,n}, \mathbf{p}_{2,n}$, which is also tabulated in Table II.

The summation over the momenta $\mathbf{p}_1, \mathbf{p}_2$ in the operators enhances their coupling to the states which belong to the A^+ representation of the cubic ($|\mathbf{d}| = 0$), tetragonal ($|\mathbf{d}| = 1$) and orthorhombic ($|\mathbf{d}| = 2$) groups. The states in A^+ representation correspond to S-wave states in the continuum, ignoring the effects from states with angular momentum $l \geq 4$ in the CM system and $l \geq 2$ in both the L1 and L2 systems.

For the source we use the different operator $\Omega_n^{(N_R)}(t)$ as

$$\Omega_n^{(N_R)}(t) = \frac{1}{N_R}\sum_{j=1}^{N_R} \pi(\mathbf{p}_{1,n}^s, t, \xi_j)\pi(\mathbf{p}_{2,n}^s, t, \eta_j), \tag{235}$$

where

$$\pi(\mathbf{p}, t, \xi_j) = \frac{1}{L^3}\left[\sum_{\mathbf{x}} \overline{q}(\mathbf{x}, t)e^{i\mathbf{p}\cdot\mathbf{x}}\xi_j^\dagger(\mathbf{x})\right]\left[\sum_{\mathbf{y}} q(\mathbf{y}, t)\xi_j(\mathbf{y})\right]. \tag{236}$$

Here $\mathbf{p}_{1,n}^s, \mathbf{p}_{2,n}^s$ are the n-th energy state momenta. Since we cannot carry out summations of the momenta in the operator $\Omega_n^{(N_R)}(t)$, we choose a typical momentum set in the actual

CM $\mathbf{P}$ = (0, 0, 0)	$n=0$	$n=1$	$n=2$	$n=3$
$\mathbf{p}_{1,n}$	(0, 0, 0)	(1, 0, 0)	(1, 1, 0)	(1, 1, 1)
$\mathbf{p}_{2,n}$	(0, 0, 0)	(-1, 0, 0)	(-1,-1, 0)	(-1,-1,-1)
N_n	1	6	12	8
L1 $\mathbf{P}$ = (1, 0, 0)	$n=0$	$n=1$	$n=2$	$n=3$
$\mathbf{p}_{1,n}$	(1, 0, 0)	(1, 1, 0)	(2, 0, 0)	(1, 1, 1)
$\mathbf{p}_{2,n}$	(0, 0, 0)	(0,-1, 0)	(-1, 0, 0)	(0,-1,-1)
N_n	2	8	2	8
L2 $\mathbf{P}$ = (1, 1, 0)	$n=0$	$n=1$	$n=2$	$n=3$
$\mathbf{p}_{1,n}$	(1, 1, 0)	(1, 0, 0)	(1, 1, 1)	(1, 0, 1)
$\mathbf{p}_{2,n}$	(0, 0, 0)	(0, 1, 0)	(0, 0,-1)	(0, 1,-1)
N_n	2	2	4	4

Table II: Typical momentum assignment. Here $\mathbf{p}_{i,n}$ is the i-th pion momentum of the n state in $2\pi/L$ unit, $\mathbf{P}$ is the total momentum of two pions $\mathbf{P} = \mathbf{p}_{1,n} + \mathbf{p}_{2,n}$, and N_n is the degeneracy of the n-th state.

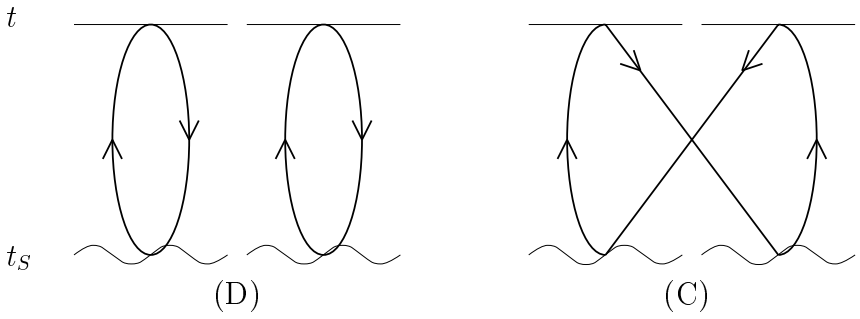

Figure 10: Contributions for the isospin $I = 2$ $\pi\pi$ four-point function. The left and right figures are direct (D) and cross (C) diagrams, respectively. Straight line denotes sink time, and wave line denotes source time.

calculation, for example, which is tabulated in Table II. The function $\xi_j(\mathbf{x})$ is complex random numbers in the three-dimensional space and has the property

$$\lim_{N_R\to\infty} \frac{1}{N_R}\sum_{j=1}^{N_R} \xi_j^\dagger(\mathbf{x})\xi_j(\mathbf{y}) = L^3\delta_{\mathbf{x},\mathbf{y}}. \tag{237}$$

The pion propagator is also calculated with the function of the random number

$$G_n^{\pi(N_R)}(t) = \frac{1}{N_R}\sum_{j=1}^{N_R}\langle 0|\pi(\mathbf{p}_n,t)\pi(-\mathbf{p}_n,t_S,\xi_j)|0\rangle. \tag{238}$$

When the numbers of N_R or the gauge configurations are large, the pion four-point function matrix $G_{nm}^{(N_R)}(t)$ and the pion propagator $G_n^{\pi(N_R)}(t)$ are expected to become

$$G_{nm}^{(N_R)}(t) \to G_{nm}(t) = \langle 0|\Omega_n(t)\Omega_m(t_S)|0\rangle, \tag{239}$$
$$G_n^{\pi(N_R)}(t) \to G_n^\pi(t) = \langle 0|\pi(\mathbf{p}_n,t)\pi(-\mathbf{p}_n,t_S)|0\rangle. \tag{240}$$

In particular $G_{nm}(t)$ is symmetric under the exchange of the sink and the source indices $n \leftrightarrow m$. We fix $N_R = 2$ in all calculations and the number of the gauge configurations are from 380 to 725.

In order to calculate the pion four-point function $G(t)$, we evaluate two diagrams which are the direct (D) and cross (C) diagrams as shown in Fig. 10. The $G(t)$ is constructed by the two diagram contributions G^D and G^C as

$$G(t) = \mathrm{Re}[G^D(t) - G^C(t)]. \tag{241}$$

The four-point function matrix is expanded by the energy eigenstate $|\overline{\Omega}_n\rangle$ as well as eq.(207)

$$G_{nm}(t) = \sum_\alpha V_{n\alpha}^T V_{\alpha m} e^{-\overline{E}_\alpha(t-t_S)}, \quad V_{\alpha m} = \langle\overline{\Omega}_\alpha|\Omega_m(0)|0\rangle, \tag{242}$$

where $\overline{E}_\alpha$ is the energy eigenvalues with the interaction, and $|\overline{\Omega}_\alpha\rangle$ is coupled to only the two-pion operator $\Omega_m(t)$ with the same $\mathbf{P}$. Since the four-point functions are constructed by a multi-exponential, it is difficult to extract the two-pion energy eigenvalues with $\alpha \neq 0$.

In order to extract the energy eigenvalues we employ the diagonalization method [7] of the matrix $M(t,t_0)$ eq.(215) which is constructed by $G(t)$ as,

$$M(t,t_0) = G(t_0)^{-1/2} G(t) G(t_0)^{-1/2}, \tag{243}$$

where t_0 is a reference time. The eigenvalues of $M(t,t_0)$ are given by

$$\lambda_n(t,t_0) = e^{-\overline{E}_n (t-t_0)}. \tag{244}$$

We then can obtain the two-pion energy eigenvalue by a single exponential fit.

The pion four-point function matrix is calculated as assuming systems contained only the two-pion states and ignoring an effect of the four-pion states. Our analysis loses its validity when the two-pion energy is over the inelastic limit, e.g. in the center of mass case $\overline{E}_n > 4m_\pi$.

Since we cannot calculate all components of the four-point function matrix, a cut-off of the state N is introduced in the actual calculation. We expect that the components of $G_{nm}(t)$ for $n,m \leq k$ are dominate for the k-th eigenvalue $\lambda_k(t)$ in the large t and t_0 region, while the components $n,m > k$ are less important. We set t and t_0 are large and check the dependence of the cut-off N by varying N later.

7.3 Parameters

We calculate the scattering phase shift on the gauge configuration, previously generated with two flavors dynamical quarks effect for the study of the light hadron spectrum [2]. The configuration generation was carried out with an renormalization group improved gauge action [56] described in Sec. 3.3.1 and clover quark action [57] described in Sec. 3.3.2 with a tadpole improved clover coefficient $c_{\rm SW}$. The tadpole improvement is explained in Sec. 3.3.3. In this simulation a mean-field improved clover coefficient $c_{\rm SW} = (P)^{-3/4}$ was adopted, where the plaquette value $P = 1 - 0.8412\beta^{-1}$ is determined by one-loop perturbation theory [56].

The parameters for the configuration generation and the number of configurations are summarized in Table III. The configuration generation was performed at $\beta = 1.80, 1.95$ and 2.10, corresponding to the lattice spacings $a = 0.2150(22)$, $0.1555(17)$ and $0.1076(13)$ fm respectively, which are determined by m_ρ at the physical quark mass. The periodic boundary condition is imposed in both the spatial and time directions. The lattice size $L^3 \times T$ at each β is $12^3 \times 24$, $16^3 \times 32$ and $24^3 \times 48$, where the spatial size corresponds to about 2.5^3 fm^3. Since the volume dependence was not seen in the scattering length calculated on the physical volume about 2.4, 3.2 and 4.8 fm with quenched approximation in Ref. [19], we assume that the dependence of the phase shift is also small in this full QCD case with the volume 2.5 fm.

In the calculation of the quark propagator we employ the same clover action as the configuration generation. The quark propagators are calculated with the periodic boundary condition in the spatial direction and the Dirichlet boundary condition in the temporal direction. For the chiral extrapolation we choose four hopping parameters κ, corresponding to $m_\pi/m_\rho \approx 0.6$–0.8 in each lattice spacing. The source operator $\Omega_n^{(N_R)}(t)$ is set at $t_S = 4$ ($\beta = 1.80, 1.95$) and $t_S = 6$ ($\beta = 2.10$) to reduce effects from the temporal boundary. To avoid effects from excited states the reference time for the diagonalization is fixed large value as $t_0 = 10, 12$ and 16 at $\beta = 1.80, 1.95$ and 2.10, respectively.

We estimate the errors of the four-point functions and pion propagators by the jackknife method. In our study of the light hadron spectrum [2], we have shown that the separation

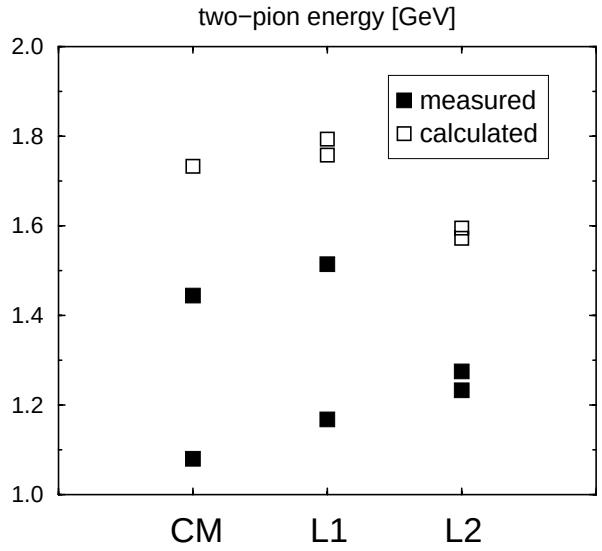

Figure 11: Center of mass energy of two-pion calculated for each system, which is evaluated with $m_\pi/m_\rho \approx 0.6$ at $\beta = 2.10$ without the interaction. We measure the scattering phase shifts at the momentum state with the closed symbols. The open symbols are used only to examine the effect of the state cut-off for the diagonalization.

of 50 trajectories covers all the autocorrelations of the configuration, so that in the present analysis we also use bins of 50 trajectories in the jackknife method. In the actual analysis bin size of 5 or 10 ($\beta = 2.10$ at the lightest quark mass) measurements are employed, because we skip 10 or 5 trajectories between two measurements.

At $\beta = 1.80$ for the lightest quark mass to reduce the statistical error we calculate extra measurements with the same configurations where the temporal origin is shifted to $t = T/2$. At this parameter we use the averaged value of the normal and extra measurements for the analysis.

To extract the phase shift in various momenta we choose the center of mass system and two laboratory systems denoted as CM, L1 and L2, respectively. These systems are described in Sec. 7.2. The total momentum $\mathbf{P}$ and the momentum set for the pion four-point function are summarized in Table III. The cut-off of the state N for the pion four-point function is chosen as $N = 2$ in the CM system and $N = 3$ in the two laboratory systems.

In Fig. 11 we display the center of mass energy without the interaction for the smallest pion mass at $\beta = 2.10$ in the three systems. As shown in the figure we know that the energies of the $n = 2$ and $n = 3$ states in both the laboratory systems are very close. This is the reason that we choose the cut-off $N = 3$ in both the laboratory systems. It is noted that in the L2 system the energies for the ground and first excited states are also close. In all systems the phase shift is obtained from the ground and first excited states, and other higher states are used to investigate the effects of N.

β	$L^3 \times T$	$c_{\rm SW}$	a [fm]	La [fm]	κ	$m_{\rm PS}/m_{\rm V}$	$N_{\rm Traj}$	$N_{\rm Skip}$	$N_{\rm Meas}$
1.80	$12^3 \times 24$	1.60	0.2150(22)	2.580(26)	0.1409	0.807(1)	6530	10	645
					0.1430	0.753(1)	5240	10	520
					0.1445	0.694(2)	7350	10	725
					0.1464	0.547(4)	5250	10	405†
1.95	$16^3 \times 32$	1.53	0.1555(17)	2.489(27)	0.1375	0.804(1)	7000	10	595
					0.1390	0.752(1)	7000	10	690
					0.1400	0.690(1)	7000	10	685
					0.1410	0.582(3)	5000	10	495
2.10	$24^3 \times 48$	1.47	0.1076(13)	2.583(31)	0.1357	0.806(1)	4000	10	395
					0.1367	0.755(2)	4000	10	390
					0.1374	0.691(3)	4000	10	380
					0.1382	0.576(3)	4000	5	640

Table III: Simulation parameters. The dagger symbol denotes that we average two measurements on the same configuration, where one is calculated with the temporal origin located at $t = 0$ and the other located at $t = T/2$. The lattice spacing a is fixed by the vector meson mass at the physical pion mass and $m_\rho = 768.4$ MeV. The $N_{\rm Traj}$ is the number of all trajectories, $N_{\rm Skip}$ is the number of separation between two measurements and $N_{\rm Meas}$ is the number of the configurations used the measurements.

8 Results

In this section we present the result of the isospin $I = 2$ S-wave $\pi\pi$ scattering phase shift calculated by the finite volume and the diagonalization methods, which are described the above sections. We examine the effect of the diagonalization by comparing the pion four-point functions before and after the diagonalization. We present the result of the scattering length, which is defined by the phase shift at the threshold, and that of the phase shift at each lattice spacing and in the continuum limit.

8.1 Effect of diagonalization

In Fig. 12 we display the several pion four-point functions defined by eq.(232) in each system. The figure shows the data at $\beta = 2.10$ for $m_\pi/m_\rho \approx 0.6$. The open symbols refer to the data of a negative value. In all systems the off-diagonal parts $G_{nm}(t)$ $(n \neq m)$ are not negligible comparing with the diagonal parts $G_{nm}(t)$ $(n = m)$. The pion four-point functions in the CM and L1 systems have similar behaviors. In the L2 system $G_{00}(t)$ is almost overlaid by $G_{11}(t)$ for all t, because these energies are very close. The figure also shows that the off-diagonal parts are symmetric under the exchange of the indices in each system, so that we employ the averaged value of the symmetric four-point functions for the diagonalization.

In order to investigate the effect of the diagonalization we define the two ratios $R_n(t)$ and $D_n(t)$ in each system as follows

$$R_n(t) = \frac{G_{nn}(t)}{G^\pi_{1,n}(t)G^\pi_{2,n}(t)}, \tag{245}$$

$$D_n(t) = \lambda_n(t,t_0)\frac{G^\pi_{1,n}(t_0)G^\pi_{2,n}(t_0)}{G^\pi_{1,n}(t)G^\pi_{2,n}(t)}, \tag{246}$$

where $G^\pi_{i,n}(t)$ is the i-th pion propagator for the n-th energy state, and $\lambda_n(t,t_0)$ is the n-th eigenvalue obtained by the diagonalization of the matrix $M(t,t_0)$ given in eq.(243). If the pion four-point function is constructed by a single exponential function, the ratio $R_n(t)$ behaves as

$$R_n(t) = A \cdot \exp(-\Delta\overline{E}^{\mathbf{P}}_n(t - t_S)), \tag{247}$$

where A is a constant and $\Delta\overline{E}^{\mathbf{P}}_n \equiv \overline{E}^{\mathbf{P}}_n - E^{\mathbf{P}}_n$, $\overline{E}^{\mathbf{P}}_n$ and $E^{\mathbf{P}}_n$ are the two-pion energy with and without the interaction in the system with the total momentum $\mathbf{P}$, respectively. If the cut-off of the state for the diagonalization is sufficiently large, the ratio $D_n(t)$ behaves as

$$D_n(t) = \exp(-\Delta\overline{E}^{\mathbf{P}}_n(t - t_0)). \tag{248}$$

In these cases we expect to extract the n-th energy shift $\Delta\overline{E}^{\mathbf{P}}_n$ from the ratios $R_n(t)$ and $D_n(t)$ by a single exponential fit.

First we focus on the results in the CM system. For the ground state $n = 0$ the ratios $R_0(t)$ and $D_0(t)$ at all β for all m_π/m_ρ are presented in Fig. 13. In the following figures the ratio $D_n(t)$ is normalized by $D_n(t_S)$ for comparing with $R_n(t)$. The cut-off of the state N for the diagonalization is chosen as $N = 2$. The diagonalization does not affect the result of the ground state, so that we can extract the two-pion energy shift without the diagonalization. We also check that the result is independent of the choice of $N = 1$ and 2.

In contrast to the case of the ground state the diagonalization is very effective for the first excited state $n = 1$ as shown in Fig. 14. The ratio $R_1(t)$ rapidly increases at large t, while the behavior cannot be shown in $D_1(t)$. Hence we can obtain the two-pion energy shift from $D_1(t)$ by a single exponential fit. We confirm that the cut-off N dependence of $D_1(t)$ is negligible by comparing with $N = 1$ and $N = 2$ in the figure. For the smaller pion mass the diagonalization effect is larger, and $D_1(t)$ is noisier. We also observe that some data of $D_1(t)$ have strange behaviors at large t. We consider that the behavior is caused by the statistics, and larger statistics are needed to reduce the behavior.

The behaviors of the ratios in the L1 system are similar to those in the CM system as shown in Figs. 15 and 16 for the ground $n = 0$ and first excited $n = 1$ states, respectively. For the ground state $R_0(t)$ agrees with $D_0(t)$ with $N = 3$. This indicates that the phase shift with $\overline{p} \neq 0$ can be extracted without the diagonalization from the calculation of the ground state. On the other hand the diagonalization is effective for the first excited state . We also show that the independence of the cut-off for $D_1(t)$ in Fig. 16. Since $D_1(t)$ at $\beta = 1.95$ and 2.10 for $m_\pi/m_\rho \approx 0.6$ do not show good exponential behaviors, the phase shifts extracted from these states are excluded from the final extrapolations.

Finally we focus on the L2 system. The results in this system are essentially different from those in the other systems. The ratios $R_n(t)$ and $D_n(t)$ for the ground $n = 0$ and first excited $n = 1$ states are shown in Figs. 17 and 18, respectively. Since the $n = 0$ and 1 states have the similar energies in the non-interacting case as shown in Fig. 11, not only the result of the $n = 1$ state but also that of the $n = 0$ state are affected by the diagonalization. In each figure we also show that the results for both the states are unchanged with the cut-off $N = 1$ and 2. Since $D_n(t)$ for the $n = 0, 1$ states at $\beta = 1.95$ in $m_\pi/m_\rho \approx 0.6$ are not clear exponential behavior, the results for these states are dropped from the final extrapolations.

In order to show the effect of the diagonalization in the L2 system clearly, we gather the ratios $R_n(t)$ and $D_n(t)$ for the $n = 0, 1$ states to Fig. 19. The data at $\beta = 2.10$ for $m_\pi/m_\rho \approx 0.6$ is shown in the figure. Before the diagonalization the ratios $R_n(t)$ have almost same shapes, while after the diagonalization the ratio $D_n(t)$ for the $n = 0$ state increases and the one for the $n = 1$ state decreases. The behavior can be understood by considering a simple eigenvalue problem of two degenerate states. We consider that the two states correspond to the $n = 0, 1$ states in the L2 system, and we approximate that both the states have the same energy E_0 in the non-interacting case. The Hamiltonian H is changed by the two-pion interaction as,

$$H = \begin{pmatrix} E_0 + \Delta & \beta \\ \beta & E_0 + \Delta \end{pmatrix}, \tag{249}$$

where $H_{nm} \equiv \langle \Omega_n | H | \Omega_m \rangle$ with the n-th non-interacting two-pion state $|\Omega_n\rangle$, and Δ and β are the interaction effects. The Δ corresponds to the slopes of $R_n(t)$ in Fig. 19. The eigenvalues $\overline{E}$ of H are given by

$$\overline{E} = E_0 + \Delta \pm \beta. \tag{250}$$

Therefore the energy eigenvalues split. The $\Delta \pm \beta$ correspond to the slopes of $D_n(t)$ for the $n = 0, 1$ states in the figure.

In the CM system we determine the two-pion energy $\overline{E}_n$ from the energy shift $\Delta\overline{E}_n^{\mathbf{P}}$ extracted by a single exponential fit for $D_n(t)$ with $\overline{E}_n = \Delta\overline{E}_n^{\mathbf{P}} + E_n$ where E_n is the two-pion energy in the free case. We evaluate the center of mass momentum $\overline{p}_n^2$ using $\overline{E}_n$. In the same manner, we can determine the two-pion energy $\overline{E}_{n,L}$ in the laboratory systems from the energy shift $\Delta\overline{E}_n^{\mathbf{P}}$ extracted from $D_n(t)$ with $\overline{E}_{n,L} = \Delta\overline{E}_n^{\mathbf{P}} + E_{n,L}$. Using $\overline{E}_{n,L}$ we

evaluate the center of mass momentum as $\overline{p}_n^2 = (\overline{E}_{n,L}^2 - \mathbf{P}^2)/4 - m_\pi^2$. We then can obtain the phase shift $\delta(\overline{p}_n)$ by substituting $\overline{p}_n^2$ in the finite volume formulae eqs.(223) and (228). The results for $\Delta\overline{E}_n^{\mathbf{P}}$, $\overline{p}_n^2$, $\delta(\overline{p}_n)$, and the fitting ranges in all systems for the $n = 0, 1$ states are summarized in Appendix D. To extrapolate the phase shift from the calculating points to the physical pion mass $m_\pi = 0.14$ GeV, we define the 'scattering amplitude' as,

$$A(m_\pi, \overline{p}) = \frac{\tan\delta(\overline{p})}{\overline{p}} \cdot \frac{\overline{E}}{2}. \tag{251}$$

The $A(m_\pi, \overline{p})$ is normalized by

$$\lim_{\overline{p}\to 0} A(m_\pi, \overline{p}) = a_0 m_\pi, \tag{252}$$

where a_0 is the scattering length. In the tables we also list the results of the amplitudes.

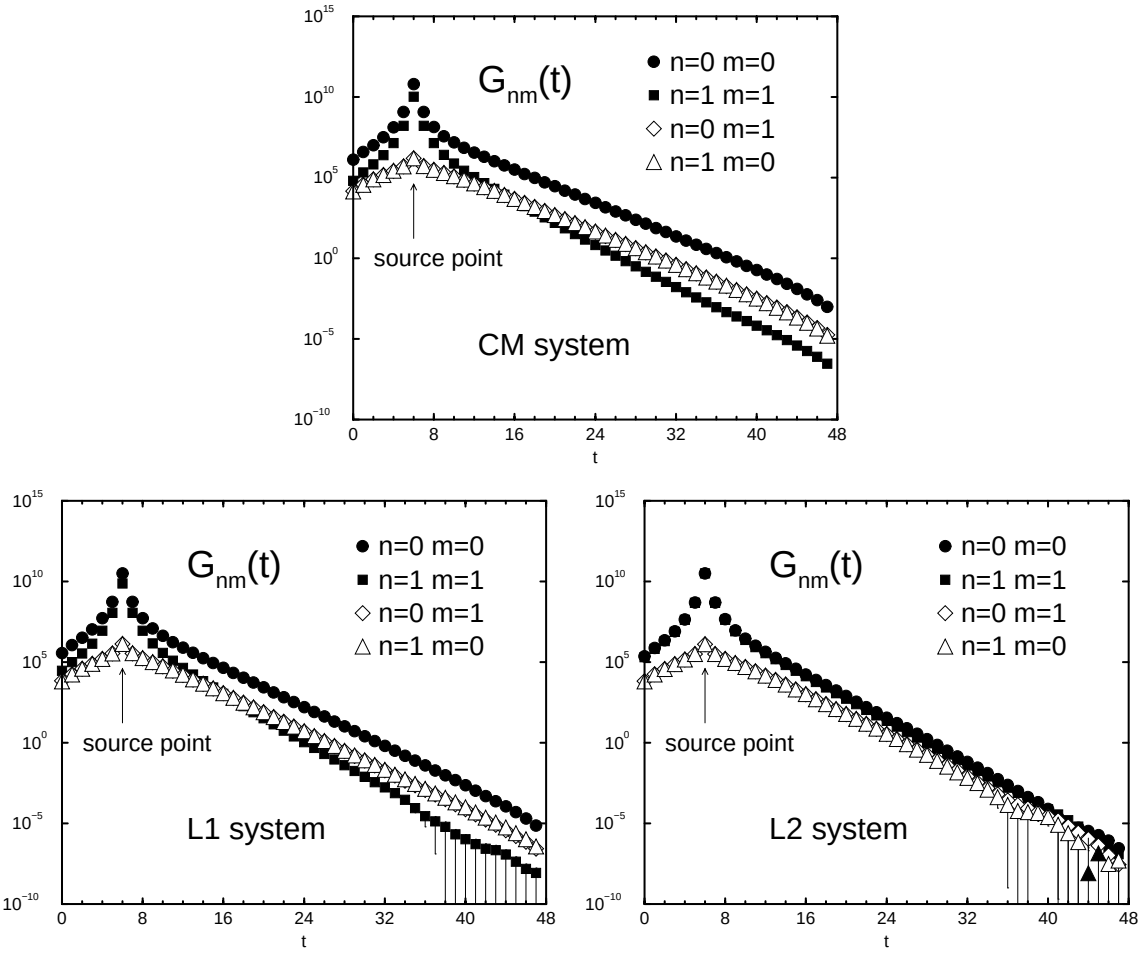

Figure 12: Typical pion four-point function $G_{nm}(t)$ at the center of mass system CM and two laboratory systems L1 and L2 at $\beta = 2.10$ for $m_\pi/m_\rho \approx 0.6$. Filled symbols denote positive values, while open symbols denote negative ones. Triangle symbol almost overlays with the diamond one.

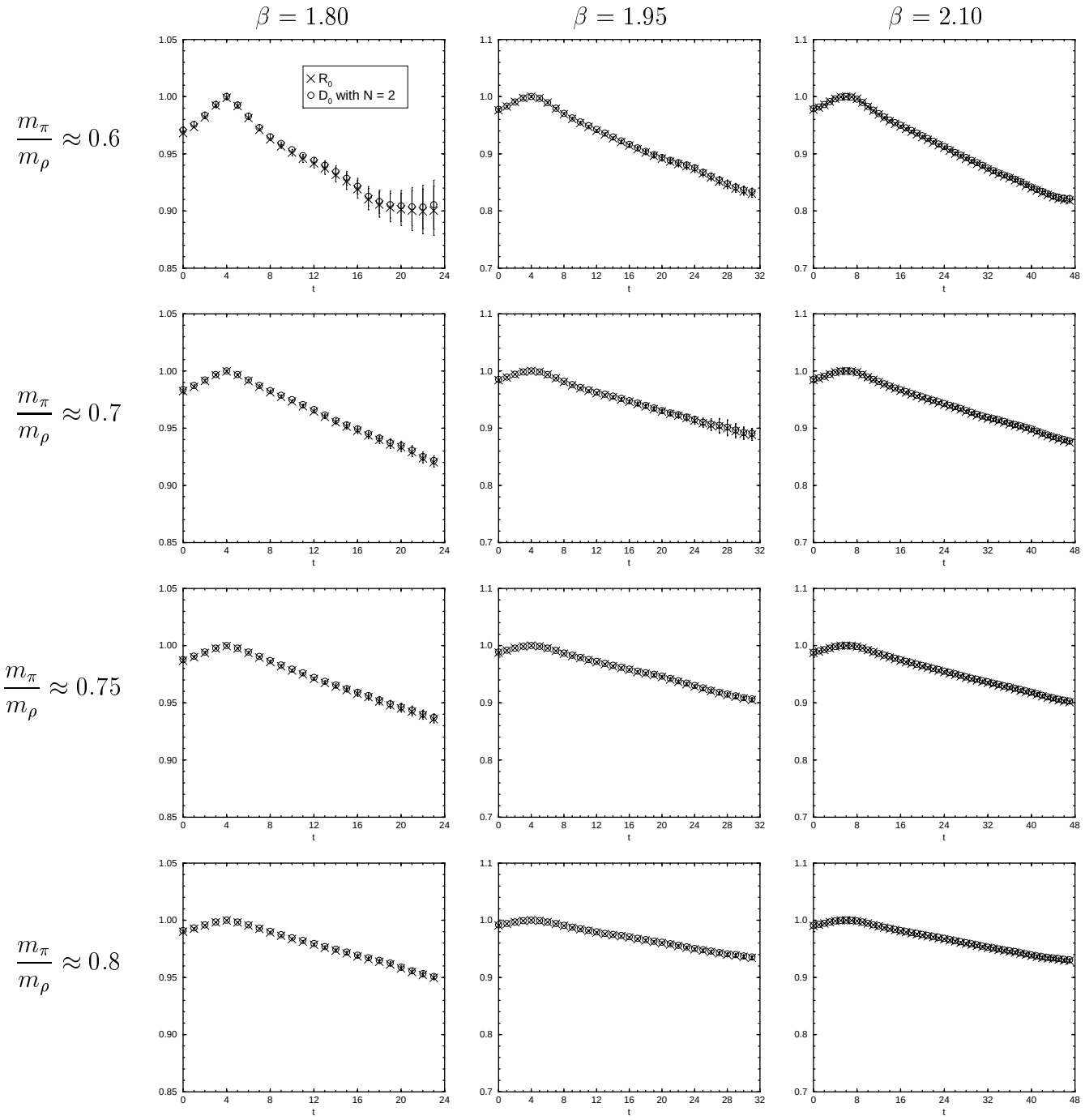

Figure 13: Ratios $R_n(t)$ and $D_n(t)$ for $n = 0$ state in the center of mass system CM with energy state cut-off $N = 2$. The m_π/m_ρ increases from top to bottom, while β increases from left to right.

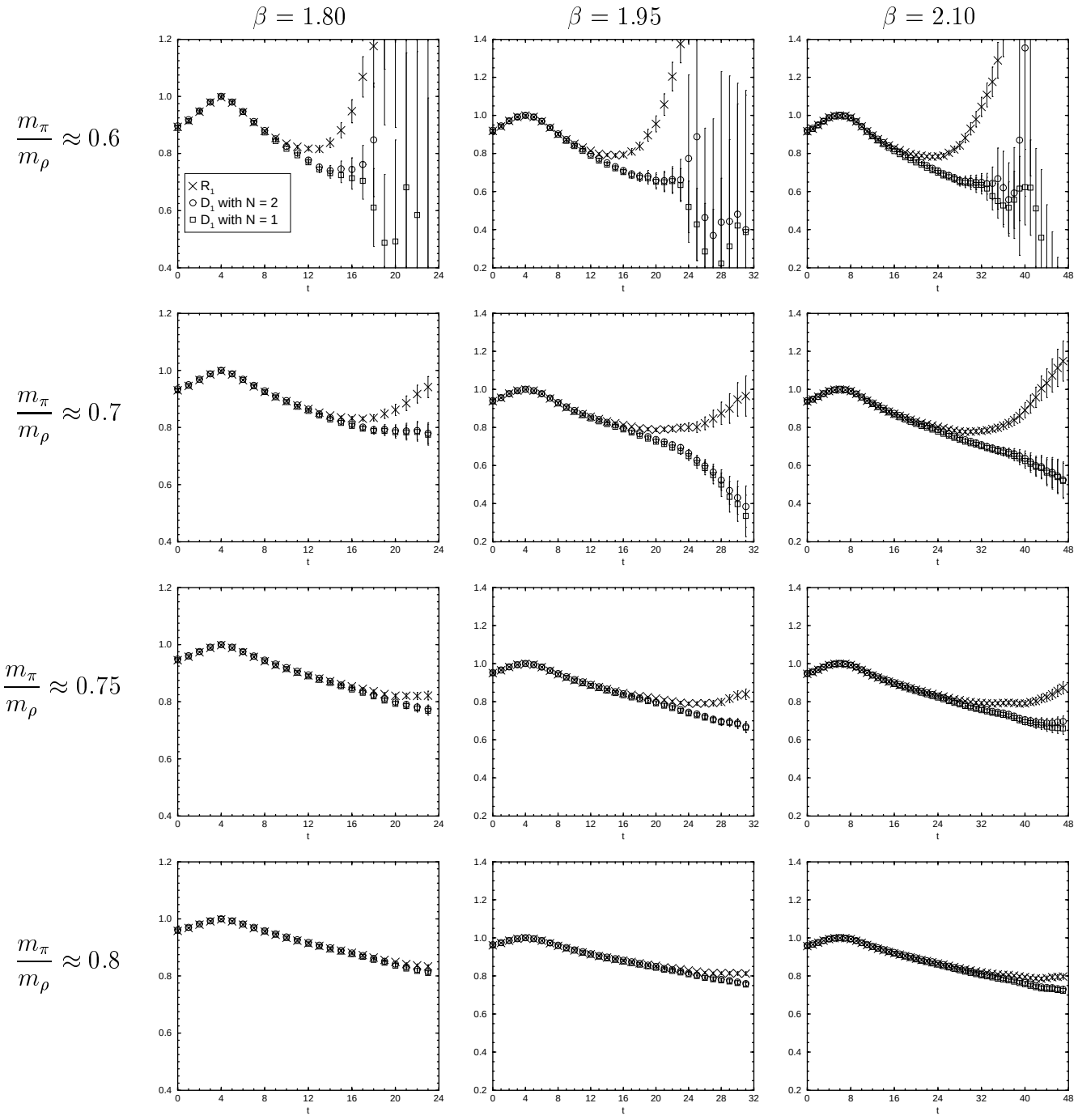

Figure 14: Ratio $R_n(t)$ and $D_n(t)$ for $n = 1$ state in the center of mass system CM with energy state cut-off $N = 1, 2$. The m_π/m_ρ increases from top to bottom, while β increases from left to right.

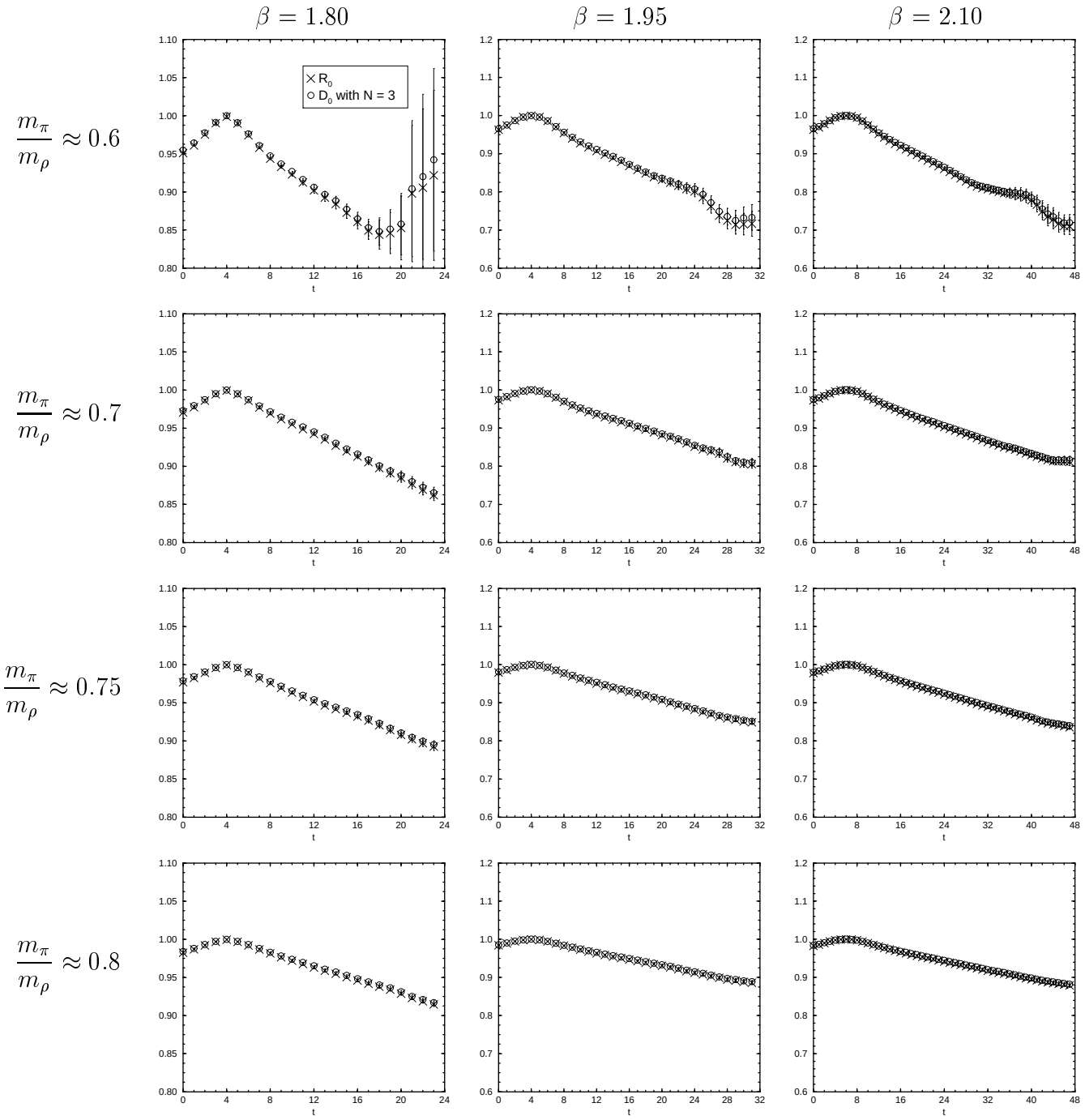

Figure 15: Ratio $R_n(t)$ and $D_n(t)$ for $n = 0$ state in the laboratory system L1 with energy state cut-off $N = 3$. The m_π/m_ρ increases from top to bottom, while β increases from left to right.

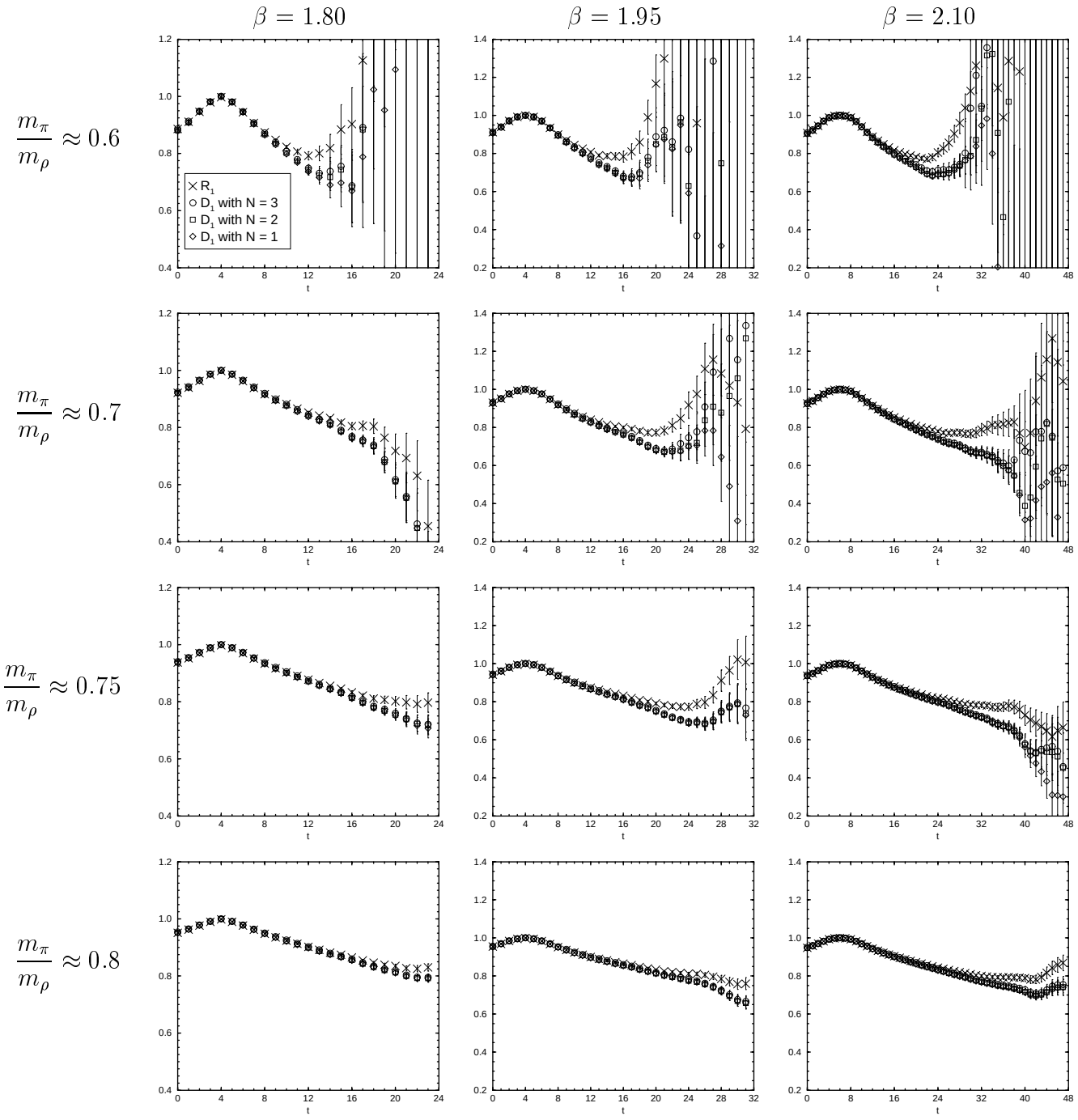

Figure 16: Ratio $R_n(t)$ and $D_n(t)$ for $n = 1$ state in the laboratory system L1 with energy state cut-off $N = 1$–3. The m_π/m_ρ increases from top to bottom, while β increases from left to right.

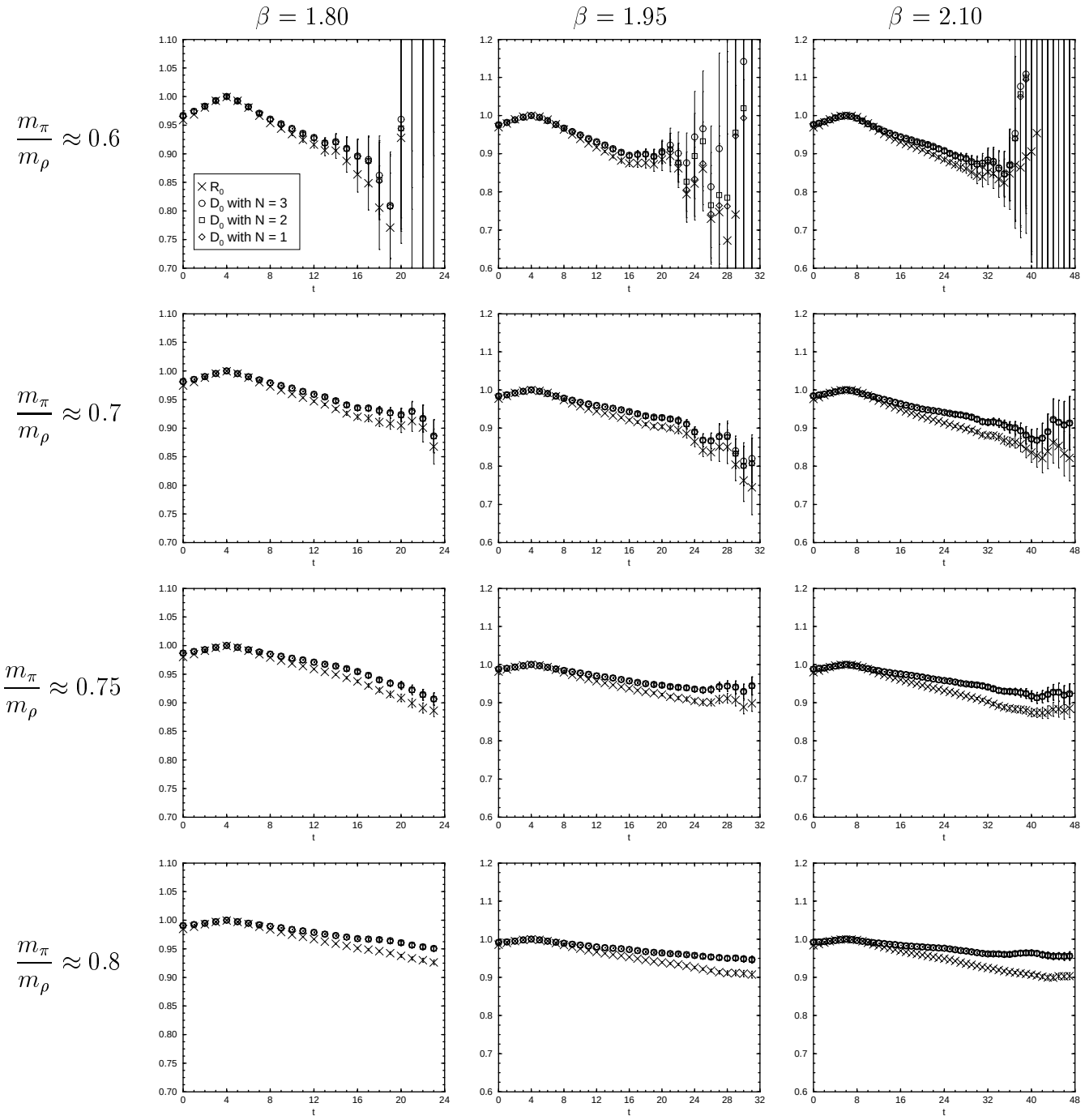

Figure 17: Ratio $R_n(t)$ and $D_n(t)$ for $n = 0$ state in the laboratory system L2 with energy state cut-off $N = 1$–3. The m_π/m_ρ increases from top to bottom, while β increases from left to right.

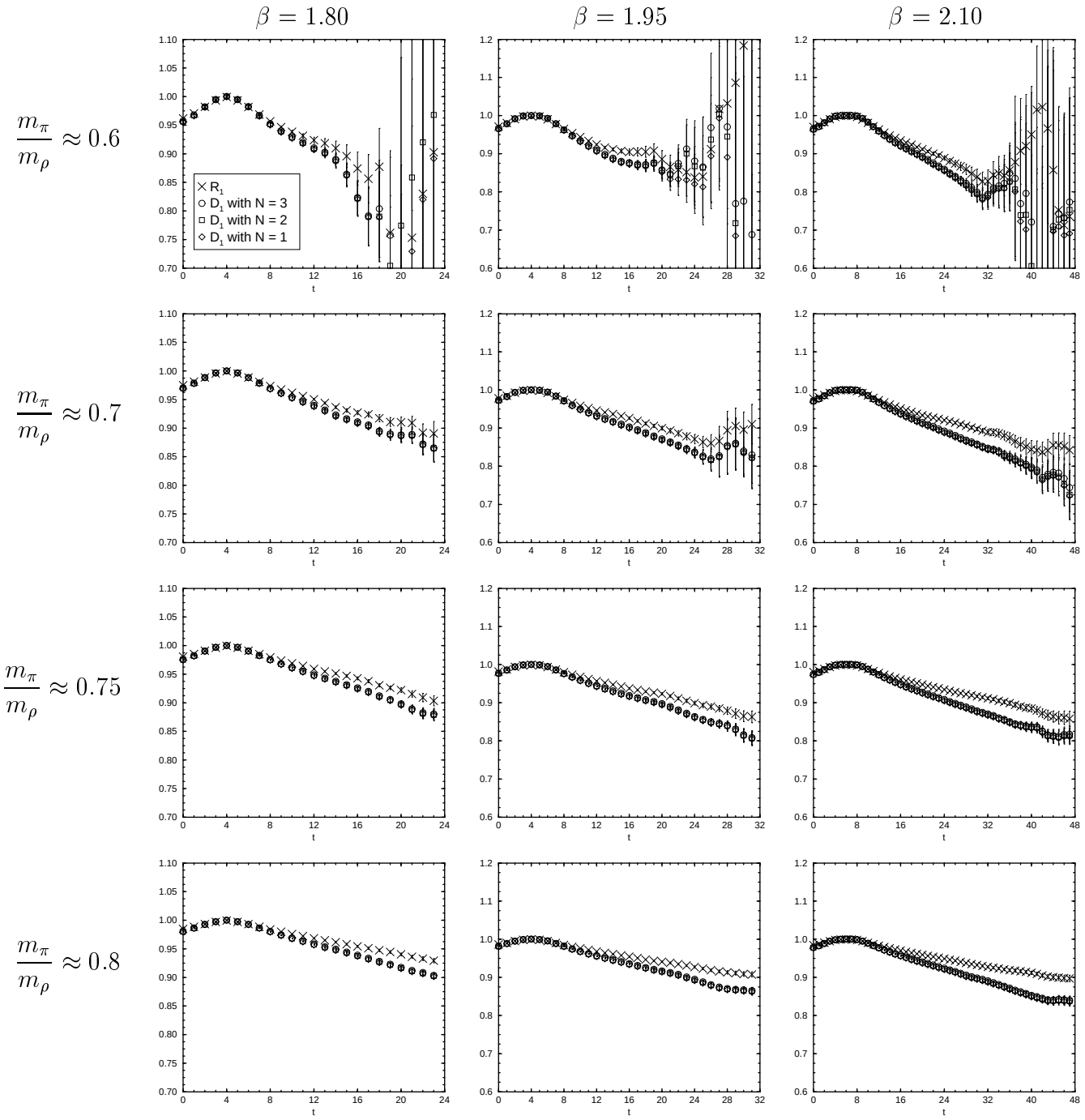

Figure 18: Ratio $R_n(t)$ and $D_n(t)$ for $n = 1$ state in the laboratory system L2 with energy state cut-off $N = 1$–3. The m_π/m_ρ increases from top to bottom, while β increases from left to right.

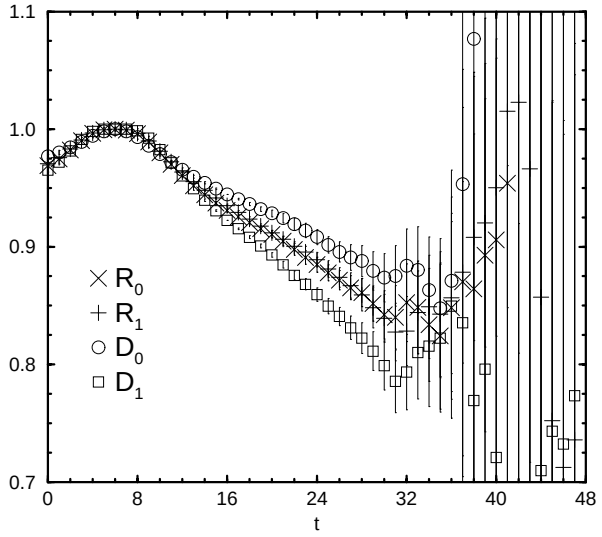

Figure 19: Ratios before $R_n(t)$ and after $D_n(t)$ the diagonalization for $n = 0$ and 1 states in the laboratory system L2 with energy state cut-off $N = 3$ at $\beta = 2.10$ for $m_\pi/m_\rho \approx 0.6$.

8.2 Result for scattering length

Since in the CM system the momentum $\overline{p}^2$ of the ground state is approximately zero, the scattering length a_0 is evaluated from the scattering amplitude defined by eq.(251) for the ground state in the CM system as $A(m_\pi, \overline{p}) \approx a_0 m_\pi$. We plot a_0/m_π as a function of m_π^2 at each β in Fig. 20. These values are tabulated in Appendix D. In the figure the large curvature exists at large β. The curvature has not been observed clearly in the previous quenched works [14, 19], as shown in Fig. 21. Due to the curvature it is not sufficient to assume a linear function for the chiral extrapolation, so that we try to fit the data with various fitting assumptions to extrapolate the scattering length to the physical pion mass $m_\pi = 0.14$ GeV.

The prediction of chiral perturbation theory (ChPT) for the scattering length at one loop order is given by Gasser and Leutwyler [32] as

$$\frac{a_0}{m_\pi} = -\frac{1}{16\pi F^2}\left\{1 - \frac{m_\pi^2}{16\pi^2 F^2}\left[L(\mu) - C_L \log\frac{m_\pi^2}{\mu^2}\right]\right\}, \tag{253}$$

where F is the pseudoscalar decay constant in the chiral limit, $L(\mu)$ is a low energy constant at a scale μ, and $C_L = 7/2$. The scale μ is fixed at 1 GeV for simplicity. When we choose F as the value in the chiral limit calculated on lattice [2], which is tabulated in Table IV, the fit with one free parameter $L(\mu)$ gives much large χ^2/d.o.f. at all β. We consider that the failure of the fit is caused by the data with $m_\pi > 0.5$ GeV and a finite lattice spacing effect in our simulation, because eq.(253) is the prediction in a small pion mass region and in the continuum limit. We also attempt to fit the data with the three parameters $F, L(\mu)$ and C_L. The results are summarized in Table V. While the values of C_L differ from the prediction of ChPT, $C_L = 7/2$, the values of F are reasonably consistent with the measured decay constants in the chiral limit at all β.

We also note about the chirality breaking effect in the scattering length with Wilson type quark action. The breaking effect causes a divergence in the chiral limit for the scattering

length [67]. The chirality breaking effect depends on the lattice spacing and should vanish in the continuum limit. We employ an improved Wilson quark action in this work and expect that the effect is small at our simulation parameters. In order to check this expectation we attempt to fit with

$$\frac{a_0}{m_\pi} = \frac{A_{00}}{m_\pi^2} + A_{10} + A_{20} m_\pi^2. \tag{254}$$

We tabulate the fit results in Table VI. The coefficient of the divergent term A_{00} increases as β increases against our expectation. We consider that the effect of the chiral breaking is not completely separated from the physical m_π^2 dependence with the fitting form in this work, if the effect exists. More detailed investigation of the effect is an important future work.

We fit the data by assuming a polynomial function in m_π^2

$$a_0/m_\pi = A_{10} + A_{20} m_\pi^2 + A_{30} m_\pi^4. \tag{255}$$

The fit result is also shown in Fig. 20 and summarized in Table VII. At $\beta = 2.10$ χ^2/d.o.f. takes the large value. This means that higher order terms, such as $A_{40} m_\pi^6$, are needed to obtain a more reasonable fit result at $\beta = 2.10$. Since we calculate the scattering length at only the four points for the pion mass, such a fitting cannot be carried out in this work.

For the following analysis we define the quantity

$$\frac{a_0^f}{m_\pi} = \left(\frac{f_\pi^{lat}}{f_\pi}\right)^2 \frac{a_0}{m_\pi}, \tag{256}$$

where f_π^{lat} is the pseudoscalar decay constant at each m_π measured on lattice, and $f_\pi = 93$ MeV. In Refs. [11, 12, 13] the authors found that the m_π dependence for a_0^f/m_π is small. In order to check the independence we plot a_0^f/m_π in Fig. 22. The values are tabulated in Appendix D denoted as $A^f(m_\pi, \overline{p})/m_\pi^2$. In the evaluation only the center value of f_π^{lat} is employed and its error is ignored, which are compiled in Table IV. We find that a_0^f/m_π is almost independent of m_π^2. This implies the strong correlation between the scattering length and decay constant measured on lattice. We carry out a constant fit for a_0^f/m_π. The results are also plotted in the figure and compiled in Table VIII. The fit gives reasonable values of χ^2/d.o.f. at all β in contrast to the polynomial fit eq.(255).

For the continuum extrapolation, we employ $a_0 m_\pi$ at the physical pion mass for the polynomial fit eq.(255) and a_0^f/m_π. The fitting results are shown in Fig. 23 and tabulated in Table IX. In the continuum limit the results are compared with the prediction of ChPT [25]: $a_0 m_\pi = -0.0444(10)$ denoted by the star symbol in the figure. We can show that the $O(a)$ effects are large in both the results, and the difference of them becomes to be smaller with the lattice spacing decreasing. The $O(a)$ effect of $a_0^f m_\pi$ is opposite to that of $a_0 m_\pi$ due to the large $O(a)$ effect of $(f_\pi^{lat})^2$.

As shown in Fig. 23 $a_0^f m_\pi$ in the continuum limit is closer to the prediction of ChPT than the other. But we should note about the decay constant which is introduced to cancel out the m_π dependence of the scattering length. From the values of f_π^{lat} tabulated in Table IV, the decay constant in the continuum limit does not seem to be consistent with the experiment $f_\pi = 93$ MeV. This causes the large uncertainty for the scattering length evaluated from a_0^f in the continuum limit. One of the possible reasons for the inconsistency is the renormalization factor of the axial vector current evaluated with perturbation theory, so that a way of avoiding the uncertainty the determination of the renormalization factor with non-perturbative method. Another way to obtain a reliable scattering length is calculation

in closer to the physical pion mass. These are important future works. Here we present on following two results estimated by a_0 and a_0^f as our results of scattering length.

$$a_0 m_\pi = -0.0558(56) \quad (257)$$
$$a_0^f m_\pi = -0.0413(28) \quad (258)$$

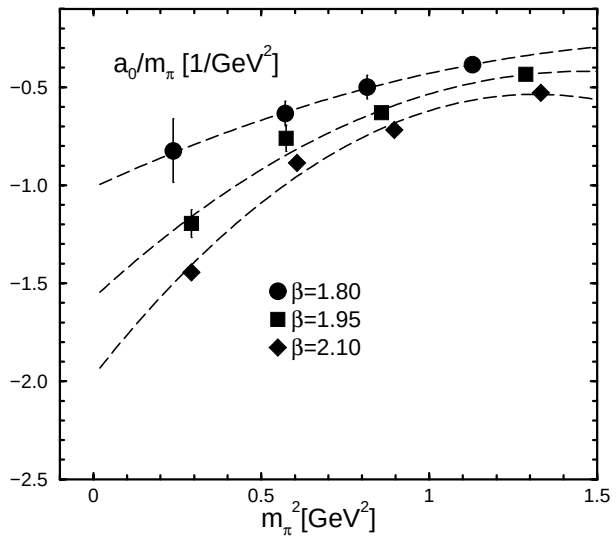

Figure 20: $I = 2$ $\pi\pi$ scattering length a_0/m_π GeV^{-2} at each β and the fitting lines with a polynomial form.

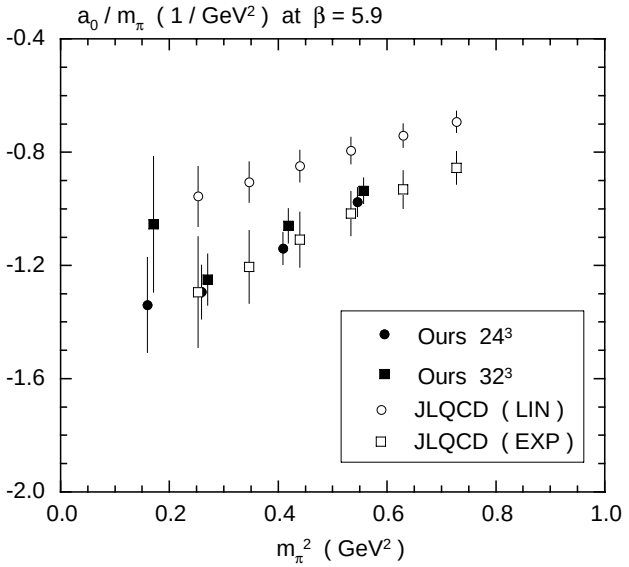

Figure 21: Previous results for $I = 2$ $\pi\pi$ scattering length a_0/m_π GeV^{-2} at $\beta = 2.10$. Open symbols are JLQCD results [14], and closed symbols are CP-PACS results [19].

$\beta = 1.80$		$\beta = 1.95$		$\beta = 2.10$	
m_π^2 [GeV^2]	f_π^{lat} [GeV]	m_π^2 [GeV^2]	f_π^{lat} [GeV]	m_π^2 [GeV^2]	f_π^{lat} [GeV]
1.128(1)	0.2516(11)	1.287(1)	0.2190(16)	1.331(2)	0.1959(19)
0.814(1)	0.2279(14)	0.857(1)	0.1908(15)	0.896(1)	0.1739(21)
0.571(1)	0.1999(11)	0.573(1)	0.1650(14)	0.605(2)	0.1540(22)
0.238(1)	0.1613(15)	0.291(2)	0.1381(21)	0.291(1)	0.1214(19)
$(m_\pi^{phys})^2$	0.1287(33)	$(m_\pi^{phys})^2$	0.1054(47)	$(m_\pi^{phys})^2$	0.0895(45)
chiral limit	0.1260(31)	chiral limit	0.1032(47)	chiral limit	0.0869(46)

Table IV: Pseudoscalar decay constant f_π^{lat} measured on lattice [2]. Here $m_\pi^{phys} = 0.14$ GeV.

β	F [GeV]	$L(\mu)$	C_L	χ^2/d.o.f.	$m_\pi = 0.14$ [GeV]
1.80	0.135(20)	1.74(15)	0.70(77)	0.04	$-1.04(40)$
1.95	0.1036(59)	1.199(72)	0.765(85)	1.55	$-1.76(20)$
2.10	0.0909(24)	0.963(28)	0.702(29)	4.78	$-2.26(11)$

Table V: Results of the fit for the scattering length a_0/m_π with eq.(253). The results at the physical pion mass are also displayed.

β	A_{00}	A_{10} [1/GeV^2]	A_{20} [1/GeV^4]	χ^2/d.o.f.
1.80	$-0.033(89)$	$-0.78(29)$	0.37(20)	0.09
1.95	$-0.184(57)$	$-0.63(18)$	0.26(12)	0.53
2.10	$-0.273(35)$	$-0.55(12)$	0.169(83)	0.55

Table VI: Results of the fit for the scattering length a_0/m_π with a divergent form $A_{00}/m_\pi^2 + A_{10} + A_{20}m_\pi^2$.

β	A_{10} [1/GeV^2]	A_{20} [1/GeV^4]	A_{30} [1/GeV^6]	χ^2/d.o.f.	$m_\pi = 0.14$ [GeV]
1.80	$-1.01(29)$	0.79(76)	$-0.20(46)$	0.02	$-0.99(28)$
1.95	$-1.57(14)$	1.58(33)	$-0.54(18)$	2.1	$-1.54(13)$
2.10	$-1.975(82)$	2.18(20)	$-0.82(11)$	8.2	$-1.932(78)$

Table VII: Results of the polynomial fit for the scattering length a_0/m_π. The results at the physical pion mass are also displayed.

β	a_0^f/m_π [1/GeV^2]	χ^2/d.o.f.
1.80	$-2.83(13)$	0.27
1.95	$-2.543(73)$	0.92
2.10	$-2.449(40)$	0.54

Table VIII: Results of a constant fit for $a_0^f/m_\pi = (f_\pi^{lat}/f_\pi)^2 a_0/m_\pi$, where f_π^{lat} is the pseudoscalar decay constant at each m_π measured on lattice, and $f_\pi = 93$ MeV.

	A	B [GeV]	χ^2/d.o.f.
$a_0 m_\pi$	$-0.0558(56)$	$0.0328(86)$	0.02
$a_0^f m_\pi$	$-0.0413(28)$	$-0.0119(43)$	0.65

Table IX: Results of the continuum extrapolations for the two scattering lengths as a function $A + aB$. Here $f_\pi = 93$ MeV.

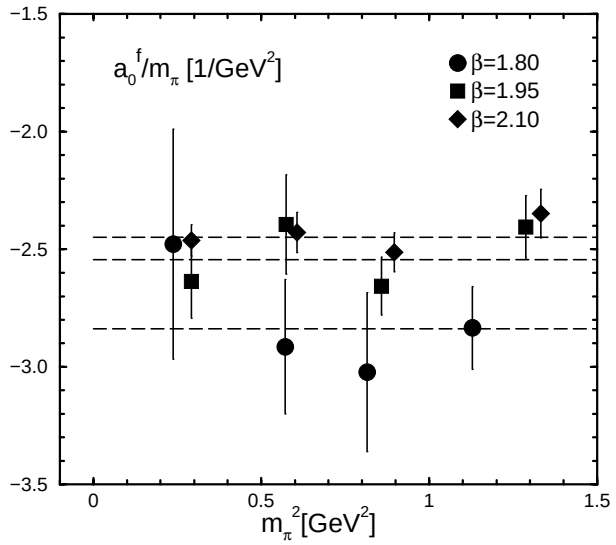

Figure 22: Scattering length $a_0^f/m_\pi = (f_\pi^{lat}/f_\pi)^2 a_0/m_\pi$ with $f_\pi = 93$ MeV at each β and results of a constant fit (dashed lines).

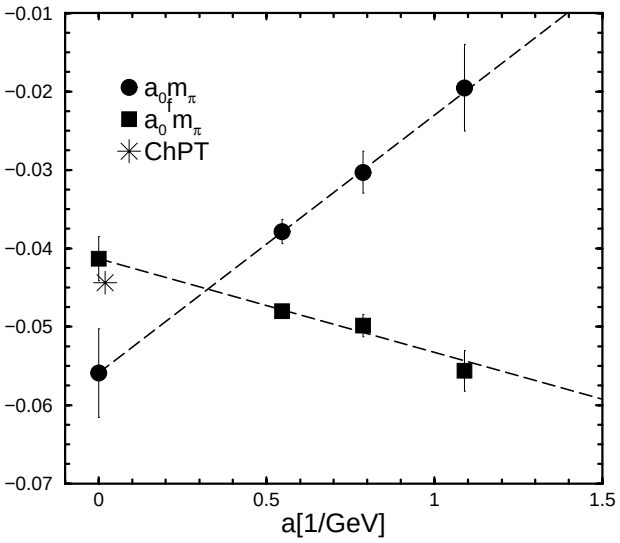

Figure 23: Continuum extrapolations for the scattering length a_0/m_π and a_0^f/m_π with $f_\pi = 93$ MeV at the physical pion mass $m_\pi = 0.14$ GeV.

8.3 Result for scattering phase shift

In order to obtain the phase shift in the continuum limit at the physical pion mass $m_\pi = 0.14$ GeV, we extrapolate the scattering amplitude $A(m_\pi, \overline{p})$ defined by eq.(251). The amplitude is plotted in Fig. 24 and tabulated in Appendix D. The CM_n in the top left figure refers to the amplitude obtained from the n-th state in the CM system, and the $\mathrm{L1}_n$ and $\mathrm{L2}_n$ to those in each laboratory system. The ordering of the amplitude, CM_0, $\mathrm{L1}_0$, $\mathrm{L2}_0$, $\cdots$, CM_1 and $\mathrm{L1}_1$, in the other figures is same as that in the top left figure. Note that we have three points between the two CM data. This shows the improvement of the momentum sampling without changing the lattice size. The open symbols in the figures are excluded from the following analysis, since $D_n(t)$ does not show a good exponential behavior as discussed in Sec. 8.1.

The statistical error of the amplitude is larger for the larger momentum, except for the L2 system. This is because in the L2 system the error of the energy shift $\Delta\overline{E}_n^{\mathbf{P}}$ for the ground state is larger than that for the first excited state as shown in Appendix D.

We extrapolate the amplitude $A(m_\pi, \overline{p})$ to the physical pion mass by a polynomial fit of m_π^2 and $\overline{p}^2$ at fixed β as

$$A(m_\pi, \overline{p}) = A_{10} m_\pi^2 + A_{20} m_\pi^4 + A_{30} m_\pi^6 + A_{01} \overline{p}^2 + A_{11} m_\pi^2 \overline{p}^2 + A_{21} m_\pi^4 \overline{p}^2. \tag{259}$$

Here the momentum independent terms correspond to the scattering length $a_0 m_\pi$. The fit results are also displayed in Fig. 24 and Table X. We find a reasonable fit to the data for both the CM and two laboratory systems. We also find that χ^2/d.o.f. at $\beta = 2.10$ is not so large in contrast to the polynomial fit for the scattering length in Sec. 8.2.

In order to check the reliability of the result, we also analyze the amplitude normalized by the pseudoscalar decay constant measured on lattice f_π^{lat} as

$$A^f(m_\pi, \overline{p}) = \left(\frac{f_\pi^{lat}}{f_\pi} \right)^2 \cdot A(m_\pi, \overline{p}). \tag{260}$$

The values of $A^f(m_\pi, \overline{p})$ are also presented in appendix D. For the calculation of $A^f(m_\pi, \overline{p})$ we use $f_\pi = 93$ MeV and only the center value of f_π^{lat}, which is tabulated in Table IV. Since as shown in Fig. 22 the normalization decreases the pion mass dependence of the scattering length, we employ the fit function eq.(259) with $A_{20} = A_{30} = A_{21} = 0$ for the extrapolation of $A^f(m_\pi, \overline{p})$. The results are tabulated in Table XI. We find that χ^2/d.o.f. is reasonable at all β, and the error of the parameter is reasonable small.

In order to obtain the amplitudes at several momenta $\overline{p}$ in the continuum limit, we employ the following procedure: At first we get the amplitudes at the physical pion mass $A(\overline{p}) = A(m_\pi^{phys}, \overline{p})$ and $A^f(\overline{p})$ for each $\overline{p}$ using the fit results, later the linear fit for the lattice spacing a at fixed $\overline{p}$ is carried out. Then we obtain the scattering amplitudes in the continuum limit at several momenta.

The extrapolations of both the amplitudes at several momenta are displayed in Fig. 25 for $\overline{p}^2 = 0$, 0.06 and 0.26 GeV^2 which roughly correspond to the momenta obtained from CM_0, $\mathrm{L1}_0$ and CM_1 respectively. The figures show the large $O(a)$ effect at each momentum. In the amplitudes we can show the tendency that the difference of $A(\overline{p})$ and $A^f(\overline{p})$ is smaller as going to the continuum limit, and they agree in the continuum limit. The result at $\overline{p}^2 = 0$ gives the scattering length $a_0 m_\pi$. In the continuum limit we obtain the scattering length $a_0 m_\pi = -0.0484(49)$ from $A(\overline{p})$ and $a_0^f m_\pi = -0.0404(24)$ from $A^f(\overline{p})$. This values are

slightly different from those in Sec. 8.2, since the result is affected by the amplitude at the non-zero momentum part. For the comparison of the result from the amplitude with that from the scattering length analysis, we also display the result obtained from the scattering length analysis denoted by the open symbols in the figure of $\overline{p}^2 = 0$.

In Fig. 26 the phase shift in the continuum limit is presented with dashed line, associated by a band of error bars. We denote the phase shift obtained from $A^f(\overline{p})$ as $\delta^f(\overline{p})$. The $\delta^f(\overline{p})$ is defined by

$$A^f(\overline{p}) = \frac{\tan\delta^f(\overline{p})}{\overline{p}} \cdot \frac{\overline{E}}{2}, \tag{261}$$

where we assume $f_\pi^{lat} = f_\pi = 93$ MeV. As discussed in Sec. 8.2, this assumption is not valid in the decay constant, so that the result $\delta^f(\overline{p})$ includes the uncertainty. The values of the phase shift at several momenta are tabulated in Table XII. The result is compared to the experimental results [23, 24], and the solid curve [25] estimated with the experimental input. Both the results in the continuum limit agree with the experiments, albeit the errors of our results are large. The large error comes from the chiral extrapolation with the data for far from the physical pion mass, and the continuum extrapolation with the data including the large $O(a)$ effect. In order to obtain a more precise result it is important to calculate the phase shift with a smaller pion mass for the chiral extrapolation, and near zero lattice spacing for the continuum extrapolation.

β	1.80	1.95	2.10
A_{10} [1/GeV^2]	−1.33(21)	−1.52(12)	−1.899(84)
A_{20} [1/GeV^4]	1.62(53)	1.51(29)	2.00(20)
A_{30} [1/GeV^6]	−0.69(31)	−0.52(16)	−0.73(11)
A_{01} [1/GeV^2]	−0.83(44)	−1.18(47)	−1.43(40)
A_{11} [1/GeV^4]	1.4(12)	1.9(11)	2.48(95)
A_{21} [1/GeV^6]	−0.46(83)	−0.65(61)	−1.04(52)
χ^2/d.o.f.	0.90	0.64	1.33

Table X: Results of a polynomial fit of m_π^2 and $\overline{p}^2$ for the scattering amplitude defined by $A(m_\pi, \overline{p}) = \tan\delta(\overline{p}) \cdot \overline{E}/2\overline{p}$.

β	1.80	1.95	2.10
A_{10}^f [1/GeV^2]	−2.84(10)	−2.546(59)	−2.438(38)
A_{01}^f [1/GeV^2]	−2.78(59)	−2.84(44)	−2.14(37)
A_{11}^f [1/GeV^4]	3.67(76)	3.36(49)	2.05(43)
χ^2/d.o.f.	0.77	0.50	0.75

Table XI: Results of the global fit for the normalized scattering amplitude defined by $A^f(m_\pi, \overline{p}) = (f_\pi^{lat}/f_\pi)^2 \tan\delta(\overline{p}) \cdot \overline{E}/2\overline{p}$ with a polynomial assumption. Here $f_\pi = 93$ MeV.

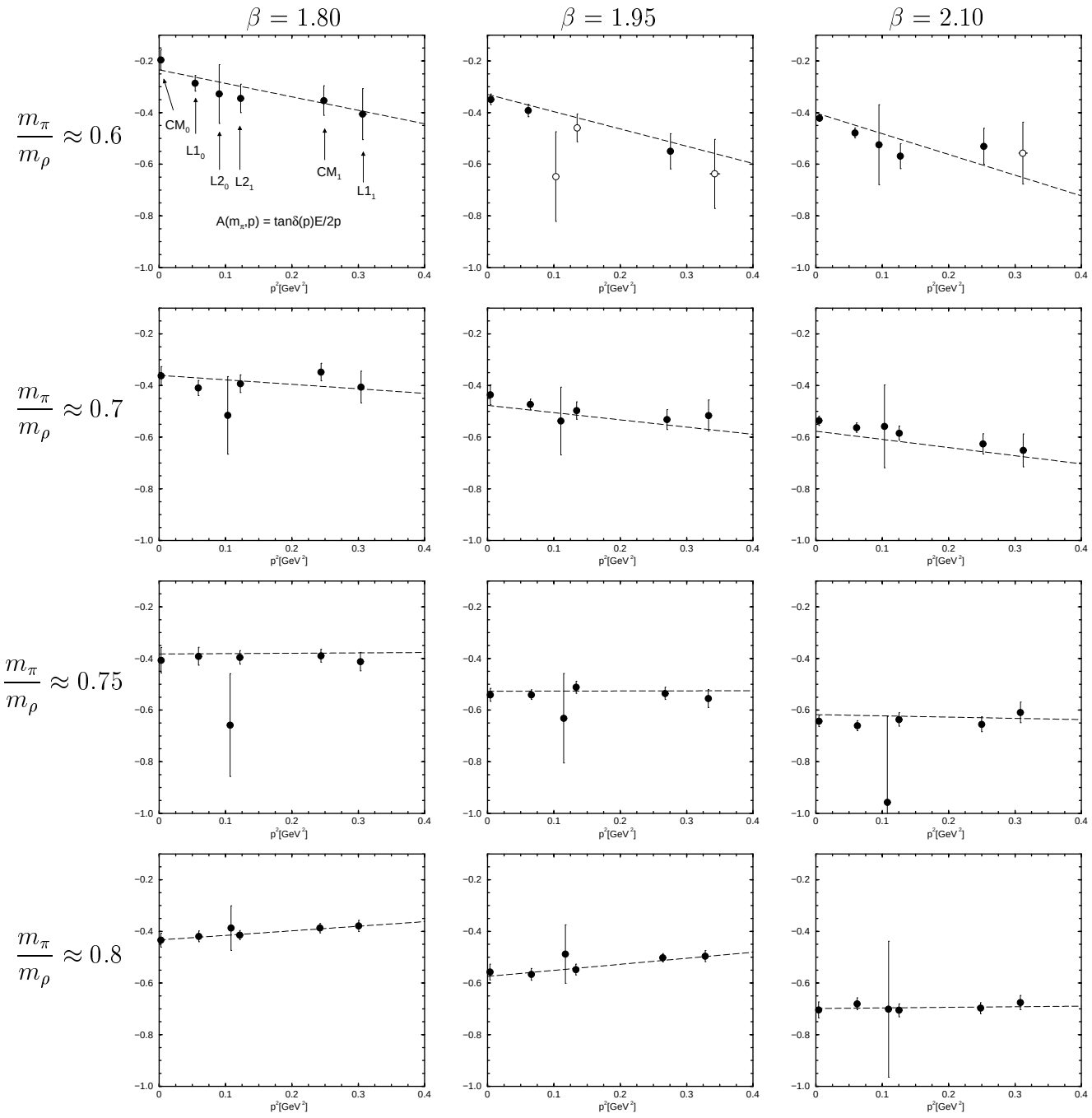

Figure 24: Measured scattering amplitudes defined by $A(m_\pi, \overline{p}) = \tan\delta(\overline{p}) \cdot \overline{E}/2\overline{p}$ and fitting lines. The CM_n refers to the amplitude obtained from the n-th state in the center of mass system, and the $\mathrm{L1}_n$ and $\mathrm{L2}_n$ to those in the laboratory systems. In the figures the open symbols are excluded from the global fit. The m_π/m_ρ increases from top to bottom, while β increases from left to right.

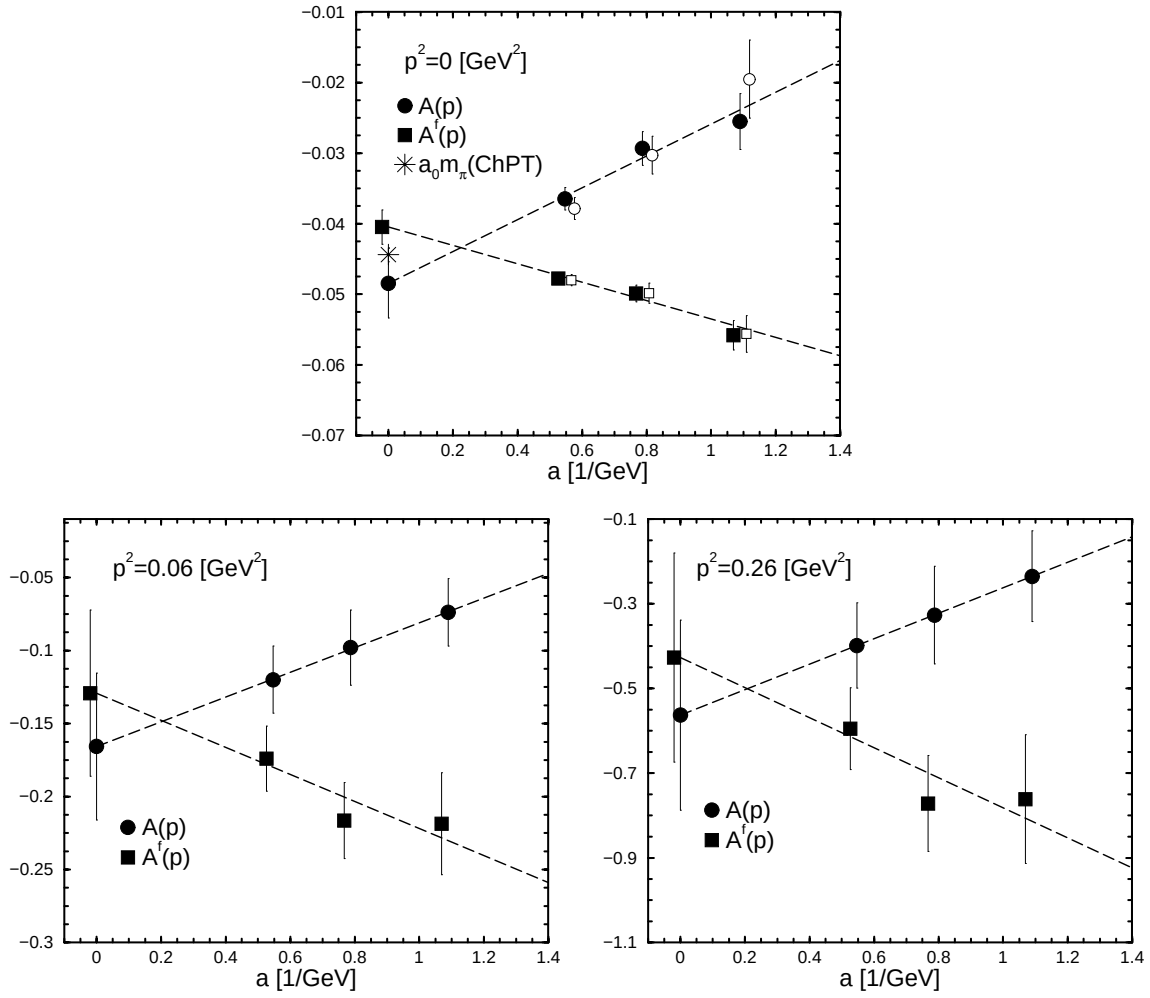

Figure 25: Continuum extrapolations of the scattering amplitudes $A(\overline{p}) = \tan\delta(\overline{p}) \cdot \overline{E}/2\overline{p}$ and $A^f(\overline{p}) = \tan\delta^f(\overline{p}) \cdot \overline{E}/2\overline{p}$ at several momenta for the physical pion mass $m_\pi = 0.14$ GeV. The results for the $A^f(\overline{p})$ are slightly shifted to smaller a. In the $\overline{p}^2 = 0$ figure open symbols are obtained from analysis of scattering length $a_0 m_\pi$, which are same as in Fig. 23. These values are also slightly moved to larger a than the corresponding closed symbols.

$\overline{p}^2$ [GeV^2]	$\sqrt{s}$ [GeV]	$\delta(\overline{p})$ [deg.]	$\delta^f(\overline{p})$ [deg.]
0.020	0.40	$-3.50(64)$	$-2.82(77)$
0.072	0.60	$-9.5(30)$	$-7.4(34)$
0.140	0.80	$-16.9(64)$	$-13.0(70)$
0.232	1.00	$-25(10)$	$-20(11)$

Table XII: Scattering phase shifts $\delta(\overline{p})$ and $\delta^f(\overline{p})$ in the continuum limit at the physical pion mass $m_\pi = 0.14$ GeV.

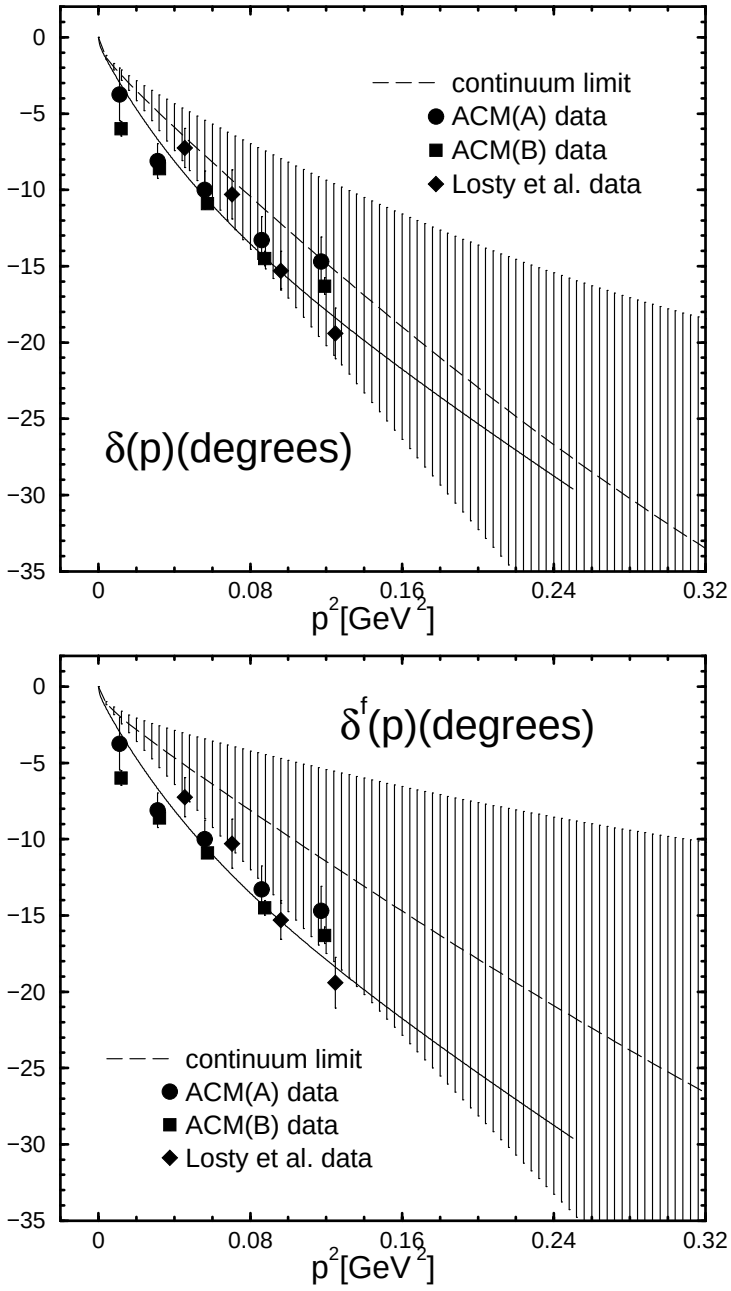

Figure 26: Scattering phase shifts obtained from the scattering amplitude $A(\overline{p}) = \tan\delta(\overline{p}) \cdot \overline{E}/2\overline{p}$ (top figure) and from $A^f(\overline{p}) = \tan\delta^f(\overline{p}) \cdot \overline{E}/2\overline{p}$ (bottom figure) in the continuum limit denoted by dashed line and a band of error bars. Symbols represent data of Aachen-Cern-Munich Collaboration [23] and one of Losty *et al.* [24]. Solid line [25] is estimated with experimental inputs.

9 Two-pion wave function in box

In this section we present an exploring work for the two-pion wave function, which contains various information about the scattering. The purposes of this work are the following two points. First is to estimate the interaction range R, where the scattering effective potential $V(r)$ vanishes at $r > R$. It is possible to extract the effective potential from the wave function, so that we can estimate the interaction range R. Since the existence of R is an important assumption in the finite volume method, this purpose is related to the reliability check of results evaluated through this method. Second is to extract the scattering phase shift from the wave function. Since the finite volume formulae are derived from the wave function on a finite box L^3 in Sec. 5, it is also possible to obtain the phase shift from the wave function directly. In this study we treat only the ground state of the $I = 2$ $\pi\pi$ scattering in the center of mass system, so that we focus on the scattering length rather than the scattering phase shift.

9.1 Definition

We define the two-pion wave function on a box L^3 with periodic boundary condition as,

$$\psi(\mathbf{r}) = \sum_{\mathbf{x}, \hat{R} \in \mathrm{O_h}} \langle 0 | \pi(\hat{R}[\mathbf{r}] + \mathbf{x}) \pi(\mathbf{x}) | \overline{\Omega}_0 \rangle, \tag{262}$$

where $\hat{R}$ is elements of cubic group, and $|\overline{\Omega}_0\rangle$ is the two-pion ground state appeared in eq.(207). The wave function is extracted from the pion four-point function $G(\mathbf{r}, t)$ given by,

$$G(\mathbf{r}, t) = \sum_{\hat{R} \in \mathrm{O_h}, \mathbf{x}} \langle 0 | \pi(\hat{R}[\mathbf{r}] + \mathbf{x}, t) \pi(\mathbf{x}, t) W(t_1) W(t_2) | 0 \rangle, \tag{263}$$

where the wall source operator $W(t)$ is given by $W(t) = \sum_{\mathbf{x}} \pi(\mathbf{x}, t)$, and t_1, t_2 are the source points. In $t \gg t_1, t_2$, only the ground state contribution remains, and we can obtain the wave function as,

$$G(\mathbf{r}, t) \to C \cdot \psi(\mathbf{r}) \cdot e^{-\overline{E} t}, \tag{264}$$

where $\overline{E} = 2\sqrt{m_\pi^2 + \overline{p}^2}$. We can obtain $\overline{E}$ from the time correlator

$$G(t) = \sum_{\mathbf{r}} G(\mathbf{r}, t), \tag{265}$$

by a single exponential fit in the large time region $t \gg t_1, t_2$.

9.2 Analysis method

When we obtain the wave function, it is straightforward to estimate the interaction range R by the effective potential $V(r)$ given by

$$\frac{\nabla^2 \psi(\mathbf{r})}{\psi(\mathbf{r})} = V(r) - \overline{p}^2, \quad r = |\mathbf{r}|, \tag{266}$$

where $V(r)$ corresponds to $2\mu V(r)$ for the definition of eq.(119). In the $r > R$ region the effective potential vanishes and the left hand side of eq.(266) becomes a constant corresponding

to $-\overline{p}^2$. We can estimate the interaction range R through the flat region of $(\nabla^2\psi(\mathbf{r}))/\psi(\mathbf{r})$, and also determine the momentum $\overline{p}^2$ at the region.

According to finite volume method, explained in Sec. 5.1, the wave function is written by the Green function eq.(133),

$$\psi(\mathbf{r}) = C \cdot \sum_{\mathbf{k}} \frac{e^{i\mathbf{k}\cdot\mathbf{r}}}{\mathbf{k}^2 - \overline{p}^2}, \tag{267}$$

where the summation is carried out in $\mathbf{k} = (2\pi/L)\cdot\mathbf{n}$ for some $\mathbf{n} \in Z^3$. Here we assume the angular momentum cut-off $\Lambda < 4$, and in $r > R$. Since the momentum can be determined by a fit with two free parameters C and $\overline{p}^2$, we can obtain the scattering phase shift by substituting $\overline{p}^2$ to the finite volume formula eq.(160). In this case we can also estimate the interaction range from the deviation of the measured wave function $\psi(\mathbf{r})$ and the fit results $\psi^f(\mathbf{r})$ as

$$\frac{|\psi(\mathbf{r}) - \psi^f(\mathbf{r})|}{\psi^f(\mathbf{r})}. \tag{268}$$

The deviation approximately implies the existence of the effective potential, since in the non-zero deviation region the measured wave function does not satisfy the Helmholtz equation eq.(121).

9.3 Parameters

Our simulation is carried out with quenched approximation employing an renormalization group improved gauge action [56], described in Sec. 3.3.1, with periodic boundary condition for the spatial and temporal directions, and clover quark action [57], described in Sec. 3.3.2, with a tadpole improved coefficient $c_{\rm SW} = (P)^{-3/4}$ which is the same choice as in Sec. 7.3. The bare coupling and the clover coefficient are chosen as $\beta = 2.334$ and $c_{\rm SW} = 1.398$ corresponding to $a = 0.1632(16)$ fm, which is determined by m_ρ at the physical pion mass. We choose five point pion masses tabulated in Table XIII.

In order to examine the interaction range, simulations are carried out for three lattice sizes, $L = 16, 20$ and 24, with a fixed temporal size $T = 80$. The number of configurations and the physical volumes are tabulated in Table XIV.

The configurations are generated with the five-hit heat bath algorithm and the over-relaxation algorithm mixed in the ratio of 1 : 4. The combination is called a sweep and we skip 200 sweeps between measurements of the physical quantities. Using the Coulomb gauge fixing configuration, the quark propagators are solved with periodic boundary condition imposed in the spatial direction and the Dirichlet boundary condition in the temporal direction. The source operators are set at $t_1 = 12$ and $t_2 = 13$ to avoid effects from the temporal boundary. In the actual calculation measurements of the wave function are carried out at every four time steps from $t = 16$. In the following analysis we focus on the result at $t = 52$, which is sufficiently large to obtain the contribution of the two-pion ground state.

We estimate the statistical errors for the four-point function, the wave function and the physical quantities by the one elimination jackknife method.

κ	0.1340	0.1349	0.1358	0.1364	0.1369
m_π [GeV]	0.8577(2)	0.7667(2)	0.6664(2)	0.5920(3)	0.5228(3)

Table XIII: Simulation parameter for quark mass used in the study for the isospin $I = 2$ $\pi\pi$ scattering wave function, and corresponding pion masses.

L	La [fm]	$N_{\rm Meas}$
16	2.61	1200
20	3.26	1000
24	3.92	506

Table XIV: Simulation parameter used in the study for the isospin $I = 2$ $\pi\pi$ scattering wave function. Lattice size, corresponding physical volume, and number of configuration using measurements $N_{\rm Meas}$.

9.4 Result

9.4.1 Result for interaction range

In Fig. 27 we show the measured wave function in a function of r at $L = 24$ for $m_\pi = 0.52$ GeV. The wave function is normalized by the value of $\psi(r_0)$ at $r_0 = 9$. The figure shows that the $I = 2$ $\pi\pi$ interaction is a repulsive force since the wave function decreases near the origin. This is consistent with the experiment.

The effective potential $V(r)$ is obtained from the derivative of $\psi(r)$ eq.(266). A typical $V(r)$ is shown in Fig. 28. The effective potential is also the repulsive force, and strongly localized near the origin. In large r we can show the flat region, where $V(r)$ vanishes.

In order to investigate the interaction range precisely, we compile the effective potential at all volumes in Fig. 29. The all effective potential vanishes in large r region, and the flat region starts almost from $r \approx 9$. This means that in $L = 16$ the effective potential $V(r)$ does not satisfy the assumption of the interaction range $0 < R < L/2$, in other words, $V(r)$ in $L = 16$ may be transformed by a boundary effect. The height of the flat region corresponds to the momentum $-\overline{p}^2$, of which volume dependence is generally given by $\overline{p}^2 = O(1/L^3)$. The $\overline{p}^2$ decreases with the volume as expected.

Since we can show that the effective potential vanishes in the region $r \geq 9$ from Fig. 29, the general solution of the Helmholtz equation eq.(267) is acceptable at this region. We try to fit the wave function in $r \geq 9$ with the fitting assumption eq.(267). We use the large L expansion form of the wave function. The calculation method of the form is described in appendix C.2. The fit result at $L = 24$ for $m_\pi = 0.52$ GeV is shown in Fig. 30. The fit is very well, and also can be explained the branch appeared in the wave function. The all results are tabulated in Table XV.

We estimate the interaction range from the deviation of the measured wave function $\psi(r)$ and the fit result $\psi^f(r)$ eq.(268). In Fig. 31 we present the deviation at all volumes for all pion masses. The figure shows that in large r region $\psi(r)$ is consistent with $\psi^f(r)$ at $r \geq 9$.

This means that the interaction range is estimated as $R \approx 9$, which is the consistent result in the effective potential analysis. Therefore we conclude that the interaction range of the isospin $I = 2$ $\pi\pi$ scattering with $\overline{p}^2 \approx 0$ is

$$R \approx 9 \quad \text{corresponding to} \quad Ra \approx 1.46 \text{ fm}. \tag{269}$$

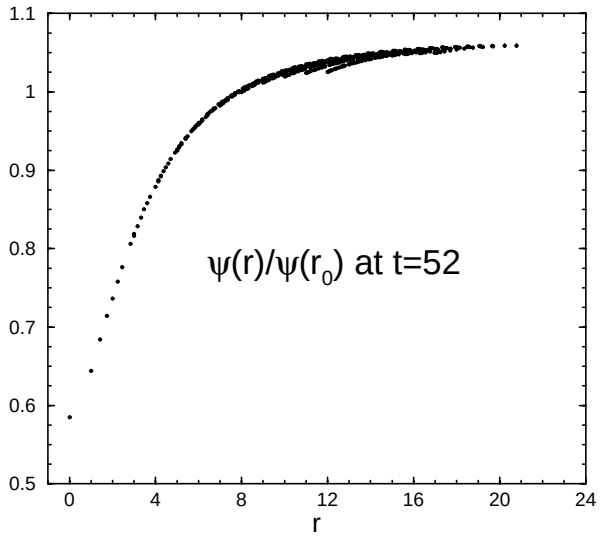

Figure 27: Wave functions $\psi(r)$ in the isospin $I = 2$ $\pi\pi$ system, which is normalized by $\psi(r_0)$ at $r_0 = 9$. Data is obtained at $L = 24$ volume for the lightest pion mass $m_\pi = 0.52$ GeV The time is fixed at $t = 52$. The horizontal axis is relative length in lattice units.

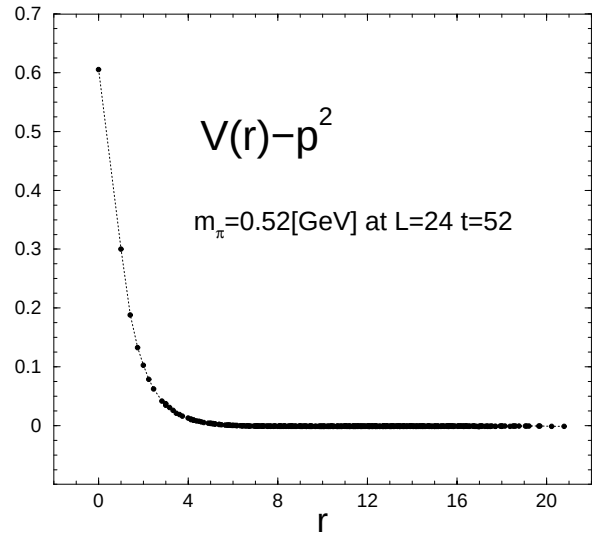

Figure 28: Effective potential of the isospin $I = 2$ $\pi\pi$ scattering defined by eq.(266). Data is obtained at $L = 24$ volume for the lightest pion mass $m_\pi = 0.52$ GeV. The time is fixed at $t = 52$. The horizontal axis is relative length in lattice units. Dotted line is a guide.

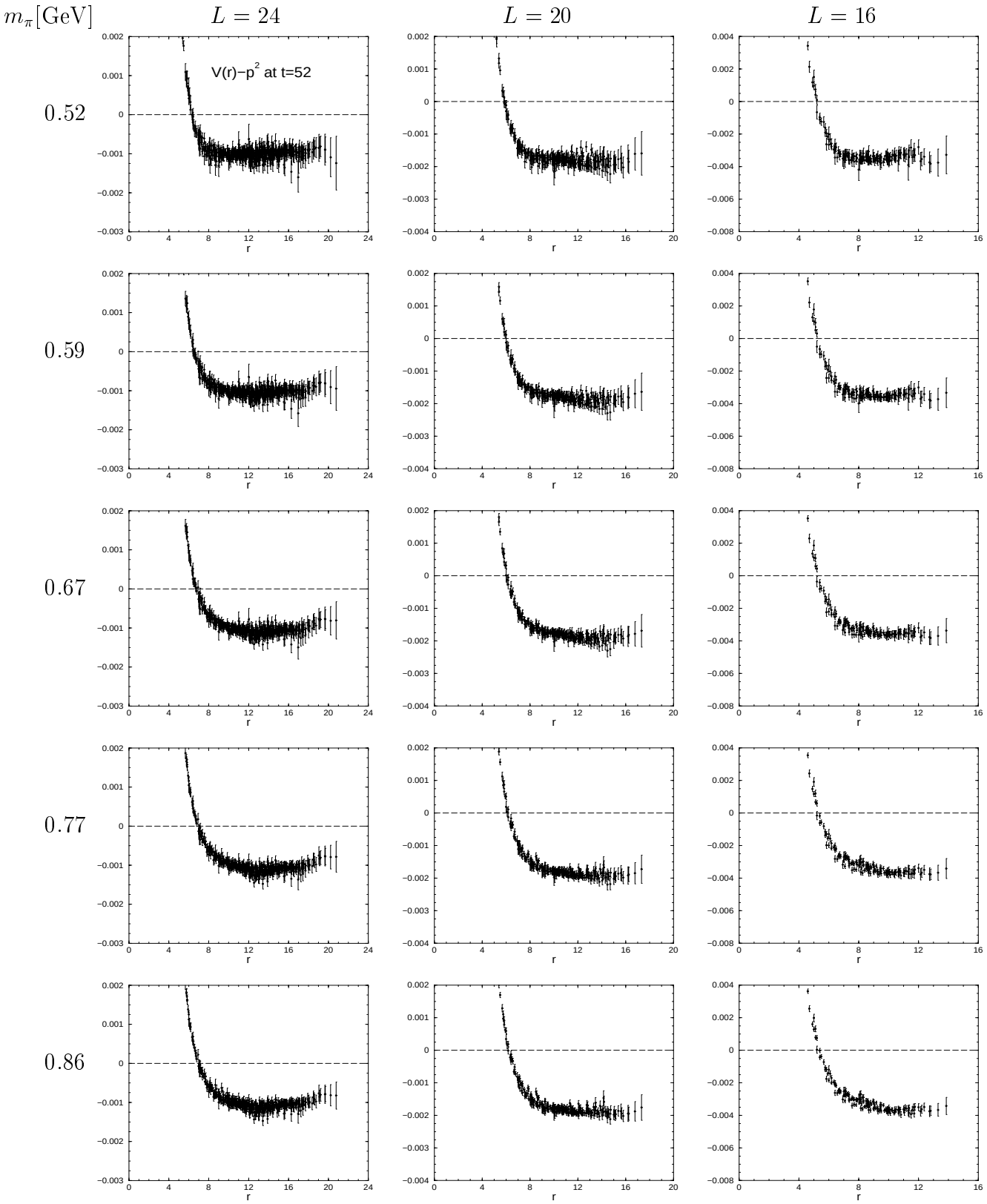

Figure 29: Effective potential $V(r) - \overline{p}^2$ in the isospin $I = 2$ $\pi\pi$ scattering system at all volumes. The horizontal axis is relative length in lattice units. The m_π increases from top to bottom, while the volume L decreases from left to right. Solid line is a guide.

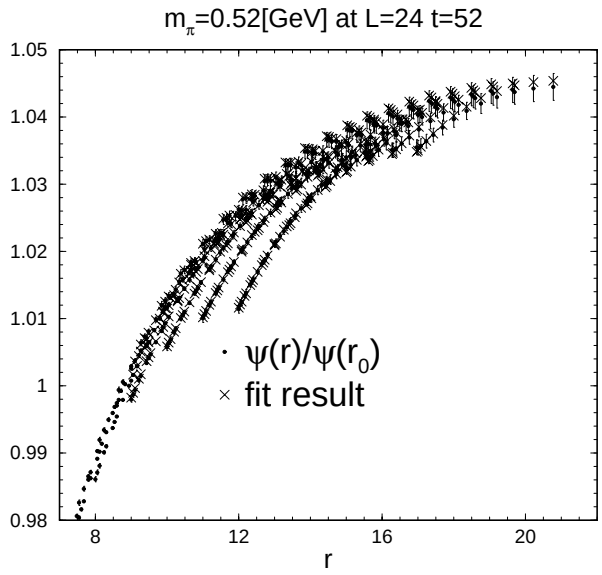

Figure 30: Fit result denoted by cross symbols. Measured wave function $\psi(r)$ denoted by dot symbol is at $L = 24$ for $m_\pi = 0.52$ GeV, and normalized by $\psi(r_0)$ at $r_0 = 9$. The horizontal axis is relative length in lattice units.

			$L = 24$		
m_π [GeV]	0.52	0.59	0.67	0.77	0.86
$\overline{p}^2$ [$\times 10^{-3}$ GeV^2]	1.46(3)	1.52(3)	1.57(3)	1.58(3)	1.56(3)
C [$\times 10^{-2}$]	$-1.47(3)$	$-1.53(3)$	$-1.58(3)$	$-1.60(3)$	$-1.58(3)$
χ^2/d.o.f	0.19	0.13	0.16	0.18	0.19
			$L = 20$		
m_π [GeV]	0.52	0.59	0.67	0.77	0.86
$\overline{p}^2$ [$\times 10^{-3}$ GeV^2]	2.67(8)	2.74(7)	2.77(7)	2.76(6)	2.73(6)
C [$\times 10^{-2}$]	$-1.84(6)$	$-1.89(5)$	$-1.91(4)$	$-1.90(5)$	$-1.88(6)$
χ^2/d.o.f	0.09	0.08	0.07	0.12	0.20
			$L = 16$		
m_π [GeV]	0.52	0.59	0.67	0.77	0.86
$\overline{p}^2$ [$\times 10^{-3}$ GeV^2]	5.12(24)	5.27(21)	5.41(18)	5.55(16)	5.55(14)
C [$\times 10^{-2}$]	$-2.22(10)$	$-2.28(9)$	$-2.34(8)$	$-2.38(7)$	$-2.40(6)$
χ^2/d.o.f	0.04	0.04	0.09	0.08	0.07

Table XV: Fit results of the isospin $I = 2$ $\pi\pi$ wave function at all volumes. The time is fixed at $t = 52$.

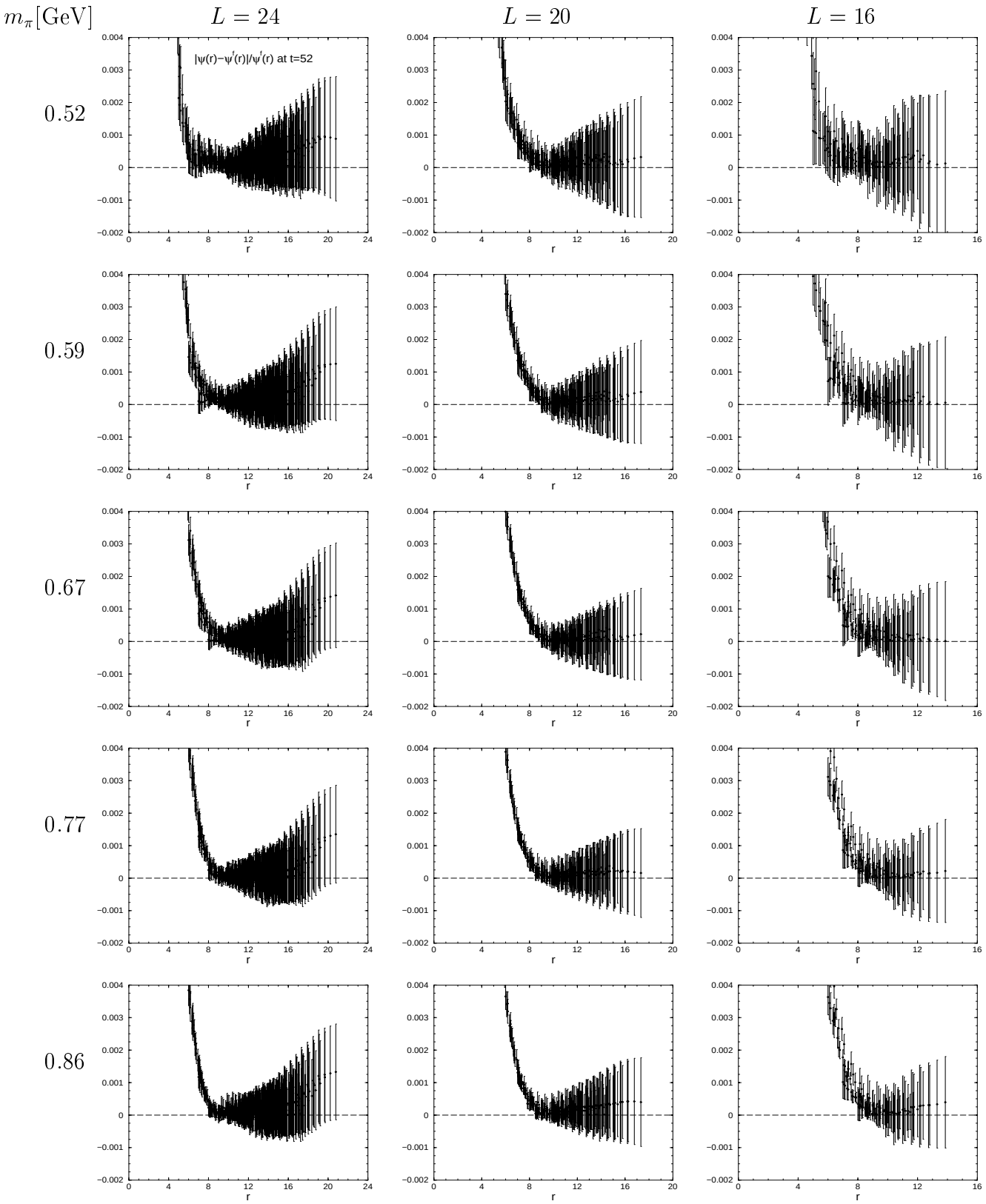

Figure 31: Deviation of measured wave function $\psi(r)$ and fit result $\psi^f(r)$. The horizontal axis is relative length in lattice units. The m_π increases from top to bottom, while the volume L decreases from left to right.

9.4.2 Result for scattering length

Now we can determine the momentum $\overline{p}^2$ with three analyses to obtain the scattering length. The first is the fit result of the wave function eq.(267), the second is a constant fit of $V(r) - \overline{p}^2$ in the flat region $r \geq 9$, and the last is the traditional method with the two-pion energy obtained from the time correlator. Using these momenta we determine the scattering length at each volume. The results are shown in Fig. 32 and tabulated in Table XVI. The consistency of the results obtained from the different analysis is very well at all volumes. In the volumes $L = 24$, the two results obtained from the effective potential and the wave function have smaller errors than that from the time correlator. This is the reason that the number of points in the exterior region of the interaction range R is larger in a larger volume, while it becomes more difficult to determine the momentum from the time correlator due to the volume dependence of the momentum $\overline{p}^2 = O(1/L^3)$. In contrast to the large volume case, the result from the time correlator does not have so larger error than the other results in the small volume $L = 16$.

From the results we cannot observe the clear volume dependence for the scattering length, even in the $L = 16$ case. This is a surprising result because we conclude in the above section that the assumption of the finite volume formula is not satisfied in the $L = 16$ case. At present it is not understood well why the results are same. The investigation of this reason is a future work.

$L = 24$					
m_π [GeV]	0.52	0.59	0.67	0.77	0.86
$\psi(r)$	−1.575(35)	−1.441(29)	−1.315(25)	−1.153(21)	−1.019(18)
$V(r) - \overline{p}^2$	−1.581(20)	−1.433(17)	−1.295(14)	−1.130(12)	−1.003(10)
$G(t)$	−1.595(60)	−1.448(52)	−1.301(45)	−1.121(38)	−0.978(34)
$L = 20$					
m_π [GeV]	0.52	0.59	0.67	0.77	0.86
$\psi(r)$	−1.622(48)	−1.466(37)	−1.313(29)	−1.136(24)	−1.005(21)
$V(r) - \overline{p}^2$	−1.584(24)	−1.420(18)	−1.271(14)	−1.107(11)	−0.984(10)
$G(t)$	−1.597(44)	−1.462(36)	−1.323(32)	−1.115(28)	−1.015(25)
$L = 16$					
m_π [GeV]	0.52	0.59	0.67	0.77	0.86
$\psi(r)$	−1.551(67)	−1.403(51)	−1.271(39)	−1.121(29)	−1.005(23)
$V(r) - \overline{p}^2$	−1.525(51)	−1.368(37)	−1.226(28)	−1.074(20)	−0.963(16)
$G(t)$	−1.536(44)	−1.413(36)	−1.287(31)	−1.135(27)	−1.014(23)

Table XVI: Isospin $I = 2$ $\pi\pi$ scattering length a_0/m_π GeV^{-2} obtained from three analyses, using wave function $\psi(r)$, effective potential $V(r) - \overline{p}^2$ and time correlator $G(t)$.

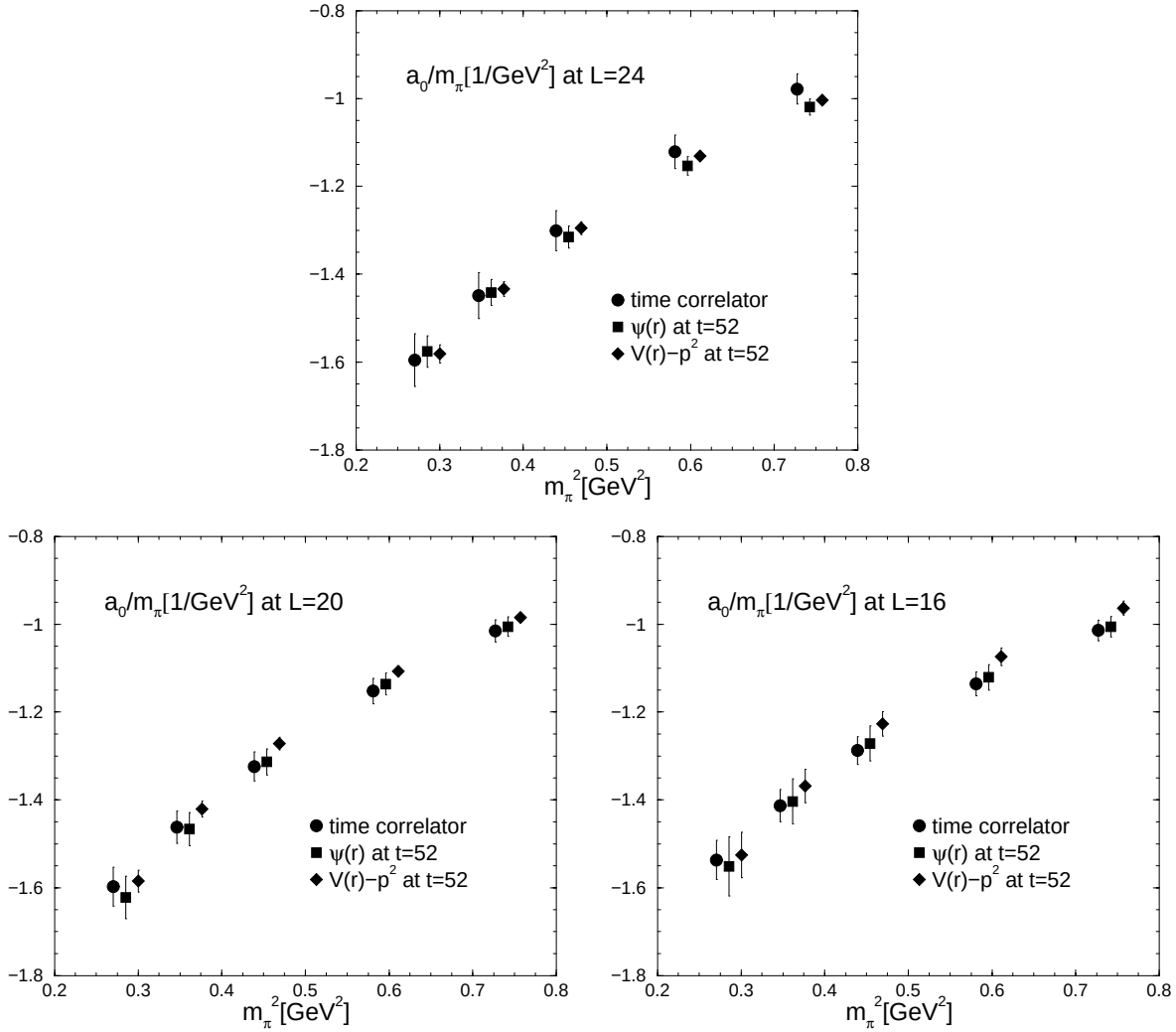

Figure 32: Scattering lengths a_0/m_π GeV^{-2} of the isospin $I = 2$ $\pi\pi$ system obtained from wave function $\psi(r)$, effective potential $V(r) - \overline{p}^2$ and time correlator for all pion masses. The results for $\psi(r)$ and $V(r) - \overline{p}^2$ are obtained at $t = 52$.

9.4.3 Time dependence for results

In Fig. 33 we show the time dependence for the scattering length obtained from $\psi(r)$ and $V(r) - \overline{p}^2$ at all volumes. The time dependence is larger as the pion mass is smaller. In the case of the lightest pion mass at $L = 16$ we cannot observe a clear plateau in the figure. We consider that a constant fit is needed to determine the value of the scattering length from the results in $L = 16$.

In the figure we also show that the large time, such as $t = 50$, is needed to obtain the plateau. This time t is much larger than in the case of the effective pion mass and the effective two-pion energy as shown in Fig. 34. The reason is not understood at present. It is an important future work to investigate the time dependence.

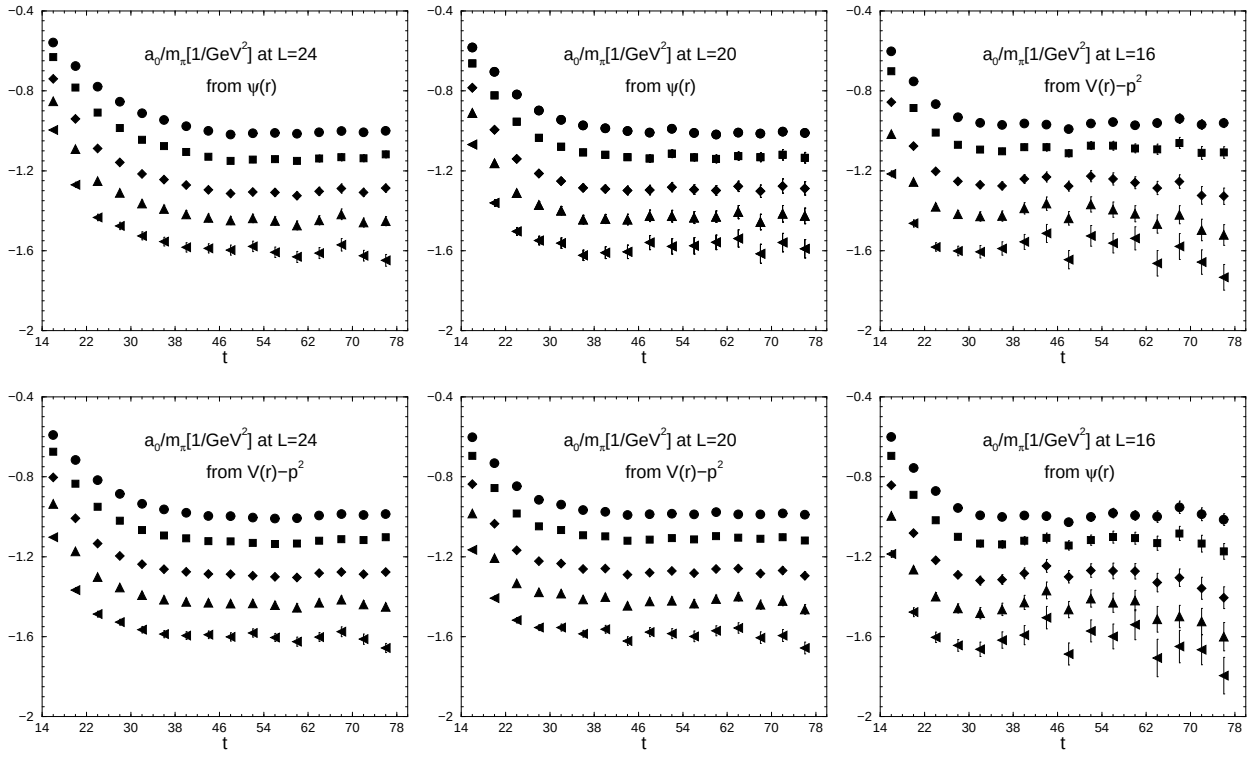

Figure 33: Time dependence of the isospin $I = 2$ $\pi\pi$ scattering length a_0/m_π GeV^{-2} obtained from wave function $\psi(r)$ and effective potential $V(r) - \overline{p}^2$, which are shown in the top and bottom lines respectively. Circle, square, diamond, triangle up and triangle left denote the data for $m_\pi = 0.52, 0.59, 0.67, 0.77$ and 0.86 GeV, respectively.

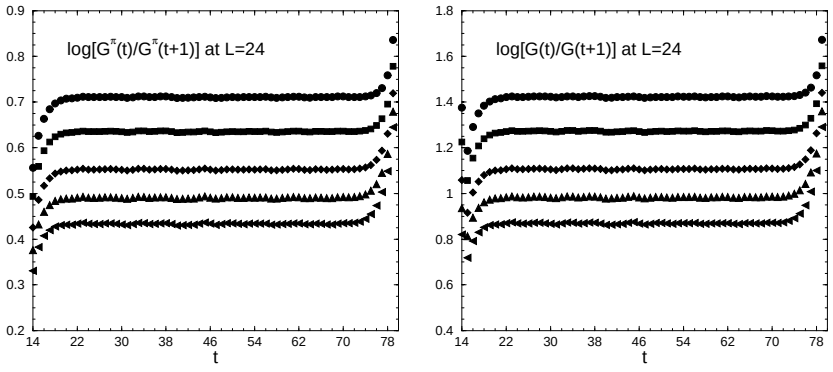

Figure 34: Effective pion mass (left figure) and effective two-pion energy (right figure). Circle, square, diamond, triangle up and triangle left denote the data for $m_\pi = 0.52, 0.59, 0.67, 0.77$ and 0.86 GeV, respectively.

10 Conclusion

In this thesis we have presented the calculation of the isospin $I = 2$ S-wave $\pi\pi$ scattering phase shift in the continuum limit with two flavor dynamical quark effect. The phase shift is evaluated with the finite volume method not only in the center of mass but also in two non-rest systems. By considering the systems we have obtained energy states at various momenta without changing the lattice size. We have demonstrated that the calculations of the phase shift is possible even in full QCD for various lattice spacings and for non-zero total momentum systems.

For the scattering length a_0 we have found that the $O(a)$ effect is large, and the curvature exists in a_0/m_π as a function of m_π^2. It is hard to extrapolate the scattering length to the physical pion mass due to the curvature. We have also found a correlation of the pion mass dependence of the scattering length and the pseudoscalar decay constant measured on lattice. We use the correlation to obtain a reliable result in the chiral extrapolation. In fact this extrapolation is more reasonable than that directly with the scattering length. However, in the continuum limit the decay constant used in this work does not seem to agree the experiment. Therefore the result with the decay constant includes an uncertainty. We have presented the two values as our results: $a_0 m_\pi = -0.0558(56)$ and $a_0^f m_\pi = -0.0413(28)$, where a_0^f is obtained from the analysis with the decay constant.

In the scattering phase shift the large $O(a)$ effect is also seen. In this analysis we find that the difficulty of the chiral extrapolation does not occur. In order to check the reliability we also made analysis with the decay constant. The difference of results becomes smaller as the lattice spacing goes to zero, and they agree in the continuum limit. The results of the phase shift in the continuum limit also agrees with the experimental results. We have also evaluated the scattering length in the continuum limit $a_0 m_\pi = -0.0484(49)$ and $a_0^f m_\pi = -0.0404(24)$ from each phase shift at the zero momentum.

The large errors of the result in the continuum limit arise from the chiral extrapolation and the continuum extrapolation. To obtain precise results it is very important to calculate with a smaller pion mass for the chiral extrapolation, and a smaller lattice spacing for the continuum extrapolation. Other future works for the chiral extrapolation are investigations of the curvature in the scattering length, the correlation of the scattering length and the decay constant measured on lattice, and effects of chiral symmetry breaking of the quark action.

A future extension of this work is calculation of other scattering processes. Since the calculation method is independent of scattering processes, it is possible to apply the method for scattering with baryons. A more interesting study is a resonance scattering phase shift. From the point of calculation it is more difficult, but it is more important for understanding hadron dynamics to investigate a decay of an unstable hadron.

Since in the finite volume method it is an assumption that the two-pion interaction range is contained in a periodic box, the validity of the results may be lost if the physical volume is smaller than the interaction range. To check the reliability of the results we also need to examine the physical volume dependence of the phase shift or the interaction range directly which we have not done in this work.

In order to examine the interaction range directly, we have made an exploring work for the isospin $I = 2$ $\pi\pi$ wave function. We have determined the interaction range R in the

scattering system from the wave function, and concluded that

$$Ra \approx 9, \quad \text{corresponding to} \quad R \approx 1.46 \text{ fm}. \tag{270}$$

This result leads to the condition that we need a physical volume larger than about 2.9 fm to obtain a reliable scattering length through the finite volume method. However, in the actual analysis we have obtained consistent results for the scattering length in the volume range from 2.6 to 3.9 fm. It is a future work to understand the reason.

We have also attempted two new analyses to determine the scattering length. The results for the scattering length obtained from the constant fit of $V(r) - \overline{p}^2$ and the fit of the wave function agree well with the result from the time correlator. Furthermore the errors for the new analyses are smaller than that from the time correlator in the large volume. This is an advantage to determine the precise scattering length on a large volume, since in such a volume the momentum may not be determined clearly from the time correlator.

In order to check the reliability for the scattering phase shift, we need the calculation of the wave function for the momentum excited states, and in the non-rest system. These are important future problems.

11 Future problems

In this section we present some future problems related to this thesis, which are calculation of the unstable hadron decay $\rho \to \pi\pi$, calculation of the weak matrix element of the $K \to \pi\pi$ decay, and extensions of the study of the two-pion wave function. These are important to understand the hadron dynamics.

11.1 $\rho \to \pi\pi$ decay

We describe here calculation of hadronic decay process. We focus on the $\rho \to \pi\pi$ decay which is an important example in QCD.

The ρ meson is a vector particle with the isospin $I = 1$. The Bose statistics constrains the two-pion state to have the symmetry $I + J =$ even, J is total angular momentum. Hence the two-pion state coupled to the ρ meson should have non-zero momentum, and at least $J = 1$ angular momentum. In an effective theory the vector coupling of the decay process is given by

$$g_{\rho\pi\pi}\rho_\mu \cdot \pi\partial^\mu\pi, \tag{271}$$

where $g_{\rho\pi\pi}$ is a coupling constant. This means that the ρ meson cannot decay unless the momentum of the two-pion is non-zero. This is a different situation from the $I = 0$ and 2 $\pi\pi$ scattering system, and σ particle decay in ϕ^4 theory, while the main strategy is same as the calculation of the $I = 2$ $\pi\pi$ scattering phase shift: At first we extract the energy eigenvalue for the two-pion and ρ states by the diagonalization method, and later the phase shift is evaluated through the finite volume method.

11.1.1 Center of mass system

First we consider in the center of mass system. We choose the two-pion operator $\Omega_n(t)$ with $I = 1$ and $J = 1$ as

$$\Omega_n^i(t) = \sum_{\mathbf{x},\mathbf{y}} f_i(\mathbf{x},\mathbf{y}) \left(\pi^+(\mathbf{x},t)\pi^-(\mathbf{y},t) - \pi^-(\mathbf{x},t)\pi^+(\mathbf{y},t)\right) e^{i\mathbf{p}_n\cdot(\mathbf{x}-\mathbf{y})}, \tag{272}$$

where $\mathbf{p}_n^2 = (2\pi/L)^2 \cdot n$, and the projection function is given by

$$f_i(\mathbf{x},\mathbf{y}) = \frac{(\mathbf{x}-\mathbf{y})_i}{|\mathbf{x}-\mathbf{y}|} \text{ for } \mathbf{x} \neq \mathbf{y}, \text{ and } f_i(\mathbf{x},\mathbf{x}) = 0, \tag{273}$$

and the pion operators $\pi^\pm$ are given by

$$\pi^+(\mathbf{x},t) = u\gamma_5\overline{d}(\mathbf{x},t), \quad \pi^-(\mathbf{x},t) = d\gamma_5\overline{u}(\mathbf{x},t). \tag{274}$$

Using the two-pion operator, the pion four-point functions is calculated in the same way as the $I = 2$ $\pi\pi$ scattering case,

$$G_{nm}(t) = \sum_{i=1}^{3}\langle 0|\Omega_n^i(t)\Omega_m^i(t_S)|0\rangle, \tag{275}$$

where t_S is the source point. After the wick contraction one finds only two diagrams, the direct diagram (D) and the rectangular diagram (R) shown in Fig. 35, are needed to calculate $G_{nm}(t)$,

$$G(t) = 2\mathrm{Im}[G^D(t) - G^R(t)]. \tag{276}$$

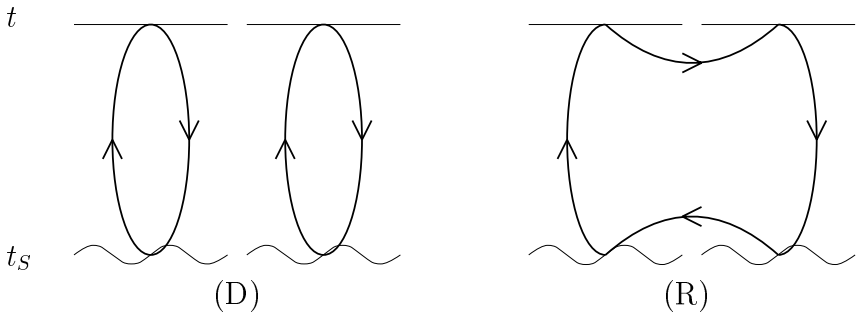

Figure 35: Diagrams contributed to the isospin $I = 1$ two-pion four-point function. The left and right figures are direct (D) and rectangular (R) diagrams. Straight line denotes sink time, and wave line denotes source time.

To evaluate the energy eigenvalues with the diagonalization method, we need to calculate the ρ meson propagator and the ρ-$\pi\pi$ three-point function as

$$G_\rho(t) = \sum_{i=1}^{3} \langle 0|\rho_i(\mathbf{0},t)\rho_i(\mathbf{0},t_S)|0\rangle, \tag{277}$$

$$G_{\rho m}(t) = \sum_{i=1}^{3} \langle 0|\rho_i(\mathbf{0},t)\Omega_m^i(t_S)|0\rangle, \tag{278}$$

where the ρ meson operator is given by

$$\rho_i(\mathbf{p},t) = \sum_{\mathbf{x}} \rho_i(\mathbf{x},t)e^{i\mathbf{p}\cdot\mathbf{x}}. \tag{279}$$

In order to extract the energy eigenvalues for the two-pion and ρ meson states, the diagonalization is carried out with the correlation function matrix

$$M_{kl}(t) = \left(\begin{array}{ccc|c} G_{11}(t) & \cdots & G_{1N}(t) & G_{1\rho}(t) \\ \vdots & \ddots & \vdots & \vdots \\ G_{N1}(t) & \cdots & G_{NN}(t) & G_{N\rho}(t) \\ \hline G_{\rho 1}(t) & \cdots & G_{\rho N}(t) & G_\rho(t) \end{array}\right), \tag{280}$$

where we assume the pion four-point function matrix $G(t)$ is $N \times N$ matrix. It is noted that $G_{00}(t) = 0$ due to the constraint of the symmetry discussed above. We then can evaluate the energy eigenvalues $\overline{E}$.

In this case to obtain the resonance phase shift, we need to modify the finite volume formula eq.(160) to the one in angular momentum $l = 1$ case. But when we assume the cut-off of angular momentum $\Lambda \leq 3$, the modification is not needed. Therefore the finite volume formula of $l = 1$ in the center of mass system is given by

$$\tan\delta_1(\overline{p}) = \frac{\pi^{3/2}\sqrt{\overline{n}}}{Z_{00}(1;\overline{n})}, \tag{281}$$

where $\overline{p} = \sqrt{\overline{E}^2/4 - m_\pi}$ and $\overline{p}^2 = (2\pi/L)^2 \cdot \overline{n}$.

11.1.2 Laboratory system

We can obtain the resonance scattering phase shift by eq.(281), but in order to investigate the detailed structure of the resonance phase shift we need results near the zero-momentum. To do this, we need a calculation with a large lattice size in the center of mass system, it is hard with present computing resources. By considering the laboratory system, however, the center of mass momentum can be decreased than the case considering only the center of mass system.

In this section we consider the system with the total momentum $\mathbf{P} = (0, 0, 2\pi/L)$. The calculation method is almost same as in Sec. 11.1.1, but several modifications are needed.

The $l = 1$ representation in the tetragonal group is reduced into two irreducible representations A_2^- and E^-, and each eigenstate splits into two states with non-degenerate energies. The state with angular momentum which is parallel to $\mathbf{P}$ belongs to the A_2^- representation, and the one with perpendicular to the E^- representation.

The two-pion operator is modified to belong to the laboratory system as

$$\Omega_n^i(t) = \sum_{\mathbf{x},\mathbf{y}} f_i(\mathbf{x}, \mathbf{y}) \left(\pi_1^+(\mathbf{x}, t)\pi_2^-(\mathbf{y}, t) - \pi_1^-(\mathbf{x}, t)\pi_2^+(\mathbf{y}, t) \right) e^{i(\mathbf{p}_{1,n}\cdot\mathbf{x} + \mathbf{p}_{2,n}\cdot\mathbf{y})}, \tag{282}$$

where the j-th pion momenta $\mathbf{p}_{j,n}$ satisfy $\mathbf{p}_{1,n} + \mathbf{p}_{2,n} = \mathbf{P}$, and the projection function $f_i(\mathbf{x}, \mathbf{y})$ is defined in eq.(273). In this case the operator $\Omega_n^3(t)$ belongs to the A_2^- representation, and $\Omega_n^i(t)$ for $i = 1, 2$ belong to the E^- representation. The pion four-point functions in each representation are given as same as eq.(275) by

$$G_{nm}^{A_2^-}(t) = \langle 0|\Omega_n^3(t)\Omega_m^3(t_S)|0\rangle, \quad G_{nm}^{E^-}(t) = \sum_{i=1}^{2} \langle 0|\Omega_n^i(t)\Omega_m^i(t_S)|0\rangle \tag{283}$$

The ρ meson propagators and the ρ-$\pi\pi$ three point functions are also given by

$$\begin{aligned} G_\rho^{A_2^-}(t) &= \langle 0|\rho_3(\mathbf{P}, t)\rho_3(\mathbf{P}, t_S)|0\rangle, & G_{\rho m}^{A_2^-}(t) &= \langle 0|\rho_3(\mathbf{P}, t)\Omega_m^3(t_S)|0\rangle, \\ G_\rho^{E^-}(t) &= \sum_{i=1}^{2} \langle 0|\rho_i(\mathbf{P}, t)\rho_i(\mathbf{P}, t_S)|0\rangle, & G_{\rho m}^{E^-}(t) &= \sum_{i=1}^{2} \langle 0|\rho_i(\mathbf{P}, t)\Omega_m^i(t_S)|0\rangle. \end{aligned} \tag{284}$$

Since the operators belonging to the A_2^- representation decouple from eigenstates which belong to the E^- representation, and vice versa, we need the diagonalizations with the correlation function matrices $M^{A_2^-}$ and M^{E^-} to extract the energy eigenvalues $\overline{E}_L$ in each representation.

From the momentum $\overline{p}^2$ evaluated by $\overline{E}_L$ as

$$\overline{p}^2 = (\overline{E}_L^2 - \mathbf{P}^2)/4 - m_\pi^2, \tag{285}$$

the phase shift is calculated through the finite volume formulae in each representation,

$$\tan\delta_1(\overline{p}) = \gamma\pi^{3/2}\sqrt{\overline{n}} \left(Z_{00}^{\mathbf{d}}(1; \overline{n}) + \frac{2}{\sqrt{5}}\overline{n}^{-1} Z_{20}^{\mathbf{d}}(1; \overline{n}) \right)^{-1} \quad A_2^- \text{ representation}, \tag{286}$$

$$\tan\delta_1(\overline{p}) = \gamma\pi^{3/2}\sqrt{\overline{n}} \left(Z_{00}^{\mathbf{d}}(1; \overline{n}) - \frac{1}{\sqrt{5}}\overline{n}^{-1} Z_{20}^{\mathbf{d}}(1; \overline{n}) \right)^{-1} \quad E^- \text{ representation}, \tag{287}$$

where $\mathbf{d} = (0, 0, 1)$ and the spherical zeta function with the $\mathbf{d}$ system $Z_{lm}^{\mathbf{d}}(s; \overline{n})$ is defined in eq.(202).

11.2 $K \to \pi\pi$ weak matrix element

Calculation of the $K \to \pi\pi$ weak matrix element has various problems. We focus on two problems of them, the first is the extraction of the on-shell amplitude, and the second is the relation of the matrix element on lattice, or a finite volume, and that in the infinite volume. In this section we show methods to solve the two problems, respectively, and restrict ourselves to the center of mass system.

11.2.1 Final state interaction

In order to calculate the matrix element we need the amplitude discussed in Sec. 6.1.2 as,

$$A^L_{K,\alpha} = \langle K|H_W|\overline{\Omega}_\alpha\rangle \ \text{ at } m_K = \overline{E}_\alpha = 2\sqrt{m_\pi^2 + \overline{p}_\alpha^2}, \tag{288}$$

where $|\overline{\Omega}_\alpha\rangle$ is the α-th two-pion state with the two-pion interaction, and H_W is effective weak interaction operator. The three-point function provides the amplitude as

$$\begin{aligned} G_n(t_1,t_2) &= \langle 0|K(t_1)H_W(t_0)\Omega_n(t_2)|0\rangle & (289)\\ &\to \langle 0|K(0)|K\rangle \sum_\beta A^L_{K,\beta}\cdot V_{\beta n}\cdot e^{-m_K(t_1-t_0)}e^{-\overline{E}_\beta(t_0-t_2)}, & (290)\\ &\quad \text{for } t_1 \gg t_0 \gg t_2, \end{aligned}$$

where $V_{\beta n} = \langle\overline{\Omega}_\beta|\Omega_n(0)|0\rangle$. Since the amplitude is contained in the summation of the two-pion state, this is a serious problem to obtain the amplitude eq.(288).

To solve the problem we introduce a method with the spectral amplitude V. The V can be extracted from the diagonalization method of the pion four-point function. The method is explained in Sec. 6.1.4. We can solve the problem by defining the new correlation function as

$$\begin{aligned} \overline{G}_\alpha(t_1,t_2) &\equiv \sum_n G_n(t_1,t_2)\cdot V^{-1}_{n\alpha} & (291)\\ &\to \langle 0|K(0)|K\rangle\cdot A^L_{K,\alpha}\cdot e^{-m_K(t_1-t_0)}e^{-\overline{E}_\alpha(t_0-t_2)}, & (292)\\ &\quad \text{for } t_1 \gg t_0 \gg t_2. \end{aligned}$$

We expect the correlation function behaves as the single exponential $e^{-\overline{E}_\alpha(t_0-t_2)}$. By dividing the normalization $\langle 0|K(0)|K\rangle$ using the K meson propagator, we can extract the amplitude $A^L_{K,\alpha}$ on a finite volume by a single exponential fit.

11.2.2 Relation to the infinite volume

Even if we succeed in the extraction of the $K \to \pi\pi$ decay amplitude A^L by lattice simulation, another problem remains. The A^L is the amplitude for two-pion energy eigenstate on a finite Euclidean space-time, but not in the infinite Minkowski space-time. We can relate A^L to the physical amplitude $A^{\rm Ph}$ in the infinite volume using some effective theory, but a calculation using such an effective theory causes large uncertainties of lattice predictions. Recently Lellouch and Lüscher [28] derived a relation between A^L and $A^{\rm Ph}$ at two-pion energy $\overline{E} = m_K$, which is called LL-formula. Here we show a brief explanation of the LL-formula.

The two-pion energy $\overline{E}$ on lattice satisfies the finite volume formula eq.(160). Introducing a weak interaction $H^W = \pi\pi K\cdot A^L$, the energy is further shifted from $\overline{E}$ to $\overline{E}'$ on finite

volumes, which also satisfies the finite volume formula, i.e.,

$$\phi(q) = n\pi - \delta(\overline{p}) \tag{293}$$
$$\phi(q^{'}) = n\pi - \delta^{'}(\overline{p}^{'}), \tag{294}$$

where $n \in Z$ and $\phi(q)$ is given by

$$\tan\phi(q) = -\frac{\pi^{3/2}q}{Z_{00}(1;q^2)}, \tag{295}$$

where we use here the quantity q^2 which is same as $\overline{n}$ in before section. The momentum $\overline{p}$ is extracted from the two-pion energy $\overline{E}$

$$\overline{p} = \sqrt{\overline{E}^2/4 - m_\pi^2}, \tag{296}$$

and $q = (\overline{p}L/2\pi)$. The quantities with the prime $(^{'})$ are also given as the same way.

The energy shift $\overline{E}^{'} - \overline{E}$ can be estimated by perturbation theory for the weak interaction on a finite volume. In the case of $\overline{E} = m_K$, one finds

$$\overline{E}^{'} - \overline{E} = \pm|A^L(\overline{E})|, \tag{297}$$

where it should be noted that the energy shift is first order in the weak interaction. This is because the energy is degenerate at $H^W = 0$. We can also estimate the difference of the phase shifts at $\overline{E}^{'}$ by the perturbation theory in the infinite volume, which yields

$$\delta^{'}(\overline{p}^{'}) - \delta(\overline{p}) = \mp\frac{1}{32\pi}\cdot\frac{\overline{p}^{'}}{\overline{E}^{'}}\cdot\frac{|A^{\rm Ph}(\overline{E}^{'})|^2}{P_K^2 + m_K^2}, \tag{298}$$

where the denominator corresponds to the s-channel K meson propagator with four-momentum $P_K = (i\overline{E}^{'}, \mathbf{0})$. Substituting eq.(298) into the relation eq.(294), and expanding around $\overline{E}^{'} = \overline{E}$ by using eq.(297), we obtain the equation at first order,

$$\Delta p\left\{\frac{\partial\phi(q)}{\partial p}\right\}_{p=\overline{p}} = -\Delta p\left\{\frac{\partial\delta(p)}{\partial p}\right\}_{p=\overline{p}} + \frac{\overline{p}|A^{\rm Ph}(\overline{E})|^2}{32\pi m_K^2|A^L(\overline{E})|}, \tag{299}$$

where $\Delta p = m_K|A^L(\overline{E})|/4\overline{p}$. One then finds the following LL-formula at $\overline{E} = m_K$ as,

$$|A^{\rm Ph}(\overline{E})|^2 = 8\pi\left\{q\frac{\partial\phi(q)}{\partial q} + p\frac{\partial\delta(p)}{\partial p}\right\}_{p=\overline{p}}\cdot\frac{m_K^3}{\overline{p}^3}\cdot|A^L(\overline{E})|^2. \tag{300}$$

From the formula we find the normalization condition in the non-interacting case $\delta(p) = 0$ as,

$$|A^{\rm Ph}(\overline{E})|^2 = \frac{4}{\nu_n}(m_K L)^3|A^L(\overline{E})|^2, \tag{301}$$

where $\nu_n \equiv \sum_{\mathbf{n}^{'}}\delta_{n,\mathbf{n}^{'2}}$. This is easy to check by using the expansion form of the spherical zeta function eq.(163). The proof is described in appendix. C.3.

11.3 Wave function

In this section calculation methods of the two-pion wave functions for higher states and in the laboratory system are briefly described.

11.3.1 Wave function for higher states

There is a problem to extract the wave function for higher states, which is a similar problem to the calculation of the weak matrix element discussed in Sec. 11.2.1. In this section we focus only on the center of mass system and lattice size L^3.

In order to calculate the wave function for higher states we need the pion four-point functions

$$G_{nm}(\mathbf{r},t) = \sum_{\hat{R}\in \mathrm{O_h},\mathbf{x}} \langle 0|\pi(\hat{R}[\mathbf{r}]+\mathbf{x},t)\pi(\mathbf{x},t)e^{i\mathbf{p}_n\cdot\hat{R}[\mathbf{r}]}\Omega_m(t_S)|0\rangle, \quad \mathbf{p}_n^2 = (2\pi/L)^2\cdot n, \tag{302}$$

where $\hat{R}$ is elements of cubic group and $\Omega_n(t_S) = \pi(\mathbf{p}_n,t_S)\pi(-\mathbf{p}_n,t_S)$. By expanding in the two-pion state $|\overline{\Omega}_\alpha\rangle$ the four-point functions are rewritten by

$$G_{nm}(\mathbf{r},t) = \sum_\beta \psi_{n\beta}(\mathbf{r})\cdot V_{\beta m}\cdot e^{-\overline{E}_\beta(t-t_S)}, \tag{303}$$

where $V_{\alpha n} = \langle\overline{\Omega}_\alpha|\Omega_n(0)|0\rangle$, and $\overline{E}_\alpha$ is the two-pion energy for the α state. Here the wave function for the α state with the n-th operator is given by

$$\psi_{n\alpha}(\mathbf{r}) = \sum_{\hat{R}\in \mathrm{O_h},\mathbf{x}} \langle 0|\pi(\hat{R}[\mathbf{r}]+\mathbf{x},t)\pi(\mathbf{x},t)e^{i\mathbf{p}_n\cdot\hat{R}[\mathbf{r}]}|\overline{\Omega}_\alpha\rangle. \tag{304}$$

Since the four-point function $G_{nm}(\mathbf{r},t)$ is not constructed by a single exponential function, it is difficult to extract the wave function $\psi_{n\alpha}(\mathbf{r})$ except for the ground state.

To solve the difficulty we use the same method described in Sec. 11.2.1. Using the inverse of the spectral amplitude $V^{-1}_{m\alpha}$, we construct a pion four-point function as

$$\overline{G}_{n\alpha}(t) = \sum_m G_{nm}(\mathbf{r},t)\cdot V^{-1}_{m\alpha}. \tag{305}$$

We expect the four-point function behaves as a single exponential. We then can extract the α state wave function in $t \gg t_S$ as

$$\overline{G}_{n\alpha}(t) \quad\to\quad \psi_{n\alpha}(\mathbf{r})e^{-\overline{E}_\alpha(t-t_S)}, \quad t\gg t_S. \tag{306}$$

The above discussion is valid not only in the center of mass system but in the laboratory system.

11.3.2 Wave function in laboratory system

In this section we consider a box L^3 with periodic boundary condition in the laboratory system, where the total momentum $\mathbf{P}\neq 0$. As discussed in Sec. 5.2, the center of mass wave function ψ_{CM}, which satisfies the Helmholtz equation, is obtained by the Lorentz transformation of the wave function ψ_{L} in the laboratory system. We show a method to calculate the wave function ψ_{CM} from lattice calculation in the laboratory system. In this section we assume that ψ_{L} can be obtained without the diagonalization method. In the case that the diagonalization is needed, we can extract ψ_{L} by the method described in Sec. 11.3.1.

We define the two-pion wave function in the laboratory system as,

$$\Psi_{\rm L}(\mathbf{X}_L, \mathbf{r}_L) = \sum_{\mathbf{x}_L, \mathbf{y}_L} \langle 0|\pi(\mathbf{x}_L) e^{i\mathbf{p}_1\cdot\mathbf{x}_L} \pi(\mathbf{y}_L) e^{i\mathbf{p}_2\cdot\mathbf{y}_L} |\overline{\Omega}\rangle \delta(\mathbf{r}_L - (\mathbf{x}_L - \mathbf{y}_L)), \tag{307}$$

where $\mathbf{X}_L = (\mathbf{x}_L + \mathbf{y}_L)/2$, $|\overline{\Omega}\rangle$ is the two-pion state in the laboratory system and $\mathbf{p}_1 + \mathbf{p}_2 = \mathbf{P}$. The $\Psi_{\rm L}(\mathbf{X}_L, \mathbf{r}_L)$ is extracted from the pion four-point function $G(\mathbf{X}_L, \mathbf{r}_L, t_L)$ given by,

$$G(\mathbf{X}_L, \mathbf{r}_L, t_L) = \sum_{\mathbf{x}_L, \mathbf{y}_L} \langle 0|\pi(\mathbf{x}_L, t_L) e^{i\mathbf{p}_1\cdot\mathbf{x}_L} \pi(\mathbf{y}_L, t_L) e^{i\mathbf{p}_2\cdot\mathbf{y}_L} \Omega(t_S)|0\rangle \delta(\mathbf{r}_L - (\mathbf{x}_L - \mathbf{y}_L)), \tag{308}$$

where $\Omega(t_S)$ is the two-pion operator with total momentum $\mathbf{P}$ at t_S. In follows we assume $t_S = 0$ for simplicity. In $t \to \infty$ we can obtain $\Psi_{\rm L}(\mathbf{X}_L, \mathbf{r}_L)$ as

$$G(\mathbf{X}_L, \mathbf{r}_L, t_L) \to C \cdot \Psi_{\rm L}(\mathbf{X}_L, \mathbf{r}_L) \cdot e^{-\overline{E}_L t_L}, \tag{309}$$

where $\overline{E}_L$ is the two-pion energy in the laboratory system.

From $\Psi_{\rm L}(\mathbf{X}_L, \mathbf{r}_L)$ we can extract the wave function $\psi_{\rm L}(\mathbf{r}_L)$ in eq.(184) as

$$\psi_{\rm L}(\mathbf{r}_L) = \sum_{\mathbf{X}_L} e^{-i\mathbf{P}\cdot\mathbf{X}_L} \Psi_{\rm L}(\mathbf{X}_L, \mathbf{r}_L). \tag{310}$$

The $\psi_{\rm L}(\mathbf{r}_L)$ satisfies the $\mathbf{d}$-periodic boundary condition eq.(186) as,

$$\psi_{\rm L}(\mathbf{r}_L) = (-1)^{\mathbf{d}\cdot\mathbf{n}} \psi_{\rm L}(\mathbf{r}_L + \mathbf{n}L), \tag{311}$$

where $\mathbf{d} = \mathbf{P}L/2\pi$ and $\mathbf{d}, \mathbf{n} \in Z^3$. The wave function in the center of mass system $\psi_{\rm CM}$ is related to $\psi_{\rm L}(\mathbf{r}_L)$ as eq.(183)

$$\psi_{\rm L}(\mathbf{r}_L) = \psi_{\rm CM}(\vec{\gamma}\mathbf{r}_L), \tag{312}$$

where $\gamma = \overline{E}_L/\sqrt{\overline{E}_L^2 - \mathbf{P}^2}$, and satisfies the Helmholtz equation eq.(179) in the exterior region of the interaction range, $r > R$,

$$(\nabla_{\mathbf{r}}^2 + \overline{p}^2)\psi_{\rm CM}(\mathbf{r}) = 0, \tag{313}$$

where $\overline{p}^2 = (\overline{E}_L^2 - \mathbf{P}^2)/4 - m_\pi^2$.

The interaction range R in the center of mass system can be estimated to use the same way with the effective potential given by eq.(266), when the Lorentz boost factor γ or the two-pion energy $\overline{E}_L$ is given. It is also possible to extract the center of mass momentum $\overline{p}^2$ in the region $r > R$.

Assuming the angular momentum cutoff $\Lambda = 0$, the center of mass wave function $\psi_{\rm CM}(\mathbf{r})$ is written by the $\mathbf{d}$-periodic Green function eq.(195),

$$\psi_{\rm CM}(\mathbf{r}) = C \cdot \sum_{k \in \Gamma_{\mathbf{d}}} \frac{e^{i\mathbf{k}\cdot\mathbf{r}}}{\mathbf{k}^2 - \overline{p}^2}, \tag{314}$$

where the sum is over the momentum

$$\Gamma_{\mathbf{d}} = \left\{ \mathbf{k} = \frac{2\pi}{L} \vec{\gamma}^{-1}(\mathbf{n} + \mathbf{d}/2) \quad \text{for all } \mathbf{n} \in Z^3 \right\}. \tag{315}$$

Since this function depends on not only the momentum $\overline{p}^2$ but also the Lorentz boost factor γ, we need the three parameters C, $\overline{p}^2$ and γ to fit the measured wave function.

Acknowledgment

I am most grateful to Professor N. Ishizuka for a kind guidance, continuous advices and discussions. I am also thankful to Professor S. Aoki, Professor A. Ukawa, Professor K. Kanaya, Professor T. Yoshié and Professor Y. Iwasaki for helpful comments and suggestions. Useful discussions with K. Ide and Y. Namekawa are gratefully acknowledged. I also would like to thank all staffs and students in the elementary particle theory group of the Institute for Theoretical Physics of the University of Tsukuba.

Numerical simulations were performed on CP-PACS at the Center for Computational Physics of the University of Tsukuba.

A Coefficients and functions in $A(s,t,u)$ of ChPT

In this appendix we show the coefficients b_i and the functions G, F, which are appeared in the scattering amplitude at two loop [33] eq.(45) in chiral perturbation theory.

A.1 Coefficient b_i

We define the coefficients $\overline{b}_i$ as

$$b_i = 16\pi^2 \overline{b}_i, \tag{A.1}$$

where the b_i is appeared in eq.(45). The coefficients $\overline{b}_i$ stand for

$$\begin{aligned}
\overline{b}_1 &= 8l_1^r + 2l_3^r - 2l_4^r + \frac{7}{6}L + \frac{1}{16\pi^2}\frac{13}{18} \\
&\quad +\xi\left\{\frac{56}{9}l_1^r + \frac{80}{9}l_2^r + 15l_3^r + \frac{26}{9}l_4^r + \frac{47}{108}L - \frac{17}{216} + \frac{1}{16\pi^2}\frac{3509}{1296}\right. \\
&\quad \left.+16\pi^2\left[\frac{1}{6}(4k_1 + 28k_2 - 6k_3 + 13k_4) + (32l_1^r + 12l_3^r - 5l_4^r)l_4^r - 8(l_3^r)^2 + r_1^r\right]\right\}, \\
\overline{b}_2 &= -8l_1^r + 2l_4^r - \frac{2}{3}L - \frac{1}{16\pi^2}\frac{2}{9} \\
&\quad +\xi\left\{-24l_1^r - \frac{166}{9}l_2^r - 18l_3^r - \frac{8}{9}l_4^r - \frac{203}{54}L + \frac{317}{3456} - \frac{1}{16\pi^2}\frac{1789}{432}\right. \\
&\quad \left.+16\pi^2\left[-\frac{1}{6}(54k_1 + 62k_2 + 15k_3 + 10k_4) - (32l_1^r + 4l_3^r - 5l_4^r)l_4^r + r_2^r\right]\right\}, \\
\overline{b}_3 &= 2l_1^r + \frac{1}{2}l_2^r - \frac{1}{2}L - \frac{1}{16\pi^2}\frac{7}{12} \\
&\quad +\xi\left\{\frac{178}{9}l_1^r + \frac{38}{3}l_2^r - \frac{7}{3}l_4^r - \frac{365}{216}L - \frac{311}{6912} + \frac{1}{16\pi^2}\frac{7063}{864}\right. \\
&\quad \left.+16\pi^2\left[\frac{1}{6}(38k_1 + 30k_2 - 3k_4) + (8l_1^r + 2l_2^r)l_4^r + r_3^r\right]\right\}, \\
\overline{b}_4 &= \frac{1}{2}l_2^r - \frac{1}{6}L - \frac{1}{16\pi^2}\frac{5}{36} \\
&\quad +\xi\left\{\frac{10}{9}l_1^r + \frac{4}{9}l_2^r - \frac{5}{9}l_4^r + \frac{47}{216}L + \frac{17}{3456} + \frac{1}{16\pi^2}\frac{1655}{2592}\right. \\
&\quad \left.+16\pi^2\left[-\frac{1}{6}(k_1 + 4k_2 + k_4) + 2l_2^r l_4^r + r_4^r\right]\right\}, \\
\overline{b}_5 &= -\frac{31}{6}l_1^r - \frac{145}{36}l_2^r + \frac{625}{288}L + \frac{7}{864} - \frac{1}{16\pi^2}\frac{66029}{20736} + 16\pi^2\left[-\frac{21}{6}k_1 - \frac{107}{96}k_2 + r_5^r\right], \\
\overline{b}_6 &= -\frac{7}{18}l_1^r - \frac{35}{36}l_2^r + \frac{257}{864}L + \frac{1}{432} - \frac{1}{16\pi^2}\frac{11375}{20736} + 16\pi^2\left[-\frac{5}{48}k_1 - \frac{25}{96}k_2 + r_6^r\right].
\end{aligned} \tag{A.2}$$

where

$$\begin{aligned}
L &= \frac{1}{16\pi^2}\ln\frac{m_\pi^2}{\mu^2}, \\
k_i &= (4l_i^r - \gamma_i L)L;\ \gamma_1 = \frac{1}{3},\ \gamma_2 = \frac{2}{3},\ \gamma_3 = -\frac{1}{2},\ \gamma_4 = 2.
\end{aligned} \tag{A.3}$$

The l_i^r and r_i^r are the renormalized couplings from $\mathcal{L}_4$ and $\mathcal{L}_6$, respectively. The parameter ξ is given by

$$\xi = \left(\frac{m_\pi^2}{4\pi f_\pi}\right)^2. \tag{A.4}$$

A.2 Functions $G^{(1)}, F^{(1)}, G^{(2)}, F^{(2)}$

We use the definition of the coefficients $\overline{b}_i$ eq.(A.1), and the normalized Mandelstam variables eq.(46)

$$\overline{s} = \frac{s}{m_\pi^2}, \quad \overline{t} = \frac{t}{m_\pi^2}, \quad \overline{u} = \frac{u}{m_\pi^2}. \tag{A.5}$$

The functions in eq.(45) are defined by

$$\begin{aligned}
F^{(1)}(\overline{s}) &= \frac{1}{2}\overline{J}(\overline{s})(\overline{s}^2-1), \\
G^{(1)}(\overline{s},\overline{t}) &= \frac{1}{6}\overline{J}(\overline{t})(14-4\overline{s}-10\overline{t}+\overline{s}\overline{t}+2\overline{t}^2), \\
F^{(2)}(\overline{s}) &= \overline{J}(\overline{s})\left\{\frac{1}{16\pi^2}\left(\frac{503}{108}\overline{s}^3-\frac{929}{54}\overline{s}^2+\frac{887}{27}\overline{s}-\frac{140}{9}\right)\right. \\
&\quad +\overline{b}_1(4\overline{s}-3)+\overline{b}_2(\overline{s}^2+4\overline{s}-4) \\
&\quad \left.+\frac{\overline{b}_3}{3}(8\overline{s}^3-21\overline{s}^2+48\overline{s}-32)+\frac{\overline{b}_4}{3}(16\overline{s}^3-71\overline{s}^2+112\overline{s}-48)\right\} \\
&\quad +\frac{1}{18}K_1(\overline{s})\left\{20\overline{s}^3-119\overline{s}^2+210\overline{s}-135-\frac{9}{16}\pi^2(\overline{s}-4)\right\} \\
&\quad +\frac{1}{32}K_2(\overline{s})\left\{\pi^2\overline{s}-24\right\}+\frac{1}{9}K_3(\overline{s})\left\{3\overline{s}^2-17\overline{s}+9\right\}, \\
G^{(2)}(\overline{s},\overline{t}) &= \overline{J}(\overline{s})\left\{\frac{1}{16\pi^2}\left(\frac{412}{27}-\frac{\overline{s}}{54}\left[\overline{t}^2+5\overline{t}+159\right]-\overline{t}\left[\frac{267}{216}\overline{t}^2-\frac{727}{108}\overline{t}+\frac{1571}{108}\right]\right)\right. \\
&\quad -\overline{b}_1(\overline{t}-2)+\frac{\overline{b}_2}{3}(\overline{t}-4)(2\overline{t}+\overline{s}-5)-\frac{\overline{b}_3}{6}(\overline{t}-4)^2(3\overline{t}+2\overline{s}-8) \\
&\quad \left.+\frac{\overline{b}_4}{6}\left(2\overline{s}(3\overline{t}-4)(\overline{t}-4)-32\overline{t}+40\overline{t}^2-11\overline{t}^3\right)\right\} \\
&\quad +\frac{1}{36}K_1(\overline{t})\left\{174+8\overline{s}-10\overline{t}^3+72\overline{t}^2-185\overline{t}-\frac{\pi^2}{16}(\overline{t}-4)(3\overline{s}-8)\right\} \\
&\quad +\frac{1}{9}K_2(\overline{t})\left\{1+4\overline{s}+\frac{\pi^2}{64}\overline{t}(3\overline{s}-8)\right\} \\
&\quad +\frac{1}{9}K_3(\overline{t})\left\{1+3\overline{s}\overline{t}-\overline{s}+3\overline{t}^2-9\overline{t}\right\}+\frac{5}{3}K_4(\overline{t})\left\{4-2\overline{s}-\overline{t}\right\}.
\end{aligned} \tag{A.6}$$

The loop functions $\overline{J}$ and K_i are given by

$$\begin{pmatrix} \overline{J} \\ K_1 \\ K_2 \\ K_3 \end{pmatrix} = \begin{pmatrix} 0 & 0 & z & -4C \\ 0 & z & 0 & 0 \\ 0 & z^2 & 0 & 8 \\ Cz\overline{s}^{-1} & 0 & \pi^2(C\overline{s})^{-1} & \pi^2 \end{pmatrix} \begin{pmatrix} h^3 \\ h^2 \\ h \\ -(2C^2)^{-1} \end{pmatrix}, \tag{A.7}$$

and

$$K_4(\overline{s}) = \frac{1}{\overline{s}z}\left(\frac{1}{2}K_1(\overline{s})+\frac{1}{3}K_3(\overline{s})+\frac{1}{C}\overline{J}(\overline{s})+\frac{(\pi^2-6)\overline{s}}{12C^2}\right), \tag{A.8}$$

where

$$h(\overline{s}) = \frac{1}{C\sqrt{z}}\ln\frac{\sqrt{z}-1}{\sqrt{z}+1}, \quad z = 1-\frac{4}{\overline{s}}, \quad C = 16\pi^2. \tag{A.9}$$

B Coefficients c_i and $\overline{p}_i$

B.1 Coefficients in $C(s,t,u)$

We show the forms of the coefficients c_i [25] in eq.(60). In this appendix the coefficients b_i given in appendix. A.1 are also used.

The coefficients c_i are given by

$$\begin{aligned}
c_1 &= -\frac{m_\pi^2}{f_\pi^2}\left\{1-\xi\left(b_1+\frac{68}{315}\right)-\xi^2\left(\frac{8b_1}{105}+\frac{32b_2}{63}+\frac{464b_3}{315}+\frac{3824b_4}{315}-\frac{601\pi^2}{945}+\frac{17947}{2835}\right)\right\},\\
c_2 &= \frac{1}{f_\pi^2}\left\{1+\xi\left(b_2-\frac{323}{1260}\right)-\xi^2\left(\frac{11b_1}{70}+\frac{211b_2}{315}+\frac{628b_3}{315}+\frac{5164b_4}{315}-\frac{5237\pi^2}{7560}+\frac{3977}{630}\right)\right\},\\
c_3 &= \frac{1}{16\pi^2 f_\pi^4}\left\{b_3+\frac{1}{42}+\xi\left(\frac{18b_1}{35}+\frac{59b_2}{105}+\frac{731b_3}{315}+\frac{3601b_4}{315}-\frac{5387\pi^2}{15120}-\frac{19121}{7560}\right)\right\},\\
c_4 &= \frac{1}{16\pi^2 f_\pi^4}\left\{b_4-\frac{31}{2520}-\xi\left(\frac{43b_1}{420}+\frac{8b_2}{63}-\frac{23b_3}{63}-\frac{997b_4}{315}-\frac{467\pi^2}{7560}+\frac{63829}{45360}\right)\right\},\\
c_5 &= \frac{1}{(16\pi^2)^2 f_\pi^6}\left\{\frac{137}{1680\xi}+\frac{b_1}{16}+\frac{379b_2}{1680}-\frac{25b_3}{28}-\frac{731b_4}{180}+b_5+\frac{269\pi^2}{15120}+\frac{61673}{18144}\right\},\\
c_6 &= \frac{1}{(16\pi^2)^2 f_\pi^6}\left\{-\frac{31}{1680\xi}+\frac{b_1}{112}-\frac{47b_2}{1680}-\frac{65b_3}{252}-\frac{547b_4}{420}+b_6+\frac{\pi^2}{15120}+\frac{44287}{92720}\right\},
\end{aligned} \tag{B.1}$$

where

$$\xi=\left(\frac{m_\pi^2}{4\pi f_\pi}\right)^2. \tag{B.2}$$

B.2 Coefficients in $\overline{P}(s,t,u)$

The coefficients $\overline{p}_i$ [25] in the polynomial term $\overline{P}(s,t,u)$ are expressed in terms of the following integrals over the imaginary parts of the partial waves $\mathrm{Im}t_l^I$,

$$\overline{I}_n^I = \sum_{l=0}^{\infty}\frac{(2l+1)}{\pi}\int_{4m_\pi^2}^{\infty}ds\frac{\mathrm{Im}t_l^I(s)}{s^{n+2}(s-4m_\pi^2)}, \tag{B.3}$$

$$H = \sum_{l=2}^{\infty}(2l+1)l(l+1)\frac{1}{\pi}\int_{4m_\pi^2}^{\infty}ds\frac{2\mathrm{Im}t_l^0(s)+4\mathrm{Im}t_l^2(s)}{9s^3(s-4m_\pi^2)}. \tag{B.4}$$

The explicit expressions of $\overline{p}_i$ are

$$\begin{aligned}
\overline{p}_1 &= -128\pi m_\pi^2\left(\overline{I}_0^1+\overline{I}_0^2+2m_\pi^2\overline{I}_1^1+2m_\pi^2\overline{I}_1^2+8m_\pi^4\overline{I}_2^2\right),\\
\overline{p}_2 &= -\frac{64\pi m_\pi^2}{3}\left(2\overline{I}_0^0-6\overline{I}_0^1-2\overline{I}_0^2-15m_\pi^2\overline{I}_1^1-3m_\pi^2\overline{I}_1^2-36m_\pi^4\overline{I}_2^2+6m_\pi^2H\right),\\
\overline{p}_3 &= \frac{8\pi}{3}\left(4\overline{I}_0^0-9\overline{I}_0^1-\overline{I}_0^2-16m_\pi^2\overline{I}_1^0-42m_\pi^2\overline{I}_1^1+22m_\pi^2\overline{I}_1^2-72m_\pi^4\overline{I}_2^2+24m_\pi^2H\right),\\
\overline{p}_4 &= 8\pi\left(\overline{I}_0^1+\overline{I}_0^2+2m_\pi^2\overline{I}_1^1+2m_\pi^2\overline{I}_1^2-24m_\pi^4\overline{I}_2^2\right),
\end{aligned}$$

$$\overline{p}_5 = \frac{4\pi}{3}\left(8\overline{I}_1^0 + 9\overline{I}_1^1 - 11\overline{I}_1^2 - 32m_\pi^2\overline{I}_2^0 + 44m_\pi^2\overline{I}_2^2 - 6H\right),$$
$$\overline{p}_6 = 4\pi\left(\overline{I}_1^1 - 3\overline{I}_1^2 + 12m_\pi^2\overline{I}_2^2 + 2H\right). \tag{B.5}$$

C Spherical zeta function

C.1 Calculation method of zeta function

In this section we present the numerical method of the spherical zeta function, which is introduced in the formulae eqs.(160) and (204) in the center of mass and laboratory systems, respectively.

The calculation has been described by Lüscher in Appendix A of Ref. [5] and in Appendix C of Ref. [6] for the center of mass system, and by Rummukainen and Gottlieb in Sec. 5.2 of Ref. [8] for general systems.

We present the calculation method of the spherical zeta function in the $\mathbf{d}$ system $Z_{00}^{\mathbf{d}}(s;\overline{n})$ with $\mathbf{d} = (L/2\pi)\mathbf{P}$ where $\mathbf{P}$ is the total momentum of the two pions. The $Z_{00}^{\mathbf{d}}(s;\overline{n})$ is defined by

$$Z_{00}^{\mathbf{d}}(s;\overline{n}) = \frac{1}{\sqrt{4\pi}}\sum_{\mathbf{r}\in P_d}(\mathbf{r}^2 - \overline{n})^{-s}, \tag{C.1}$$

where $P_d = \{\mathbf{r} = \vec{\gamma}^{-1}(\mathbf{n} + \mathbf{d}/2), \mathbf{n} \in Z^3\}$, $\vec{\gamma}^{-1}\mathbf{n} = \gamma^{-1}\mathbf{n}_{||} + \mathbf{n}_\perp$ where $\mathbf{n}_{||}$ and $\mathbf{n}_\perp$ are components of $\mathbf{n}$ parallel and perpendicular to the direction $\mathbf{d}$, i.e., $\mathbf{n}_{||} = (\mathbf{n}\cdot\mathbf{d})\mathbf{d}/\mathbf{d}^2$ and $\mathbf{n}_\perp = \mathbf{n} - \mathbf{n}_{||}$. Here γ is the Lorentz boost factor defined by $\gamma = E_L/\sqrt{E_L^2 - \mathbf{P}^2}$ where E_L is the two-pion energy in the $\mathbf{d}$ system. We can obtain the one in the center of mass system $Z_{00}(s;\overline{n})$ by taking $|\mathbf{d}| = 0$ in the representation of $Z_{00}^{\mathbf{d}}(s;\overline{n})$.

The zeta function $Z_{00}^{\mathbf{d}}(s;\overline{n})$ takes a finite value in $\mathrm{Re}\, s > 3/2$, so that $Z_{00}^{\mathbf{d}}(1;\overline{n})$ in the formula eq.(204) is defined by the analytic continuation from $\mathrm{Re}\, s > 3/2$.

The summation in $Z_{00}^{\mathbf{d}}(s;\overline{n})$ is divided by the two parts as,

$$\sum_{\mathbf{r}}(\mathbf{r}^2 - \overline{n})^{-s} = \sum_{\mathbf{r}^2<\overline{n}}(\mathbf{r}^2 - \overline{n})^{-s} + \sum_{\mathbf{r}^2>\overline{n}}(\mathbf{r}^2 - \overline{n})^{-s}, \tag{C.2}$$

where the summation of $\mathbf{r}$ is carried out with $\mathbf{r} \in P_{\mathbf{d}}$. The second term is written by the integral form as follows,

$$\sum_{\mathbf{r}^2>\overline{n}}(\mathbf{r}^2 - \overline{n})^{-s} = \frac{1}{\Gamma(s)}\sum_{\mathbf{r}^2>\overline{n}}\int_0^\infty dt\, t^{s-1}e^{-t(\mathbf{r}^2-\overline{n})} \tag{C.3}$$
$$= \frac{1}{\Gamma(s)}\sum_{\mathbf{r}^2>\overline{n}}\left[\int_0^1 dt\, t^{s-1}e^{-t(\mathbf{r}^2-\overline{n})} + \int_1^\infty dt\, t^{s-1}e^{-t(\mathbf{r}^2-\overline{n})}\right] \tag{C.4}$$
$$= \frac{1}{\Gamma(s)}\int_0^1 dt\, t^{s-1}e^{t\overline{n}}\sum_{\mathbf{r}}e^{-t\mathbf{r}^2} - \sum_{\mathbf{r}^2<\overline{n}}(\mathbf{r}^2 - \overline{n})^{-s} + \sum_{j=1}^{s}\frac{1}{(s-j)!}\sum_{\mathbf{r}}\frac{e^{-(\mathbf{r}^2-\overline{n})}}{(\mathbf{r}^2-\overline{n})^j}. \tag{C.5}$$

The second term is canceled out with the first term in eq.(C.2). We rewrite the first term in eq.(C.5) by the Poisson's summation formula,

$$\sum_{\mathbf{n}\in Z^3} f(\mathbf{n}) = \sum_{\mathbf{n}\in Z^3} \int d^3x f(\mathbf{x}) e^{i2\pi \mathbf{n}\cdot\mathbf{x}}. \tag{C.6}$$

By integrating for $\mathbf{x}$ we obtain the following formula as,

$$\frac{1}{\Gamma(s)} \int_0^1 dt\, t^{s-1} e^{t\overline{n}} \sum_{\mathbf{r}} e^{-t\mathbf{r}^2} = \frac{\gamma}{\Gamma(s)} \int_0^1 dt\, t^{s-1} e^{t\overline{n}} \left(\frac{\pi}{t}\right)^{3/2} \sum_{\mathbf{n}\in Z^3} (-1)^{\mathbf{n}\cdot\mathbf{d}} e^{-\left(\frac{\pi^2(\vec{\gamma}\mathbf{n})^2}{t}\right)}. \tag{C.7}$$

In $s = 1$, the $|\mathbf{n}| = 0$ part of the integration of the right hand side in eq.(C.7) diverges, while other parts of the integration give finite values. We divide the integrand to the divergent part ($|\mathbf{n}| = 0$) and the finite part ($|\mathbf{n}| \neq 0$). The divergent part can be evaluated in $\mathrm{Re}\, s > 3/2$ as

$$\int_0^1 dt\, t^{s-1} e^{t\overline{n}} \left(\frac{\pi}{t}\right)^{3/2} = \sum_{l=0}^{\infty} \frac{\pi^{3/2}}{s+l-3/2} \frac{\overline{n}^l}{l!}. \tag{C.8}$$

The final expression is finite at $s = 1$.

In $s = 1$ using eq.(C.8) the all parts of the spherical zeta function takes finite values, so that we can calculate the value of $Z_{00}^{\mathbf{d}}(1;\overline{n})$ as follows,

$$\begin{aligned} Z_{00}^{\mathbf{d}}(1;\overline{n}) &= \frac{1}{\sqrt{4\pi}} \left\{ \sum_{\mathbf{r}} \frac{e^{-(\mathbf{r}^2-\overline{n})}}{\mathbf{r}^2-\overline{n}} \right. \\ &\left. + \gamma \int_0^1 dt\, e^{t\overline{n}} \left(\frac{\pi}{t}\right)^{3/2} {\sum_{\mathbf{n}\in Z^3}}' (-1)^{\mathbf{n}\cdot\mathbf{d}} e^{-\left(\frac{\pi^2(\vec{\gamma}\mathbf{n})^2}{t}\right)} + \gamma \sum_{l=0}^{\infty} \frac{\pi^{3/2}}{l-1/2} \frac{\overline{n}^l}{l!} \right\}, \end{aligned} \tag{C.9}$$

where $\sum'_{\mathbf{n}\in Z^3}$ is the summation without $|\mathbf{n}| = 0$ case. This is the integral representation of the spherical zeta function in the $\mathbf{d}$ system introduced in eq.(204).

Substituting $|\mathbf{d}| = 0$ and $\gamma = 1$ in the above expression, we obtain the representation of the zeta function in the center of mass system appeared in eq.(160),

$$Z_{00}(1;\overline{n}) = \frac{1}{\sqrt{4\pi}} \left\{ \sum_{\mathbf{n}\in Z^3} \frac{e^{-(\mathbf{n}^2-\overline{n})}}{\mathbf{n}^2-\overline{n}} + \int_0^1 dt\, e^{t\overline{n}} \left(\frac{\pi}{t}\right)^{3/2} {\sum_{\mathbf{n}\in Z^3}}' e^{-\left(\frac{\pi^2\mathbf{n}^2}{t}\right)} + \sum_{l=0}^{\infty} \frac{\pi^{3/2}}{l-1/2} \frac{\overline{n}^l}{l!} \right\}. \tag{C.10}$$

C.2 Calculation method of wave function

We explain calculation of the wave function in the center of mass system eq.(267)

$$\psi(\mathbf{r}) = C \cdot \sum_{\mathbf{k}} \frac{e^{i\mathbf{k}\cdot\mathbf{r}}}{\mathbf{k}^2-\overline{p}^2} = C' \cdot \sum_{\mathbf{n}} \frac{e^{i\mathbf{n}\cdot\mathbf{r}'}}{\mathbf{n}^2-\overline{n}}, \quad \mathbf{k} = \left(\frac{2\pi}{L}\right)\mathbf{n}, \tag{C.11}$$

where $C' = C \cdot (L/2\pi)^2$, $\mathbf{r}' = \mathbf{r} \cdot (2\pi/L)$ and $\overline{p}^2 = (2\pi/L)^2 \cdot \overline{n}$. We restrict the region of the wave function in $\mathbf{r} \neq 0$, since in the actual analysis we use the form only in the exterior region of the interaction range R, i.e., $r > R$. For the wave function analysis the expansion form of the wave function is useful. In this section we show the form.

We omit the over all constant $C^{'}$, and define an integer $n^{'}$ as $n^{'} - \overline{n} = O(1/L)$. In free case $n^{'} = \overline{n}$. Using $n^{'}$ we expand $\psi(\mathbf{r})$ around $\overline{n} = n^{'}$ and find

$$\psi(\mathbf{r}) = -\frac{1}{\Delta}\sum_{i=1}^{\nu_{n^{'}}} e^{i\mathbf{n}\cdot\mathbf{r}^{'}} + \sum_{s=1}^{\infty}\Delta^{s-1}Z^{sub}(s, n^{'}, \mathbf{r}^{'}), \tag{C.12}$$

where $\nu_{n^{'}} = \sum_{\mathbf{n}}\delta_{n^{'},\mathbf{n}^2}$, $\Delta = \overline{n} - n^{'}$, and

$$Z^{sub}(s, n^{'}, \mathbf{r}) = \sum_{\mathbf{n}^2 \neq n^{'}} \frac{e^{i\mathbf{n}\cdot\mathbf{r}}}{(\mathbf{n}^2 - n^{'})^s}. \tag{C.13}$$

We can obtain the integral expression of eq.(C.13) in the same manner in appendix. C.1: The summation is divided by two parts, and we use the Poisson's summation formula eq.(C.6). We then find

$$\begin{aligned} Z^{sub}(s, n^{'}, \mathbf{r}) &= \frac{1}{\Gamma(s)}\left\{\sum_{\mathbf{n}^2 \neq n^{'}} e^{i\mathbf{n}\cdot\mathbf{r} - (\mathbf{n}^2 - n^{'})}\sum_{j=1}^{s}\frac{1}{(\mathbf{n}^2 - n^{'})^j}\frac{(s-1)!}{(s-j)!}\right. & \text{(C.14)} \\ &\left. + \int_0^1 dt\, t^{s-1}e^{tn^{'}}\left(\frac{\pi}{t}\right)^{3/2}\sum_{\mathbf{n}} e^{-(\pi\mathbf{n} - \mathbf{r}/2)^2/t} - \frac{1}{s}\right\}. & \text{(C.15)} \end{aligned}$$

Substituting the integral expression into eq.(C.12), we obtain the wave function for desired precision.

C.3 Property of zeta function in free case

In this section first we prove the equation

$$q\frac{\partial\phi(q)}{\partial q}\bigg|_{q^2=n} = \frac{4\pi^2 q^3}{\nu_n}, \tag{C.16}$$

where $\nu_n \equiv \sum_{\mathbf{m}}\delta_{n,\mathbf{m}^2}$. Here $\phi(q)$ is defined by eq.(295)

$$\tan\phi(q) = -\frac{\pi^{3/2}q}{Z_{00}(1; q^2)}, \tag{C.17}$$

where $\overline{n}$ in the above sections corresponds to q^2 in this section. Substituting the large-L expansion form of the spherical zeta function eq.(163) into eq.(C.17) we find

$$\tan\phi(q) = \frac{2\pi^2 q\Delta}{\nu_n}\left(1 + \Delta\frac{Z_{00}^{sub}(1; q^2)}{\nu_n} + O(\Delta^2)\right), \quad \Delta = q^2 - n, \tag{C.18}$$

where the subtracted spherical zeta function $Z_{00}^{sub}(1; q^2)$ is defined in eq.(162). Since $\tan\phi(q)$ is $O(\Delta)$ as shown in eq.(C.18), we can show $\phi(q) = 0$ at $\Delta = 0$.

The derivative of $\tan\phi(q)$ up to $O(\Delta^2)$ is given by

$$\frac{1}{\cos^2(\phi(q))}\frac{\partial\phi(q)}{\partial q} = \frac{4\pi^2 q^2}{\nu_n}\left(1 + \Delta\left(\frac{1}{2q^2} + 2\frac{Z_{00}^{sub}(1; q^2)}{\nu_n}\right)\right). \tag{C.19}$$

Hence at $\Delta = 0$ we can show the equation eq.(C.16).

Substituting eq.(C.16) and $\delta(p) = 0$ to eq.(300) and using the relation $p = (2\pi/L)q$, we can show eq.(301).

D Table for Results of scattering length and scattering phase shift

In Tables XVII – XXII we tabulate fitting ranges, energy shift $\Delta\overline{E}_n^{\mathbf{P}}$, center of mass momentum $\overline{p}^2$, Lorentz boost factor γ, scattering phase shift $\delta(\overline{p})$, and scattering amplitudes,

$$A(m_\pi, \overline{p}) = \frac{\tan\delta(\overline{p})}{\overline{p}} \cdot \frac{\overline{E}}{2}, \tag{D.1}$$

$$A^f(m_\pi, \overline{p}) = \left(\frac{f_\pi^{lat}}{f_\pi}\right)^2 \cdot A(m_\pi, \overline{p}), \tag{D.2}$$

where f_π^{lat} is the pseudoscalar decay constant for each pion mass measured on lattice and $f_\pi = 93$ MeV, in each system for the ground $n = 0$ and first excited $n = 1$ states. In the center of mass system for the ground state, the values

$$\frac{A(m_\pi, \overline{p})}{m_\pi^2} \quad \text{and} \quad \frac{A^f(m_\pi, \overline{p})}{m_\pi^2} \tag{D.3}$$

are also listed, which may be approximated the scattering length a_0/m_π and a_0^f/m_π.

$\beta = 1.80$	κ	0.1464	0.1445	0.1430	0.1409
$a^{-1} = 0.9176(93)$[GeV]	m_π/m_ρ	0.547(4)	0.694(2)	0.753(1)	0.807(1)
	m_π^2 [GeV^2]	0.238(1)	0.571(1)	0.814(1)	1.128(1)
Fitting Range		10 – 20	12 – 20	12 – 20	12 – 20
$\Delta\overline{E}_n^{\mathbf{P}}$	[$\times 10^{-4}$ GeV]	46.1(98)	36.2(39)	28.4(37)	21.7(14)
$\overline{p}_n^2$	[$\times 10^{-4}$ GeV^2]	24.5(52)	29.9(32)	27.9(37)	25.1(17)
$\delta(\overline{p}_n)$	[degrees]	−1.13(34)	−1.49(22)	−1.36(25)	−1.17(11)
$A(m_\pi, \overline{p}_n)$		−0.196(38)	−0.362(35)	−0.406(49)	−0.434(26)
$A(m_\pi, \overline{p}_n)/m_\pi^2$	[1/GeV^2]	−0.82(16)	−0.633(62)	−0.499(60)	−0.384(23)
$A^f(m_\pi, \overline{p}_n)$		−0.59(11)	−1.66(16)	−2.44(29)	−3.17(19)
$A^f(m_\pi, \overline{p}_n)/m_\pi^2$	[1/GeV^2]	−2.47(48)	−2.91(28)	−3.02(33)	−2.83(17)
$\beta = 1.95$	κ	0.1410	0.1400	0.1390	0.1375
$a^{-1} = 1.268(13)$[GeV]	m_π/m_ρ	0.582(3)	0.690(1)	0.752(1)	0.804(1)
	m_π^2 [GeV^2]	0.291(2)	0.573(1)	0.857(1)	1.287(1)
Fitting Range		12 – 23	13 – 25	13 – 25	13 – 25
$\Delta\overline{E}_n^{\mathbf{P}}$	[$\times 10^{-4}$ GeV]	109.5(73)	68.9(69)	57.4(30)	38.6(23)
$\overline{p}_n^2$	[$\times 10^{-4}$ GeV^2]	46.7(31)	41.2(41)	41.9(22)	34.5(21)
$\delta(\overline{p}_n)$	[degrees]	−2.50(23)	−2.10(29)	−2.16(15)	−1.65(14)
$A(m_\pi, \overline{p}_n)$		−0.348(20)	−0.436(38)	−0.540(25)	−0.557(30)
$A(m_\pi, \overline{p}_n)/m_\pi^2$	[1/GeV^2]	−1.195(70)	−0.759(67)	−0.630(29)	−0.433(23)
$A^f(m_\pi, \overline{p}_n)$		−0.769(45)	−1.37(12)	−2.27(10)	−3.09(17)
$A^f(m_\pi, \overline{p}_n)/m_\pi^2$	[1/GeV^2]	−2.63(15)	−2.39(21)	−2.65(12)	−2.40(13)
$\beta = 2.10$	κ	0.1382	0.1374	0.1367	0.1357
$a^{-1} = 1.833(22)$[GeV]	m_π/m_ρ	0.576(3)	0.691(3)	0.755(2)	0.806(1)
	m_π^2 [GeV^2]	0.291(1)	0.605(2)	0.896(1)	1.331(2)
Fitting Range		18 – 35	18 – 35	18 – 35	18 – 35
$\Delta\overline{E}_n^{\mathbf{P}}$	[$\times 10^{-4}$ GeV]	173.3(54)	104.8(42)	84.9(32)	61.6(30)
$\overline{p}_n^2$	[$\times 10^{-4}$ GeV^2]	51.3(16)	44.6(17)	44.0(16)	38.9(19)
$\delta(\overline{p}_n)$	[degrees]	−3.17(13)	−2.62(14)	−2.57(13)	−2.17(14)
$A(m_\pi, \overline{p}_n)$		−0.421(12)	−0.536(18)	−0.643(20)	−7.04(30)
$A(m_\pi, \overline{p}_n)/m_\pi^2$	[1/GeV^2]	−1.444(38)	−0.885(31)	−0.718(23)	−0.528(23)
$A^f(m_\pi, \overline{p}_n)$		−0.718(20)	−1.471(49)	−2.251(72)	−3.12(13)
$A^f(m_\pi, \overline{p}_n)/m_\pi^2$	[1/GeV^2]	−2.462(66)	−2.429(85)	−2.512(82)	−2.34(10)

Table XVII: Result for $n = 0$ state in the center of mass system CM with energy state cut-off $N = 2$. The $A(m_\pi, \overline{p}_n)$ and $A^f(m_\pi, \overline{p}_n)$ are defined by eqs.(D.1) and (D.2), respectively. The values for $A(m_\pi, \overline{p})/m_\pi^2$ and $A^f(m_\pi, \overline{p})/m_\pi^2$ are approximated the scattering length a_0/m_π and a_0^f/m_π, respectively.

$\beta = 1.80$	κ	0.1464	0.1445	0.1430	0.1409
$a^{-1} = 0.9176(93)$[GeV]	m_π/m_ρ	0.547(4)	0.694(2)	0.753(1)	0.807(1)
	m_π^2 [GeV^2]	0.238(1)	0.571(1)	0.814(1)	1.128(1)
Fitting Range		10 – 18	12 – 18	12 – 20	12 – 20
$\Delta\overline{E}_n^{\mathbf{P}}$	[$\times 10^{-3}$ GeV]	22.5(34)	13.2(12)	11.42(70)	8.78(40)
$\overline{p}_n^2$	[$\times 10^{-2}$ GeV^2]	24.80(26)	24.40(12)	24.380(78)	24.222(51)
$\delta(\overline{p}_n)$	[degrees]	−14.1(22)	−10.7(10)	−10.59(66)	−9.25(43)
$A(m_\pi, \overline{p}_n)$		−0.353(57)	−0.348(33)	−0.389(24)	−0.387(18)
$A^f(m_\pi, \overline{p}_n)$		−1.06(17)	−1.59(15)	−2.34(14)	−2.83(13)
$\beta = 1.95$	κ	0.1410	0.1400	0.1390	0.1375
$a^{-1} = 1.268(13)$[GeV]	m_π/m_ρ	0.582(3)	0.690(1)	0.752(1)	0.804(1)
	m_π^2 [GeV^2]	0.291(2)	0.573(1)	0.857(1)	1.287(1)
Fitting Range		12 – 23	13 – 25	13 – 25	13 – 25
$\Delta\overline{E}_n^{\mathbf{P}}$	[$\times 10^{-3}$ GeV]	45.7(51)	29.9(20)	22.70(95)	15.50(49)
$\overline{p}_n^2$	[$\times 10^{-2}$ GeV^2]	27.55(30)	27.02(14)	26.761(79)	26.389(48)
$\delta(\overline{p}_n)$	[degrees]	−20.9(24)	−16.7(11)	−14.63(63)	−11.70(38)
$A(m_\pi, \overline{p}_n)$		−0.549(68)	−0.531(38)	−0.535(23)	−0.502(16)
$A^f(m_\pi, \overline{p}_n)$		−1.21(15)	−1.67(12)	−2.225(99)	−2.787(91)
$\beta = 2.10$	κ	0.1382	0.1374	0.1367	0.1357
$a^{-1} = 1.833(22)$[GeV]	m_π/m_ρ	0.576(3)	0.691(3)	0.755(2)	0.806(1)
	m_π^2 [GeV^2]	0.291(1)	0.605(2)	0.896(1)	1.331(2)
Fitting Range		18 – 35	18 – 35	18 – 35	18 – 35
$\Delta\overline{E}_n^{\mathbf{P}}$	[$\times 10^{-3}$ GeV]	58.8(69)	44.1(25)	34.6(14)	26.80(78)
$\overline{p}_n^2$	[$\times 10^{-2}$ GeV^2]	25.30(28)	25.17(13)	24.969(84)	24.789(53)
$\delta(\overline{p}_n)$	[degrees]	−19.8(24)	−18.7(11)	−16.99(73)	−15.44(46)
$A(m_\pi, \overline{p}_n)$		−0.530(69)	−0.626(39)	−0.654(28)	−0.697(21)
$A^f(m_\pi, \overline{p}_n)$		−0.90(11)	−1.71(10)	−2.29(10)	−3.097(94)

Table XVIII: Result for $n = 1$ state in the center of mass system CM with energy state cut-off $N = 2$. The $A(m_\pi, \overline{p}_n)$ and $A^f(m_\pi, \overline{p}_n)$ are defined by eqs.(D.1) and (D.2), respectively.

$\beta = 1.80$	κ	0.1464	0.1445	0.1430	0.1409
$a^{-1} = 0.9176(93)$[GeV]	m_π/m_ρ	0.547(4)	0.694(2)	0.753(1)	0.807(1)
	m_π^2 [GeV^2]	0.238(1)	0.571(1)	0.814(1)	1.128(1)
Fitting Range		10 – 18	12 – 20	12 – 20	12 – 20
$\Delta\overline{E}_n^{\mathbf{P}}$	[$\times 10^{-3}$ GeV]	9.5(10)	6.72(50)	4.65(43)	3.70(19)
$\overline{p}_n^2$	[$\times 10^{-3}$ GeV^2]	54.16(69)	58.93(46)	59.04(45)	59.56(23)
γ		1.09436(62)	1.04481(11)	1.032523(71)	1.024028(25)
$\delta(\overline{p}_n)$	[degrees]	−7.03(76)	−7.14(52)	−5.81(52)	−5.36(27)
$A(m_\pi, \overline{p}_n)$		−0.286(30)	−0.409(28)	−0.391(34)	−0.419(20)
$A^f(m_\pi, \overline{p}_n)$		−0.862(91)	−1.88(13)	−2.35(20)	−3.07(15)
$\beta = 1.95$	κ	0.1410	0.1400	0.1390	0.1375
$a^{-1} = 1.268(13)$[GeV]	m_π/m_ρ	0.582(3)	0.690(1)	0.752(1)	0.804(1)
	m_π^2 [GeV^2]	0.291(2)	0.573(1)	0.857(1)	1.287(1)
Fitting Range		12 – 23	13 – 25	13 – 25	13 – 25
$\Delta\overline{E}_n^{\mathbf{P}}$	[$\times 10^{-3}$ GeV]	17.3(11)	11.99(55)	9.62(35)	6.92(30)
$\overline{p}_n^2$	[$\times 10^{-3}$ GeV^2]	61.40(58)	64.47(36)	65.73(28)	65.91(28)
γ		1.08447(51)	1.04758(13)	1.033120(56)	1.022720(32)
$\delta(\overline{p}_n)$	[degrees]	−9.29(59)	−8.55(38)	−8.20(29)	−7.12(30)
$A(m_\pi, \overline{p}_n)$		−0.392(24)	−0.473(20)	−0.540(18)	−0.566(23)
$A^f(m_\pi, \overline{p}_n)$		−0.865(53)	−1.491(63)	−2.276(79)	−3.14(12)
$\beta = 2.10$	κ	0.1382	0.1374	0.1367	0.1357
$a^{-1} = 1.833(22)$[GeV]	m_π/m_ρ	0.576(3)	0.691(3)	0.755(2)	0.806(1)
	m_π^2 [GeV^2]	0.291(1)	0.605(2)	0.896(1)	1.331(2)
Fitting Range		18 – 35	18 – 35	18 – 35	18 – 35
$\Delta\overline{E}_n^{\mathbf{P}}$	[$\times 10^{-3}$ GeV]	27.8(12)	17.7(65)	14.75(48)	10.45(38)
$\overline{p}_n^2$	[$\times 10^{-3}$ GeV^2]	58.78(42)	61.02(29)	62.22(26)	61.97(25)
γ		1.07874(41)	1.04214(13)	1.029504(58)	1.020373(39)
$\delta(\overline{p}_n)$	[degrees]	−11.09(46)	−9.66(33)	−9.55(29)	−8.16(28)
$A(m_\pi, \overline{p}_n)$		−0.478(19)	−0.563(18)	−0.660(19)	−0.680(23)
$A^f(m_\pi, \overline{p}_n)$		−0.816(32)	−1.544(50)	−2.311(68)	−3.02(10)

Table XIX: Result for $n = 0$ state in the laboratory system L1 with energy state cut-off $N = 3$. The $A(m_\pi, \overline{p}_n)$ and $A^f(m_\pi, \overline{p}_n)$ are defined by eqs.(D.1) and (D.2), respectively.

$\beta = 1.80$	κ	0.1464	0.1445	0.1430	0.1409
$a^{-1} = 0.9176(93)$[GeV]	m_π/m_ρ	0.547(4)	0.694(2)	0.753(1)	0.807(1)
	m_π^2 [GeV^2]	0.238(1)	0.571(1)	0.814(1)	1.128(1)
Fitting Range		10 – 18	12 – 18	12 – 20	12 – 20
$\Delta\overline{E}_n^{\mathbf{P}}$	[$\times 10^{-3}$ GeV]	28.70(63)	18.1(26)	14.6(12)	10.62(59)
$\overline{p}_n^2$	[$\times 10^{-2}$ GeV^2]	30.65(53)	30.41(27)	30.31(14)	30.006(79)
γ		1.05169(54)	1.03245(10)	1.025510(52)	1.020014(19)
$\delta(\overline{p}_n)$	[degrees]	−16.9(39)	−13.4(20)	−12.1(10)	−9.86(56)
$A(m_\pi, \overline{p}_n)$		−0.405(98)	−0.406(61)	−0.412(35)	−0.379(21)
$A^f(m_\pi, \overline{p}_n)$		−1.22(29)	−1.86(28)	−2.47(21)	−2.77(15)
$\beta = 1.95$	κ	0.1410	0.1400	0.1390	0.1375
$a^{-1} = 1.268(13)$[GeV]	m_π/m_ρ	0.582(3)	0.690(1)	0.752(1)	0.804(1)
	m_π^2 [GeV^2]	0.291(2)	0.573(1)	0.857(1)	1.287(1)
Fitting Range		12 – 16	13 – 20	13 – 20	13 – 25
$\Delta\overline{E}_n^{\mathbf{P}}$	[$\times 10^{-3}$ GeV]	57(10)	34.0(37)	28.3(16)	18.98(79)
$\overline{p}_n^2$	[$\times 10^{-2}$ GeV^2]	34.21(67)	33.30(28)	33.26(14)	32.788(81)
γ		1.04789(53)	1.03371(12)	1.025787(45)	1.019069(26)
$\delta(\overline{p}_n)$	[degrees]	−25.0(47)	−17.3(19)	−16.35(99)	−12.59(53)
$A(m_\pi, \overline{p}_n)$		−0.63(13)	−0.516(60)	−0.555(34)	−0.495(21)
$A^f(m_\pi, \overline{p}_n)$		−1.40(29)	−1.62(19)	−2.33(14)	−2.75(11)
$\beta = 2.10$	κ	0.1382	0.1374	0.1367	0.1357
$a^{-1} = 1.833(22)$[GeV]	m_π/m_ρ	0.576(3)	0.691(3)	0.755(2)	0.806(1)
	m_π^2 [GeV^2]	0.291(1)	0.605(2)	0.896(1)	1.331(2)
Fitting Range		18 – 22	18 – 35	18 – 35	18 – 35
$\Delta\overline{E}_n^{\mathbf{P}}$	[$\times 10^{-3}$ GeV]	68(13)	53.9(48)	39.3(24)	32.4(12)
$\overline{p}_n^2$	[$\times 10^{-2}$ GeV^2]	31.16(58)	31.23(24)	30.82(14)	30.798(89)
γ		1.04646(43)	1.03077(10)	1.023545(48)	1.017343(30)
$\delta(\overline{p}_n)$	[degrees]	−21.8(43)	−20.7(19)	−17.1(10)	−16.32(64)
$A(m_\pi, \overline{p}_n)$		−0.55(12)	−0.651(63)	−0.608(39)	−0.675(27)
$A^f(m_\pi, \overline{p}_n)$		−0.95(20)	−1.78(17)	−2.13(13)	−3.00(12)

Table XX: Result for $n = 1$ state in the laboratory system L1 with energy state cut-off $N = 3$. The $A(m_\pi, \overline{p}_n)$ and $A^f(m_\pi, \overline{p}_n)$ are defined by eqs.(D.1) and (D.2), respectively.

$\beta = 1.80$	κ	0.1464	0.1445	0.1430	0.1409
$a^{-1} = 0.9176(93)$[GeV]	m_π/m_ρ	0.547(4)	0.694(2)	0.753(1)	0.807(1)
	m_π^2 [GeV^2]	0.238(1)	0.571(1)	0.814(1)	1.128(1)
Fitting Range		10 – 18	12 – 18	12 – 18	12 – 20
$\Delta\overline{E}_n^{\mathbf{P}}$	[$\times 10^{-4}$ GeV]	72(21)	47.9(84)	38.1(50)	20.3(27)
$\overline{p}_n^2$	[$\times 10^{-2}$ GeV^2]	9.03(15)	10.316(82)	10.682(57)	10.820(34)
γ		1.1626(11)	1.08224(20)	1.06082(12)	1.045678(45)
$\delta(\overline{p}_n)$	[degrees]	−9.7(33)	−11.4(32)	−12.6(37)	−6.5(14)
$A(m_\pi, \overline{p}_n)$		−0.32(11)	−0.51(15)	−0.65(19)	−0.387(86)
$A^f(m_\pi, \overline{p}_n)$		−0.98(34)	−2.37(69)	−3.9(11)	−2.83(63)
$\beta = 1.95$	κ	0.1410	0.1400	0.1390	0.1375
$a^{-1} = 1.268(13)$[GeV]	m_π/m_ρ	0.582(3)	0.690(1)	0.752(1)	0.804(1)
	m_π^2 [GeV^2]	0.291(2)	0.573(1)	0.857(1)	1.287(1)
Fitting Range		12 – 16	13 – 20	13 – 25	13 – 25
$\Delta\overline{E}_n^{\mathbf{P}}$	[$\times 10^{-3}$ GeV]	15.5(25)	7.5(10)	5.49(71)	3.12(37)
$\overline{p}_n^2$	[$\times 10^{-2}$ GeV^2]	10.28(14)	11.043(77)	11.473(59)	11.726(36)
γ		1.14682(99)	1.08709(25)	1.06202(10)	1.043336(60)
$\delta(\overline{p}_n)$	[degrees]	−18.3(46)	−12.1(29)	−12.2(32)	−8.0(18)
$A(m_\pi, \overline{p}_n)$		−0.64(17)	−0.53(13)	−0.63(17)	−0.48(11)
$A^f(m_\pi, \overline{p}_n)$		−1.42(38)	−1.69(41)	−2.66(73)	−2.70(62)
$\beta = 2.10$	κ	0.1382	0.1374	0.1367	0.1357
$a^{-1} = 1.833(22)$[GeV]	m_π/m_ρ	0.576(3)	0.691(3)	0.755(2)	0.806(1)
	m_π^2 [GeV^2]	0.291(1)	0.605(2)	0.896(1)	1.331(2)
Fitting Range		18 – 30	18 – 35	18 – 35	18 – 35
$\Delta\overline{E}_n^{\mathbf{P}}$	[$\times 10^{-3}$ GeV]	17.5(35)	9.3(15)	7.83(88)	4.45(61)
$\overline{p}_n^2$	[$\times 10^{-2}$ GeV^2]	9.48(13)	10.332(76)	10.746(50)	10.932(42)
γ		1.13877(72)	1.07789(27)	1.05563(10)	1.039047(74)
$\delta(\overline{p}_n)$	[degrees]	−14.5(41)	−12.0(33)	−17.3(56)	−10.9(40)
$A(m_\pi, \overline{p}_n)$		−0.52(15)	−0.55(16)	−0.95(33)	−0.70(26)
$A^f(m_\pi, \overline{p}_n)$		−0.89(26)	−1.53(44)	−3.3(11)	−3.1(11)

Table XXI: Result for $n = 0$ state in the laboratory system L2 with energy state cut-off $N = 3$. The $A(m_\pi, \overline{p}_n)$ and $A^f(m_\pi, \overline{p}_n)$ are defined by eqs.(D.1) and (D.2), respectively.

$\beta = 1.80$	κ	0.1464	0.1445	0.1430	0.1409
$a^{-1} = 0.9176(93)$[GeV]	m_π/m_ρ	0.547(4)	0.694(2)	0.753(1)	0.807(1)
	m_π^2 [GeV^2]	0.238(1)	0.571(1)	0.814(1)	1.128(1)
Fitting Range		10 – 18	12 – 18	12 – 20	12 – 20
$\Delta\overline{E}_n^{\mathbf{P}}$	[$\times 10^{-4}$ GeV]	95(18)	68.0(73)	53.8(44)	44.7(24)
$\overline{p}_n^2$	[$\times 10^{-2}$ GeV^2]	12.26(13)	12.217(71)	12.152(49)	12.120(30)
γ		1.14900(84)	1.08007(19)	1.05990(11)	1.045213(44)
$\delta(\overline{p}_n)$	[degrees]	−11.3(18)	−9.36(82)	−8.12(54)	−7.35(32)
$A(m_\pi, \overline{p}_n)$		−0.329(55)	−0.393(34)	−0.397(24)	−0.413(18)
$A^f(m_\pi, \overline{p}_n)$		−1.03(16)	−1.80(15)	−2.37(15)	−3.03(13)
$\beta = 1.95$	κ	0.1410	0.1400	0.1390	0.1375
$a^{-1} = 1.268(13)$[GeV]	m_π/m_ρ	0.582(3)	0.690(1)	0.752(1)	0.804(1)
	m_π^2 [GeV^2]	0.291(2)	0.573(1)	0.857(1)	1.287(1)
Fitting Range		12 – 16	13 – 25	13 – 25	13 – 25
$\Delta\overline{E}_n^{\mathbf{P}}$	[$\times 10^{-3}$ GeV]	18.2(26)	13.6(11)	10.81(61)	8.71(41)
$\overline{p}_n^2$	[$\times 10^{-2}$ GeV^2]	13.49(15)	13.415(83)	13.333(51)	13.288(40)
γ		1.13642(69)	1.08428(22)	1.060890(97)	1.042870(58)
$\delta(\overline{p}_n)$	[degrees]	−14.4(16)	−12.20(83)	−10.63(48)	−9.51(36)
$A(m_\pi, \overline{p}_n)$		−0.459(53)	−0.496(33)	−0.511(23)	−0.547(20)
$A^f(m_\pi, \overline{p}_n)$		−1.01(11)	−1.56(10)	−2.156(98)	−3.04(11)
$\beta = 2.10$	κ	0.1382	0.1374	0.1367	0.1357
$a^{-1} = 1.833(22)$[GeV]	m_π/m_ρ	0.576(3)	0.691(3)	0.755(2)	0.806(1)
	m_π^2 [GeV^2]	0.291(1)	0.605(2)	0.896(1)	1.331(2)
Fitting Range		18 – 30	18 – 35	18 – 35	18 – 35
$\Delta\overline{E}_n^{\mathbf{P}}$	[$\times 10^{-3}$ GeV]	31.5(32)	21.2(12)	17.99(92)	15.12(66)
$\overline{p}_n^2$	[$\times 10^{-2}$ GeV^2]	12.72(13)	12.542(63)	12.522(53)	12.511(45)
γ		1.12865(64)	1.07562(21)	1.05469(10)	1.038631(69)
$\delta(\overline{p}_n)$	[degrees]	−17.4(14)	−13.61(65)	−12.56(52)	−11.68(42)
$A(m_\pi, \overline{p}_n)$		−0.568(48)	−0.584(27)	−0.636(26)	−0.705(24)
$A^f(m_\pi, \overline{p}_n)$		−0.969(81)	−1.603(75)	−2.226(91)	−3.13(11)

Table XXII: Result for $n = 1$ state in the laboratory system L2 with energy state cut-off $N = 3$. The $A(m_\pi, \overline{p}_n)$ and $A^f(m_\pi, \overline{p}_n)$ are defined by eqs.(D.1) and (D.2), respectively.

Reference

[1] CP-PACS Collaboration: S. Aoki *et al.*, Phys. Rev. Lett. **84** (2000) 238; Phys. Rev. **D67** (2003) 034503.

[2] CP-PACS Collaboration: A. Ali Khan *et al.*, Phys. Rev. Lett. **85** (2000) 4674; Phys. Rev. **D65** (2002) 054505.

[3] HPQCD/UKQCD/MILC/Fermilab Collaborations: C. T. H. Davies *et al*, hep-lat/0304004.

[4] CP-PACS/JLQCD Collaborations: K. Kanaya *et al*, hep-lat/0310040.

[5] M. Lüscher, Commun. Math. Phys. **105** (1986) 153.

[6] M. Lüscher, Nucl. Phys. **B354** (1991) 531.

[7] M. Lüscher and U. Wolff, Nucl. Phys. **B339** (1990) 222.

[8] K. Rummukainen and S. Gottlieb, Nucl. Phys. **B450** (1995) 397.

[9] C. R. Gattringer and C. B. Lang, Nucl. Phys. **B391** (1993) 463; H. R. Fiebig, R. M. Woloshyn, and A. Dominiguez, Nucl. Phys. **B418** (1994) 649; M. Göckeler, H. A. Kastrup, J. Westphalen, and F. Zimmermann, Nucl. Phys. **B425** 413 (1994); M. Göckeler, H. A. Kastrup, J. Viola, and J. Westphalen, Nucl. Phys. **B** (Proc. Suppl.) **47** 831 (1996); C. Gutsfeld, H. A. Kastrup, K. Stergios, and J. Westphalen, Nucl. Phys. **B** (Proc. Suppl.) **63** 266 (1998); C. Gutsfeld, H. A. Kastrup, and K. Stergios, Nucl. Phys. **B560** 431 (1999).

[10] M. Guagnelli, E. Marinari, and G. Parisi, Phys. Lett. **B240** (1990) 188.

[11] S. R. Sharpe, R. Gupta and G. W. Kilcup, Nucl. Phys. **B383** (1992) 309.

[12] R. Gupta, A. Patel and S. R. Sharpe, Phys. Rev. **D48** (1993) 388.

[13] Y. Kuramashi, M. Fukugita, H. Miho, M. Okawa and A. Ukawa, Phys. Rev. Lett. **71** (1993) 2387; M. Fukugita, Y. Kuramashi, M. Okawa, H. Miho and A. Ukawa, Phys. Rev. **D52** (1995) 3003.

[14] JLQCD Collaboration: S. Aoki *et al.*, Phys. Rev. **D66** (2002) 077501.

[15] C. Liu, J. Zhang, Y. Chen and J. P. Ma, Nucl. Phys. **B624** (2002) 360.

[16] G. Meng, C. Miao, X. Du and C. Liu, hep-lat/0309048.

[17] BGR Collaboration: K. J. Juge *et al.*, hep-lat/0309075.

[18] H. R. Fiebig, K. Rabitsch, H. Markum and A. Mihàly, Few-Body Syst. **29** (2000) 95.

[19] CP-PACS Collaboration: S. Aoki *et al.*, Phys. Rev. **D67** (2003) 014502.

[20] C. Kim, hep-lat/0311003.

[21] C. W. Bernard and M. F. L. Golterman, Phys. Rev. **D53** (1996) 476.

[22] G. Colangelo and E. Pallante, Nucl. Phys. **B520** (1998) 433.

[23] Aachen-Cern-Munich Collaboration: W. Hoogland *et al.*, Nucl. Phys. **B69** (1974) 266: *ibid.* **B126** (1977) 109.

[24] M. J. Losty *et al.*, Nucl. Phys. **B69** (1974) 185.

[25] G. Colangelo, J. Gasser and H. Leutwyler, Nucl. Phys. **B603** (2001) 125.

[26] J. Balog, M. Nierdermaier, F. Niedermayer, A. Patrascioiu, E. Seiler and P. Weisz, Nucl. Phys. **B618** (2001) 315.

[27] L. Maiani and M. Testa, Phys. Lett. **B245** (1990) 585.

[28] L. Lellouch and M. Lüscher, Commun. Math. Phys. **219** (2001) 31.

[29] C. Bernard, T. Draper, A. Soni, H. D. Politzer and M. B. Wise, Phys. Rev. **D33** (1985) 2343; C. Bernard, T. Draper, G. Hockney and A. Soni, Nucl. Phys. **B** (Proc. Suppl.) **4** (1988) 483; SPQCDR Collaboration: D. Becirevic *et al.*, Nucl. Phys. **B** (Proc. Suppl.) **119** (2003) 359.

[30] JLQCD Collaboration: S. Aoki *et al.*, Phys. Rev. **D58** (1998) 054503; D. Pekurovsky and G. Kilcup, Phys. Rev. **D64** (2001) 074502; RBC Collaboration: T. Blum *et al.*, hep-lat/0110075; CP-PACS Collaboration: J. I. Noaki *et al.*, Phys. Rev. **D68** (2003) 014501.

[31] N. Ishizuka, Nucl. Phys. **B** (Proc. Suppl.) **119** (2003) 84.

[32] J. Gasser and H. Leutwyler, Annals Phys. **158** (1984) 142.

[33] J. Bijnens, G. Colangelo, G. Ecker, J. Gasser and M. E. Sainio, Phys. Lett. **B374** (1996) 210; Nucl. Phys. **B508** (1997) 263.

[34] A. Schenk, Nucl. Phys. **B363** (1991) 97.

[35] H. W. Fearing and S. Scherer, Phys. Rev. **D53** (1996) 315.

[36] J. Bijnens, G. Colangelo and J. Gasser, Nucl. Phys. **B427** (1994) 427.

[37] S. M. Roy, Phys. Lett. **B36** (1971) 353.

[38] B. Hyams *et al.*, Nucl. Phys. **B64** (1973) 134.

[39] S. D. Protopopescu *et al.*, Phys. Rev. **D7** (1973) 1279.

[40] B. Ananthanarayan, G. Colangelo, J. Gasser and H. Leutwyler, Phys. Rep. **353** (2001) 207.

[41] Geneva-Saclay Collaboration: L. Rosselet *et al.*, Phys. Rev. **D15** (1977) 574.

[42] C. D. Froggatt and J. L. Petersen, Nucl. Phys. **B129** (1977) 89.

[43] M. M. Nagels *et al.*, Nucl. Phys. **B147** (1979) 189.

[44] E865 Collaboration: S. Pislak *et al.*, Phys. Rev. Lett. **87** (2001) 221801.

[45] S. Pislak *et al.*, Phys. Rev. **D67** (2003) 072004.

[46] NA48 Collaboration: A. L. D. Marras *et al.*, Eur. Phys. J. **C30** (2003) 33.

[47] KLOE Collaboration: A. Aloisio *et al.*, hep-ex/0308023.

[48] A. V. Kravtsov *et al.*, Nucl. Phys. **B134** (1978) 413.

[49] M. E. Sevior *et al.*, Phys. Rev. Lett. **66** (1991) 2569: Phys. Rev. **D48** (1993) 3987.

[50] OMICRON Collaboration: G. Kernel *et al.*, Z. Phys. **C48** (1990) 201; G. Kernel *et al.*, Phys. Lett. **B225** (1989) 198.

[51] J. B. Lange *et al.*, Phys. Rev. **C61** (2000) 025201.

[52] CHAOS Collaboration: F. Bonutti *et al.*, Nucl. Phys. **A677** (2000) 213.

[53] DIRAC Collaboration: C. Santamarina *et al.*, hep-ex/0309335.

[54] J. Gasser, V. E. Lyubovitskij, A. Rusetsky and A. Gall, Phys. Rev. **D64** (2001) 016008.

[55] K. G. Wilson, in *New Phenomena in Subnuclear Physics*, ed. A. Zichichi (Plenum Press, New York 1975), p.69.

[56] Y. Iwasaki, Nucl. Phys. **B258** (1985) 141; University of Tsukuba preprint UTHEP-118 (1983) (Unpublished).

[57] B. Sheikholeslami and R. Wohlert, Nucl. Phys. **B259** (1985) 572.

[58] G. P. Lepage and P. B. Mackenzie, Phys. Rev. **D48** (1993) 2250.

[59] F. Niedermayer, P. Rüfenacht and U. Wenger, Nucl. Phys. **B597** (2001) 413.

[60] BGR Collaboration: C. Gattringer *et al.*, hep-lat/0307013.

[61] M. Jarrell and J. E. Gubernatis, Phys. Rep. **269** (1996) 133.

[62] T. Yamazaki and N. Ishizuka, Phys. Rev. **D67** (2003) 077503.

[63] Ph. de Forcrand *et al.*, Nucl. Phys. **B** (Proc. Suppl.) **63** (1998) 460; Y. Nakahara, M. Asakawa, and T. Hatsuda, Phys. Rev. **D60** (1999) 091503; M. Asakawa, T. Hatsuda and Y. Nakahara, Prog. Part. Nucl. Phys. **46** (2001) 459; CP-PACS Collaboration: T. Yamazaki *et al.*, Phys. Rev. **D65** (2002) 014501; K. Sasaki, S .Sasaki, T. Hatsuda and M. Asakawa, hep-lat/0309177.

[64] I. Wetzorke and F. Karsch, presented at International Workshop on Strong and Electroweak Matter (SEWM 2000), hep-lat/0008008; M. Oevers, C. Davies and J. Shigemitsu, Nucl. Phys. **B** (Proc. Suppl.) **94** (2001) 423; F. Karsch, E. Laermann, P. Petreczky and S.Stickan, Phys. Rev. **D68** (2003) 014504; M. Asakawa and T. Hatsuda, hep-lat/0308034.

[65] M. Imachi, Y. Shinno and H. Yoneyama, hep-lat/0309156.

[66] C. R. Allton, J. E. Clowser, S. J. Hands, J. B. Kogut, and C. G. Strouthos, Phys. Rev. **D66** (2002) 094511.

[67] N. Kawamoto and J. Smit, Nucl. Phys. **B192** (1981) 100.